Unravelling Galaxy Components

Rebecca Kennedy

Thesis submitted to the University of Nottingham
for the degree of Doctor of Philosophy

June 2017

Supervisor:	Dr. Steven Bamford
Examiners:	Professor Michael Merrifield
	Dr. Vivienne Wild
Submitted:	20th March 2017
Examined:	11th April 2017
Final version:	22nd June 2017

Contents

List of Figures

List of Tables

Abstract

This thesis aims to understand more about the developmental histories of galaxies and their internal components by studying the wavelength dependence of their spatial structure. I use a large sample of low-redshift galaxies with optical–near-IR imaging from the GAMA survey, which have been fitted with Sérsic and Sérsic + exponential functions in nine wavebands simultaneously, using software developed by the MegaMorph project.

The first section of this thesis examines how the sizes and radial profiles of galaxies vary with wavelength. To quantify the wavelength dependence of effective radius I use the ratio, $\mathcal{R}$, of measurements in two restframe bands. The dependence of Sérsic index on wavelength, $\mathcal{N}$, is computed correspondingly. I show that accounting for different redshift and luminosity selections partly reconciles variations between several recent studies. Dividing galaxies by visual morphology confirms the behaviour inferred using morphological proxies, although our quantitative measurements allow me to study larger and fainter samples. I then demonstrate that varying dust opacity and disc inclination can account for features of the joint distribution of $\mathcal{R}$ and $\mathcal{N}$ for late-type galaxies. However, dust does not appear to explain the highest values of $\mathcal{R}$ and $\mathcal{N}$. The bulge-disc nature of galaxies must also contribute to the wavelength-dependence of their structure.

The second section of this thesis studies radial colour gradients across the galaxy population. I use the multi-wavelength information provided by MegaMorph analysis of galaxy light profiles to calculate intrinsic colour gradients, and divide into six subsamples split by overall Sérsic index (n) and galaxy colour.

continued

I find a bimodality in the colour gradients of high- and low-n galaxies in all wavebands which varies with overall galaxy luminosity. Global trends in colour gradients therefore result from combining the contrasting behaviour of a number of different galaxy populations. The ubiquity of strong negative colour gradients supports the picture of inside-out growth through gas accretion for blue, low-n galaxies, and through dry minor mergers for red, high-n galaxies. An exception is the blue high-n population which has properties indicative of dissipative major mergers.

In the third section of this thesis I apply bulge-disc decompositions to my sample of galaxies, in order to discover the structural origin of the wavelength dependences found in the previous two chapters. I find that most galaxies with a substantial disc, even those with no discernible bulge, display a high value of $\mathcal{N}$. The increase in Sérsic index to longer wavelengths is therefore intrinsic to discs, apparently resulting from radial variations in stellar population and/or dust reddening. Similarly, low values of $\mathcal{R}$ (< 1) are found to be ubiquitous, implying an element of universality in galaxy colour gradients. I also study how bulge and disc colour distributions vary with galaxy type. I find that, rather than all bulges being red and all discs being blue in absolute terms, both components become redder for galaxies with redder total colours. I even observe that bulges in bluer galaxies are typically bluer than discs in red galaxies, and that bulges and discs are closer in colour for fainter galaxies. Trends in total colour are therefore not solely due to the colour or flux dominance of the bulge or disc.

Published work

Much of the work in this thesis has been previously presented in several papers:

I Kennedy, R., Bamford, S. P., Baldry, I., Häußler, B., Holwerda, B. W., Hopkins, A. M., Kelvin, L. S., Lange, R., Moffett, A. J., Popescu, C. C., Taylor, E. N., Tuffs, R. J., Vika, M. and Vulcani, B., 2015, "Galaxy And Mass Assembly (GAMA): the wavelength dependence of galaxy structure versus redshift and luminosity", MNRAS, 2015, 454, 806

II Kennedy, R., Bamford, S. P., Häußler, B., Baldry, I., Bremer, M., Brough, S., Brown, M. J. I, Driver, S., Duncan, K., Graham, A. W., Holwerda, B. W., Hopkins, A. M., Kelvin, L. S., Lange, R., Phillipps, S., Vika, M. and Vulcani, B., 2016, "Galaxy And Mass Assembly (GAMA): understanding the wavelength dependence of galaxy structure with bulge-disc decompositions", MNRAS, 2016, 460, 3458

III Kennedy, R., Bamford, S. P., Häußler, B., Brough, S., Holwerda, B. W., Hopkins, A. M., Vika, M. and Vulcani, B., 2016, "Galaxy And Mass Assembly (GAMA): Galaxy colour gradients versus colour, structure and luminosity", A&A, 2016, 593, A84

Paper I contains the work detailed in chapter 3 of this thesis. Paper II describes the work presented in chapter 5. Just to mix things up a bit, Paper III contains most of the work presented in chapter 4.

The vast majority of the work presented in this thesis was performed by the author, with advice from the paper coauthors listed above. Where the material presented is the result of more collaborative work, this is mentioned at the beginning of the relevant chapter.

Chapter 1

Introduction

1.1 Motivation

This thesis aims to understand more about the developmental histories of galaxies. The stars within a given galaxy have typically formed over a range of times and through different mechanisms. The formation history of a galaxy is recorded in the age, metallicity and phase space distributions of a galaxy's stellar population. The observed spatial structure of galaxies, and their wavelength dependence, can therefore be used to learn how galaxies have formed and evolved.

1.2 Galaxy Formation

Our current picture of the history of the Universe begins with a 'Big Bang' approximately 13.8 billion years ago. For a fraction of a second after the big bang the Universe expanded and cooled extremely quickly, during a period called 'inflation'.

As the Universe continued to cool after inflation, protons and neutrons were able to bind together to form atomic nuclei. After further cooling, electrons bound to these nuclei to form neutral atoms during 'recombination'. At this point, 380,000 years after the big bang, photons were able to free stream throughout the Universe, making it transparent. This is known as the 'surface of last scattering', which we can observe today as the Cosmic Microwave

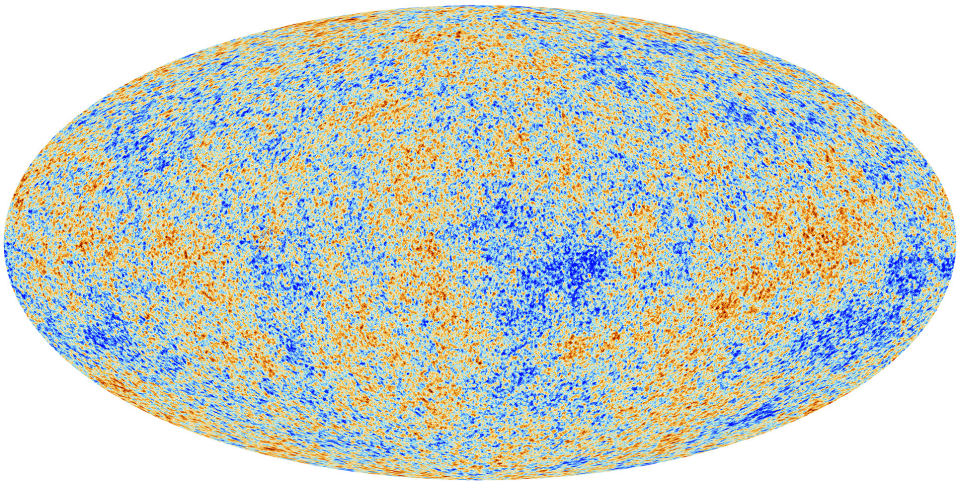

Figure 1.1. The anisotropies of the Cosmic microwave background (CMB) as observed by Planck (2013).

Background (CMB), see Fig. 1.1.

The variations in temperature we see on the CMB were created by quantum fluctuations before inflation, and formed the basis for the large scale structure we see in the universe today. Initially the growth of structure was dominated by dark matter in the standard model, which was first proposed by Zwicky (1933). Dark matter, as its name suggests, cannot be seen because it does not interact with the electromagnetic field, and only interacts with gravity. Dark matter halos attracted baryonic 'light' matter, i.e. visible matter. As clouds of protogalactic gas slowly cooled they began to collapse, and as they collapsed they began to rotate, causing the gas to settle into a rotating disc which became dense enough for the first stars to form. These stars, and their resulting supernovae, became the building blocks for the first galaxies. The scenario of hierarchical structure formation (Lacey & Cole 1993) in which smaller dark matter halos coalesce to make larger halos, which have a greater gravitational potential, allowing them to attract more galaxies, causing further merging events, is responsible for the evolved galaxies we observe today.

1.3 Galaxy Evolution

Galaxies today form a bimodal distribution in colour-mass space, with a divide between the blue cloud (which contains a young, star forming population), and the red sequence (which contains older, quenched galaxies) (Strateva et al.

2001). The space between these populations is referred to as the 'green valley'. The red and blue populations have been modelled as separate Gaussian distributions (Baldry et al. 2004), implying that these green valley galaxies are outliers of the red sequence and blue cloud rather than being a distinct population. Other studies (e.g. Mendez et al. 2011) support this theory by finding that the green valley contains a mix of populations in terms of (amongst other descriptors), morphological type. It is also well documented that many members of the green valley population are dusty, highly-inclined systems (e.g. Morselli et al. 2016 and references therein).

A galaxy's evolution is closely linked to its morphology (Smethurst et al. 2015); some late-type star-forming galaxies quench on very short timescales and join the red sequence, whilst other late-type galaxies retain their discy morphology and experience a much slower decline in star formation (see Schawinski et al. 2014).

After its formation a galaxy can undergo a number of processes throughout its lifetime which will shape its individual characteristics. However, we can often only see the signatures of a galaxy's latest evolutionary process, so we may never be able to fully understand the full formation history of a population of galaxies without the use of simulations. In this section I therefore discuss evidence from both observations and simulations.

The processes affecting a galaxy's evolution can generally be split into two categories, which are detailed below: internal processes, and environmental (external) processes. I then go on to discuss in more detail some of the prevailing theories of how the types of galaxies studied in this project may have evolved.

1.3.1 Internal processes

Inside-out disc growth Spiral galaxies are thought to grow through the infall of gas from within the dark matter halo of a protogalaxy (first introduced by Fall & Efstathiou 1980). As the gas is accreted onto the growing disc, it gains angular momentum and forms an exponential profile, with a mass and angular momentum proportional to the corresponding properties of the dark matter halo in which it resides (Mo, Mao & White

1998).

Star-formation feedback Supernovae are able to heat large amounts of their surrounding ISM, preventing the collapse of more gas, which in turn regulates the star formation rate (Efstathiou 2000). Stellar winds are also a significant feedback mechanism; low-mass stars (i.e. below $\sim M_{\odot}$) return large quantities of their mass to the surrounding interstellar medium during their lifetime, leaving behind white dwarf remnants (Stinson et al. 2006).

Radio jets Star formation within a galaxy may be shut off when a black hole at its centre expels powerful jets, which prevents the cooling of hot halo gas, thus halting star formation (see Fabian 2012 for a review). Simulations of radio jets emerging from black holes support this theory (Gabor et al. 2011), and help to explain why the products of major mergers (discussed in Section 1.3.2) don't have renewed star formation after the gas heated by the merger has naturally cooled.

Secular bulge growth Whereas classical bulges may be the products of mergers, pseudo-bulges are more likely to have formed via disc instabilities (Kormendy & Kennicutt 2004). Boxy bulges are thought to have formed from bars which have buckled, leaving a central component which looks boxy when viewed edge-on. In this scenario, the structure of the pseudo-bulge is likely to be younger than its stars, which originally part resided in the inner disc (see Combes et al. 1990 and references therein). Discy pseudo-bulges are thought to form when angular momentum transport via bars drives material into the centre of a galaxy, forming a bulge-like structure (Kormendy 1993).

1.3.2 Environmental processes

External processes are numerous and varied, and are particularly prevalent in galaxies within clusters and groups. It has been demonstrated that low-mass galaxies within clusters and groups are significantly more likely to be quenched compared to field galaxies at a given stellar mass (Baldry et al. 2006; Slater & Bell 2014), and that quenching occurs on shorter timescales than morphological transformations (Bamford et al. 2009). At higher masses Dressler (1980)

showed a remarkable relationship between local density and galaxy type, with ellipticals preferentially residing in the densest regions. This environmental dependence is particularly important at more recent times: both the median star formation rate (SFR) and the specific star formation rate (sSFR) depend on environment below z <1, but are independent of environment above $z = 1$ (Darvish et al. 2016). Below I provide an overview of the environmental processes which can alter galaxies. Although evidence has been found for particular mechanisms to be prevalent in particular environments, this does not mean that other mechanisms aren't also at play; multiple mechanisms can (and do) act simultaneously on a galaxy.

Harassment Or 'tidal interactions'; when two galaxies interact gravitationally without merging. This can result in (amongst other things) tidal tails, asymmetry, and bars (Moore et al. 1996), and can have a similar effect to ram pressure stripping, described below (see e.g. Willman et al. 2004; Bahé & McCarthy 2015 and references therein). The main evidence for harassment comes from the observation that clusters at higher redshifts contain many discy galaxies, while clusters at low redshift primarily contain redder, quenched galaxies. Modelling these systems reproduces observations, with the modelled galaxies having undergone multiple harassment events during the simulation (Moore et al. 1996).

Accretion E.g. in binary systems, or gas from the IGM accreting onto galaxies (see e.g. Rees & Ostriker 1977). In the latter scenario, gas is accreted along filaments of the cosmic web, providing ample cool gas to fuel star formation (Stewart et al. 2011). In practice these cool flows are difficult to observe, but the presence of multiple bursts of star formation in dwarf galaxies provides indirect evidence for their existence (see Tolstoy, Hill & Tosi 2009 for an overview of star formation histories in dwarf galaxies).

Galaxy mergers Two or more galaxies colliding and subsequently merging through dynamical friction. Mergers between galaxies of very different masses are classed as minor mergers, whilst mergers between galaxies of similar massess are classed as major mergers. If both galaxies are gas-rich, this is classed as a wet merger and is likely to produce lots of star formation (Bekki & Shioya 1998). Dry mergers, between older, gas-

poor galaxies, have little effect on star formation rate (Bekki 1998). It is widely postulated that major mergers at higher redshift are a likely formation mechanism for older, quenched red sequence galaxies; the discs of the merging galaxies are disrupted and the gas reservoirs are quickly destroyed, halting star formation. Similar conclusions are found in simulations, which can trace the merging of disc-dominated systems to create the spheroidal galaxies we observe today, with one final burst of star formation during the merger (Steinmetz & Navarro 2002).

Ram pressure stripping Explains the absence of late-type galaxies in the centre of clusters (see e.g. Gunn & Gott 1972). As a galaxy falls inwards towards the centre of a cluster, the pressure of the intracluster medium strips the galaxy of its gas. Simulations have shown that ram pressure stripping can be responsible for the loss of around half the cool gas within a galaxy (Bahé & McCarthy 2015).

Strangulation In which the gas supply to a galaxy is shut off, but the gas reservoir is not removed (as it would be in ram pressure stripping). This allows the galaxy to continue forming stars for some time using its available gas, thereby increasing its stellar mass and metallicity (Peng, Maiolino & Cochrane 2015).

1.3.3 Size Evolution

Studying galactic size evolution is an important step in understanding the formation history of galaxies and the dark matter halos in which they reside. van der Wel et al. (2014) find over a redshift range of $0 < z < 3$, early-type galaxies are, on average, smaller than late-type galaxies. They also find a significantly different rate of average size evolution at fixed galaxy mass, with fast size evolution for the early-type population, and moderate evolution for the late-type population. These findings for the late-type population, particularly below z = 1, are consistent with the work of Barden et al. (2005), who demonstrate that the size evolution of disc galaxies is decoupled from the size evolution of the dark matter halos in which they reside. The size evolution of late-types is therefore thought to be due to the inside-out growth of their discs, which is discussed in section 1.3.1.

Previous studies have shown that compact passive galaxies, or 'red nuggets' were significantly more prevalent in the early universe compared to the present day (see e.g. Daddi et al. 2005; Longhetti et al. 2007; Cimatti et al. 2008; Hopkins et al. 2009; Cassata et al. 2010; Szomoru, Franx & van Dokkum 2012; Davari et al. 2017). The fast size growth of early-type galaxies has been postulated as being due to tidal disruption of satellite galaxies leading to gradual stellar accretion in the outskirts of early-types. Both simulations (e.g. Naab, Johansson & Ostriker 2009 and references therein) and observations (see e.g. van Dokkum et al. 2010; Davari et al. 2017 and references therein) corroborate this theorised inside-out evolution process via minor mergers, particularly in low-mass systems (Hopkins et al. 2010). These processes are not thought to be responsible for the growth of discy galaxies; too few late-types are found in simulations, having undergone mergers which destroy their discs (Steinmetz & Navarro 2002).

1.4 Galaxy Morphology

Historically, galaxies were visually classified as elliptical ('E'), lenticular ('S0') or spiral ('S') in morphology (Hubble 1936 , see Fig. 1.2). Elliptical galaxies are traditionally characterised by their one-component spheroidal shape. They are thought to be the product of early and/or dry mergers, and therefore predominantly contain older, redder stars (Dressler et al. 1997; Kauffmann et al. 2003; Brinchmann et al. 2004). Many of the objects initially classified as 'elliptical' were later found to have a disc component (Kormendy & Bender 1996), which led to the introduction of the 'ES' classification for galaxies lying between ellipticals and lenticulars on the Hubble tuning fork diagram (Liller 1966). They have since been referred to as E/S0 galaxies and discy ellipticals (Nieto, Capaccioli & Held 1988; Simien & Michard 1990). This view was later augmented to include parallel sequences for spirals and lenticulars, with 'early' and 'late' types described by their disc-to-bulge ratios (van den Bergh 1976). As the quality of observational data improved over time, the need for a continuum of bulge-to-disc ratios in early-type galaxies also became necessary (Capaccioli, Piotto & Rampazzo 1988). This version of the Hubble diagram was then extended to include spheroidal galaxies at the end of the S0a-S0b-S0c

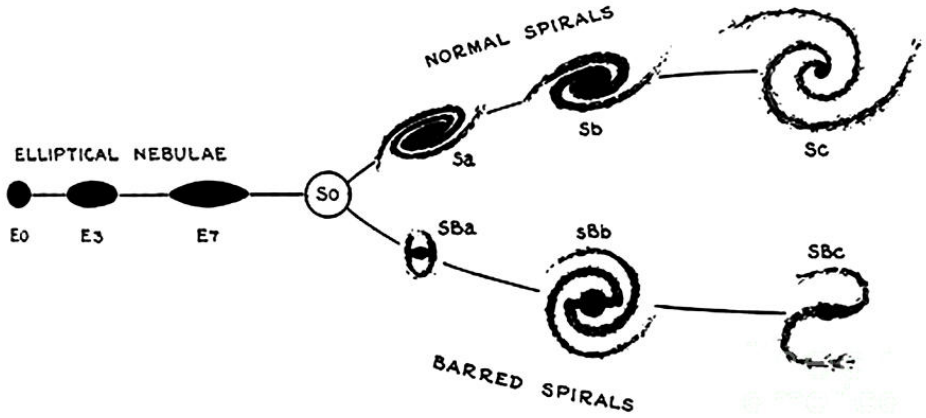

Figure 1.2. Hubble's tuning fork diagram, published in 'The realm of the nebulae', (Hubble 1936).

sequence, as shown in Fig. 1.3 (Cappellari et al. 2011).

Apparent visual morphology is strongly dependent on inclination; for example, face-on S0s are commonly mis-classified as ellipticals, whilst it is difficult to ascertain whether an edge-on spiral has a bar or not. To resolve this, Graham (2014) uses both bulge-to-disc flux ratio and Hubble type in conjunction with one another in order to minimise the effect of the random orientation of a galaxy's disc on its morphological classification.

The colour of a galaxy and its components can be used as a proxy for morphology to aid differentiation between early and late types, however Conselice (2006) and Bamford et al. (2009) caution against using color as a sole classifier. The colour cut used varies between studies, but is commonly defined at around $u - r = 2.22$, regardless of magnitude (e.g. Strateva et al. 2001). $u - r$ versus $g - i$ colour space has also been found as an effective proxy for classifying galaxies in the Sloan Digital Sky Survey (SDSS) as either early- or late-type. The location of a galaxy in this colour space also reflects the degree and locality of star formation activity (Park & Choi 2005), and correlates well with stellar population age.

Structural classifications based on kinematics are more sensitive to the presence of discs than any photometric attempt (e.g. Emsellem et al. 2007; Cappellari et al. 2011). For example, work based on ATLAS-3D data finds that discs are common in all but the most massive galaxies (Emsellem et al. 2011). Kinematics can also distinguish between, for example, fast and slow rotating

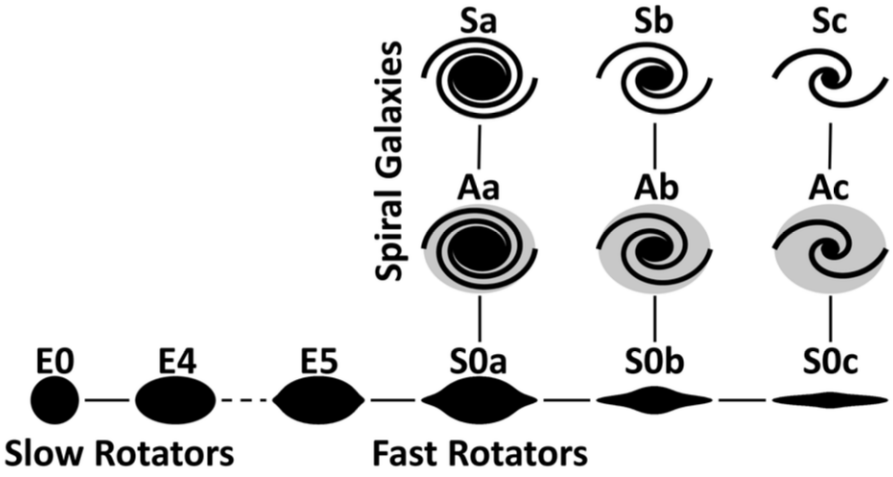

Figure 1.3. Cappellari's updatedtuning fork diagram, which extends Hubble's tuning fork diagram to include spheroidal galaxies at the end of the S0a-S0b-S0c sequence (Cappellari et al. 2011).

early-type galaxies, which can shine a light on both their underlying stellar structure, and their possible formation mechanisms (e.g. Emsellem et al. 2011; Krajnović et al. 2011; Krajnovic et al. 2013 and references therein).

1.4.1 Measuring structural properties

Radial luminosity profiles of galaxies, and their components, are commonly described by a Sérsic function, which models the variation in the projected light distribution with radius. These are typically defined on elliptical isophotes (Sérsic 1963; Graham & Driver 2005):

$$I(r) = I_e \left\{ -b_n \left[\left(\frac{r}{R_e} \right)^{\frac{1}{n}} - 1 \right] \right\} \tag{1.1}$$

where n is the Sérsic index, which controls the shape of the profile, $I(r)$ is the surface brightness at a given radius, R_e is the effective radius (the radius containing half of the model light), I_e is the intensity at the effective radius, and b_n is a function of Sérsic index such that $\Gamma(2n) = 2\gamma(2n, b_n)$, where Γ and γ represent the complete and incomplete gamma functions, respectively (Ciotti 1991). The shape of the Sérsic function for a range of Sérsic indices is shown in Fig. 1.4.

Elliptical galaxies are typically well-described by a single Sérsic profile. The

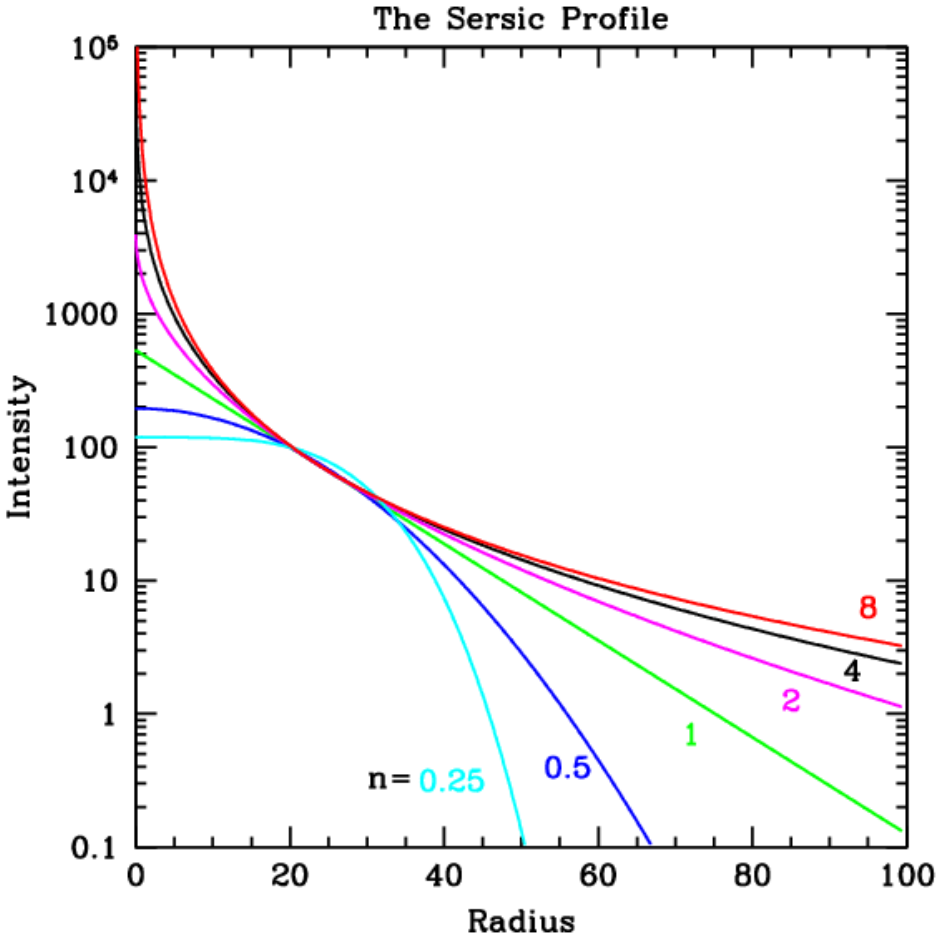

Figure 1.4. The Sérsic function for a range of Sérsic indices, where R_e and b_n are held fixed (Peng et al. 2010).

index is often taken to be fixed at $n = 4$ (de Vaucouleurs 1948), although it has been shown to vary from $n \lesssim 2$ at low masses to $n \gtrsim 4$ for high mass ellipticals (Hodge 1971; Caon, Capaccioli & D'Onofrio 1993; Graham 2013).

Spiral galaxies, on the other hand, generally require a superposition of two different Sérsic profiles. Some studies also account for the presence of a bar, commonly with a third Sérsic profile (Gadotti 2011). The discs of spirals (and lenticulars) can usually be accurately described by an exponential ($n = 1$) profile (e.g., Kormendy 1977, Allen et al. 2006). Bulges are often described by a de Vaucouleurs ($n = 4$) profile. As with elliptical galaxies, this is usually not accurate (Andredakis, Peletier & Balcells 1995; Graham & Prieto 2001; de Souza, Gadotti & dos Anjos 2004), so recent studies (including the work described in this thesis) tend to adopt a general Sérsic profile, where n is not fixed. In fact, it is rare to find bulges with $n > 3$ (Balcells et al. 2003),

and the bulges of many spiral galaxies (particularly intermediate-type discs) exhibit the exponential profiles of pseudo bulges and are supported by rotation (Andredakis & Sanders 1994; Carollo 1999; de Jong et al. 2004; Gadotti 2009; McDonald et al. 2011).

Pseudo-bulges generally have younger stellar populations than classical bulges, and are likely formed by secular processes. Due to their flattened light profiles they are often difficult to detect at high inclination (Carollo et al. 1997; Kormendy et al. 2006; Drory & Fisher 2007; Gadotti 2009). Conversely, early-type spiral galaxies by definition appear to have significantly bigger and brighter bulges than late-type spiral galaxies, which tend to have small, faint bulges (Graham & Prieto 2001; Möllenhoff 2004). A possible reason for this difference in bulge size and luminosity with morphology is that in late-type spirals the bulge is 'submerged' in the disc, masking some of the bulge light (Graham & Prieto 2001). This is consistent with the Hubble sequence pattern of increasing D/T flux ratio for later-type spirals (de Lapparent, Baillard & Bertin 2011).

It should be noted that using a single Sérsic fit as an indicator of whether a galaxy is early- or late-type can sometimes be misleading, due to the intrinsic variations in n and measurement uncertainties (Binggeli & Jerjen 1998; Graham & Guzman 2003; Krajnovic et al. 2013). Elliptical galaxies commonly have discs (e.g. Kormendy & Bender 1996 and references therein), or disc-like structures (Emsellem et al. 2007; Krajnović et al. 2011; Emsellem et al. 2011; Cappellari et al. 2011), and can exhibit a large range of disc-to-total (D/T) flux ratios (Krajnovic et al. 2013), with $D/T \sim 0.4$ typical. This calls into question the tradition of classifying galaxies by their Sérsic index or visual morphology (Vika et al. 2015).

1.4.2 Wavelength dependence of structural parameters

Previous studies have shown a strong relationship between measured sizes of galaxies and wavelength: on average, galaxies of all morphologies are found to be smaller in redder wavebands (Evans 1994; La Barbera et al. 2010b; McDonald et al. 2011; Kelvin et al. 2012; Vulcani et al. 2014 (hereafter V14); Kennedy et al. 2015; Lange et al. 2015). Sérsic index is also known to change with wavelength; Sérsic index measured in the NIR is generally significantly

larger than in the optical for low-n galaxies, with high-n galaxies exhibiting a similar, if less pronounced, trend (Taylor-Mager et al. 2007; Kelvin et al. 2012; V14, Vika et al. 2015). These trends, and their implications for galaxy structure, are discussed in more detail in Section 3.1.

Variations in structural properties with wavelength directly imply that the colour of a galaxy must change with distance from its centre. This can be measured as a colour gradient, or the radial change in colour. As a non-parametric way of quantifying galaxy properties, this can be instrumental in characterising the stellar populations within a galaxy.

1.4.3 Colour gradients

The existence of negative colour gradients (i.e. redder in the centre and bluer in the outskirts) in elliptical galaxies is well-documented (see Peletier, Valentijn & Jameson 1990; Gonzalez-Perez, Castander & Kauffmann 2011 and references therein). La Barbera et al. (2010a) find that these colour gradients can be linked to the overall colour and luminosity of an early-type galaxy (ETG); steeper negative colour gradients are more commonly found in bluer or more luminous ETGs. Steep negative colour gradients have also been observed in late-type galaxies (LTGs) and are thought to indicate the presence of young stars in their outer regions (Gonzalez-Perez, Castander & Kauffmann 2011). There are, however, inherent difficulties in measuring consistently accurate stellar population colours in LTGs due to interstellar extinction caused by dust. This dust extinction is most problematic in optical wavebands (see de Jong & van der Kruit 1994 and references therein). Moving to longer wavelengths combats this problem as observations in the near-infrared (NIR) are less affected by dust. The NIR is also better able to measure the older stellar populations within a galaxy, which contain most of the stellar mass (de Jong & van der Kruit 1994).

Recently, advances have been made in using colour information to constrain age and metallicity gradients in ETGs (e.g. La Barbera et al. 2010a; Carter et al. 2011). Fewer studies of a similar nature have been attempted for spiral galaxies, partly due to their increased dust content compared to elliptical galaxies, and partly due to their more complex structure. Bell & de Jong

(2000) find that the inner regions of most low-inclination spiral galaxies are older and more metal-rich than their outskirts which supports inside-out formation, although age gradients do not necessarily correlate with metallicity gradients (e.g. Tortora et al. 2010; Sánchez-Blázquez et al. 2014 and references therein). Similarly, $g-r$ and $g-i$ rest-frame global colours are mainly related to the age of the galaxy, and do not depend strongly on metallicity (Gonzalez-Perez, Castander & Kauffmann 2011).

1.5 Stellar populations

In order to draw meaningful conclusions about a galaxy's formation history from its current colour information, one must consider stellar population models and their connection to observed colours. Stellar population synthesis (SPS) models can be used to derive the likely spectral evolution of a stellar population as a function of its metallicity and age, given an initial mass function (IMF) (e.g. see Taylor et al. 2011 for an overview). The SPS modelling procedure implemented for this thesis is described in more detail in Chapter 6.

We can use a galaxy's spectrum to tell us about its past and present star formation, because transitions in the star formation rate within a galaxy leave marked signatures in the light of its stellar population. Dust, and the interstellar medium, can also affect the properties observed, so these must be taken into account when making inferences about a galaxy's stellar populations. In Chapter 3 I study the effect of dust on galaxy properties, and show that dust alone cannot account for the trends observed. This leaves age and metallicity to drive the wavelength dependence of galaxy properties for the sample studied in this thesis, as described in the following section.

The age of a stellar population, commonly measured in Gyr, describes the time since its formation. The oldest stellar populations in the universe reside in giant elliptical galaxies, which had a very early formation time and have been aging ever since (Bruzual 2000). Younger stellar populations are formed when, for example, two galaxies have undergone a recent interaction and a burst of star formation occurs, or in galaxies which have ongoing star formation (as described in section 1.2).

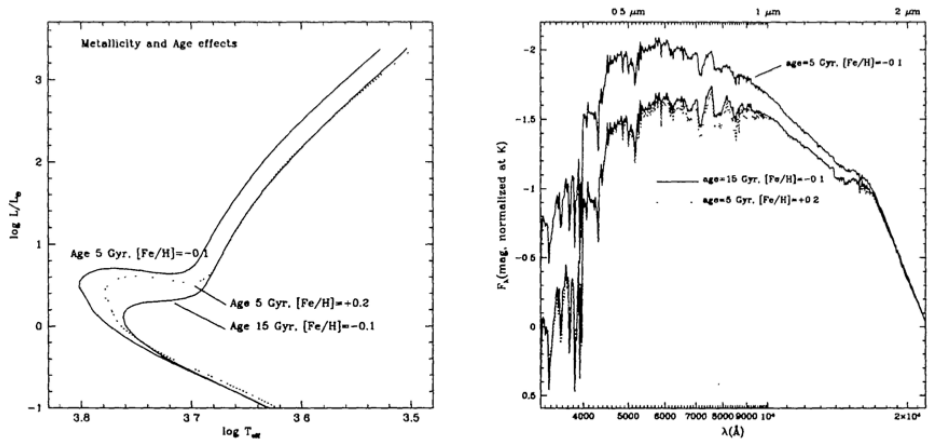

Figure 1.5. The 3/2 age-metallicity degeneracy as presented in Worthey (1994). This figure considers an isochrone of 5 Gyr age (left-hand panel), with a metallicity slightly lower than solar abundance. Isochrones of three times the age or twice the metallicity have nearly identical spectra (right-hand panel).

The fraction of a galaxy's mass which is in the form of metals (i.e. not hydrogen or helium) is referred to as it's 'metallicity' (Z). As the universe ages, and stars age, lighter elements synthesise to produce heavier elements (see Bruzual 2000 for an overview). In spiral galaxies there are generally two types of stellar population: Population I and Population II. Population I stars make up the disc of the galaxy and are young, blue, and metal-rich. Population II stars usually make up the central bulge, have very low metallicities, and are redder in colour.

1.5.1 Age-metallicity degeneracy

Age and metallicity are degenerate properties, and their effects are easily confused with one another; a combination of the two can be used to describe almost any galaxy colour and spectral index. Plotted against one another, the slope in the δlog(age) vs δ log(Z) = 3/2, or 'the 3/2 degeneracy' (Worthey 1994, 1999). This degeneracy is neatly demonstrated in Figure 1.5 which is taken from Worthey (1994). The isochrones show that a 30% change in age can compensate for a -20% change in metallicity, and vice versa.

One way in which this age-metallicity degeneracy can be broken is by using spectroscopy; different spectral lines have different sensitivities to age and metallicity. For example, the absorption of radiation from metals in stellar

atmospheres, and the absence of hot, blue stars, causes a clear signature in the SED of a galaxy. This feature therefore occurs most strongly in elliptical galaxies, and less commonly in spiral galaxies. The 4000Åbreak is a spectral feature which tells us about the luminosity-weighted mean stellar age of a population, and the fraction of stars formed in recent bursts ($<$ 1Gyr) (Poggianti & Barbaro 1997).

More recently, colours have been used to derive the age and metallicity of stellar populations (e.g. Li & Han 2007). This technique has a number of advantages over spectral analysis; colours are more widely available for large numbers of galaxies, and are independent of a galaxy's distance. However, this technique has been shown to be particularly sensitive to the presence of young stellar populations, which can obscure the detection of and older, more metal-rich stellar population. Principle Component Analysis (PCA, e.g. Wild et al. 2007) is a technique that aims to circumvent both the problems with using a stellar population model (not every stellar population will have a good fit to a model), and using colours alone (young stars tend to dominate the light). PCA compares the output of stellar population models to the eigenspectra of particular features, in order to combine the wide availability of colours with known spectral features.

In this study I use the methods of Taylor et al. (2011) to derive ages and metallicities for the galaxies in my sample. This is discussed in more detail in section 6.2.

1.6 Structure of thesis

This thesis aims to understand more about the developmental histories of galaxies and their internal components by studying the wavelength dependence of their spatial structure. I use a large sample of low-redshift galaxies with optical–near-IR imaging from the GAMA survey, which have been fitted with Sérsic and Sérsic + exponential functions simultaneously in nine wavebands using software developed by the MegaMorph project.

I begin by describing the origin of the data used in this project, and the structural analysis methods that have been employed.

Chapter 3 of this thesis investigates how the sizes and radial profiles of galaxies vary with wavelength, as well as how this behaviour varies with luminosity and the robustness of these trends to the effects of redshift.

Chapter 4 of this thesis studies radial colour gradients across the galaxy population. I use the multi-wavelength information provided by MegaMorph analysis of galaxy light profiles to calculate intrinsic colour gradients, and divide into six subsamples split by overall Sérsic index (n) and galaxy colour.

In Chapter 5 of this thesis I apply bulge-disc decompositions to my sample of galaxies, in order to discover the structural origin of the wavelength dependences found in the previous two chapters.

Finally, in Chapter 7, I present an overview of the work conducted in this thesis, and I discuss my results in the context of contemporary studies.

Chapter 2

Data and methods

2.1 Galaxy And Mass Assembly (GAMA)

2.1.1 Overview

The Galaxy And Mass Assembly (GAMA; Driver et al. 2009, 2011; Liske et al. 2015) is the largest homogeneous, multi-wavelength dataset currently available for the low-redshift Universe. Its aim is to exploit the latest generation of space- and ground-based survey facilities to study cosmology and galaxy formation and evolution. Primarily, this involves the study of structure on scales of 1 kpc to 1 Mpc, which includes galaxy clusters, groups, mergers and coarse measurements of galaxy structure (i.e. bulges and discs).

The imaging data GAMA has assembled, from both SDSS (York et al. 2000) and UKIDSS (Lawrence et al. 2007), provides a consistent set of pixel-registered multi-wavelength data, covering the ($ugriz$) optical bands and the ($YJHK$) near-infrared (NIR) bands, respectively (Hill et al. 2011). It has been demonstrated that these data have sufficient depth and resolution to allow Sérsic profiles to be fit to large samples (Kelvin et al. 2012; Häußler et al. 2013).

The current GAMA survey (GAMA-II) consists of three equatorial regions, each of 72 deg^2, and two regions in the south, each of 85.8 deg^2 (see Fig. 2.1). Redshifts and spectra have been obtained for 238,000 objects, down to a limiting magnitude of r <19.8 using the AAOmega spectrograph on the Anglo-Australian Telescope. The redshift completeness is 98.3%. The majority of the

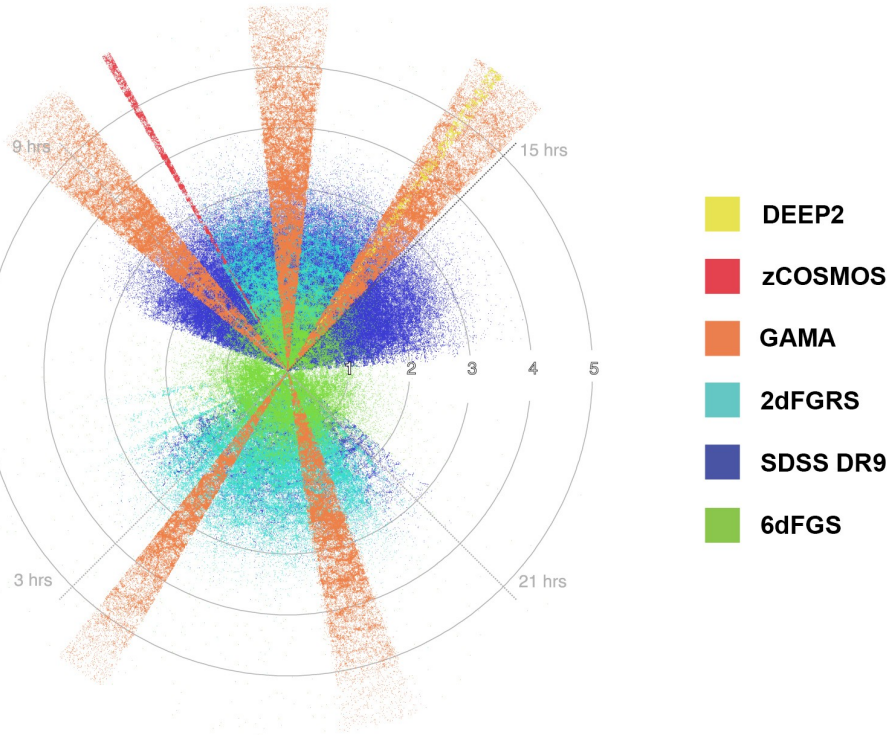

Figure 2.1. GAMA-II survey area shown in orange, versus lookback time. Credit: ICRAR/GAMA.

GAMA database is publicly available at http://www.gama-survey.org, with catalogues which are accessible via a schema browser.

In addition to the optical and NIR bands, GAMA has also collated data from a number of independent surveys, in order to build an imaging database which spans a wide wavelength range of 1nm - 1m. The depth and completeness of the spectroscopy means that group and environment have also been characterised; this is documented in more detail in Robotham et al. (2011).

2.1.2 Data management

The data included in the GAMA survey is stored in Data Management Units (DMUs), which are 'packets' containing the result of some specific data reduction or analysis. Each DMU stands alone, and no data should be repeated in multiple DMUs. This allows users to easily access the GAMA database to find data products relevant to their science.

Each DMU must contain the information necessary for a fellow researcher to use it without any additional comments or tools. Catalogues must be in

the form of FITS-plus files and contain no repeated information (with the exception of a unique identifier for each row in the table), and no entries may be left blank; null or missing information must follow GAMA's convention for 'dummy values'. Meta data must be included in the DMU in the form of a .par file containing each column name, number, unit (if applicable), and brief description. Additionally, a .notes file is necessary which should include a detailed description of how the data products in the DMU were derived, and which data products served as inputs to this DMU.

Before a DMU is 'published' to the database it must undergo quality control (QC) which is undertaken by both fellow team members and a dedicated QC team. As a member of the GAMA team, I performed a round of quality control for the SIGMA structural decomposition catalogue (Kelvin et al. 2012), and also compiled the MegaMorph DMU (see section 2.2).

2.2 MegaMorph

The MegaMorph project uses GALAPAGOS-2[1] with GALFITM[2] to fit a single wavelength-dependent 2D model to many images of a galaxy simultaneously. Fitting in multiple wavebands simultaneously increases the accuracy of measured parameters, and avoids the number of 'failed' fits which occur in single-band fitting by allowing smooth, physically meaningful, transitions between wavebands.

The present catalogue was primarily produced to examine the pros and cons of multi-band fitting in a large galaxy survey. To limit the required computing requirements, initially only G09 GAMA I region was considered (Fig. 2.2). The single-Sérsic results were originally presented in Häußler et al. (2013) and studied further in Vulcani et al. (2014) and Kennedy et al. (2015, 2016b); the latter two papers forms the basis of Chapters 3 and 4 of this thesis. The bulge-disc results are to be presented in Häußler et al. (in prep.) and are studied further in Kennedy et al. (2016a), which is presented in Chapter 5 of this

[1]Multi-band version of GALAPAGOS: Galaxy Analysis over Large Areas: Parameter Assessment by GALFITting Objects from SExtractor. Code designed by Barden et al. (2012) to automate source detection, two-dimensional light-profile Sérsic modelling and catalogue compilation in large surveys

[2]GALFITM: A multi-wavelength extension to GALFIT3 (Peng et al. 2002; Peng et al. 2010)

thesis. The data used in this thesis is from a previous run on SDSS+UKIDSS which was completed before the start of my PhD. I have since repeated this process on the new SDSS+VIKING data, using the techniques described in Section 2.3.

GALFITM is a modified version of GALFIT 3 (Peng et al. 2010) which replaces each single waveband parameter with a wavelength-dependent function. In the data presented in this thesis, the wavelength dependent parameters are magnitude, Sérsic index, effective radius, position, axis ratio and position angle. The degrees of freedom afforded to each of these parameters is set by a set of Chebyshev polynomials chosen by the user.

In this work, galaxy magnitudes are allowed to vary freely, while Sérsic index and effective radius are modelled as quadratic functions of wavelength. All other parameters are not permitted to vary with wavelength. GALFITM accounts for seeing by convolving the model with a PSF (produced by Kelvin et al. 2012) before comparing to the data.

To test the reliability of this new fitting technique, simulated galaxies were created which closely matched the distribution of galaxy parameters expected of a sample such as the GAMA G09 region (Häußler et al. 2013). Whilst these simulated images are an idealised case which assumes that real galaxies are well represented by perfect Sérsic profiles, they are suitable for giving a lower limit on the error bars for real data. Poisson noise was added to each galaxy in the simulated catalogue, and they were then placed onto an empty sky image from real GAMA imaging. Having been fitted using exactly the same setup as would be used for the real data, Häußler et al. (2013) could compare the recovered values to the known input parameters. It was found that, compared to single-band fitting, this new multi-band fitting technique performed particularly well for galaxies which had low signal-to-noise wavebands, allowing meaningful fits for a much larger sample, and at fainter magnitudes, than before.

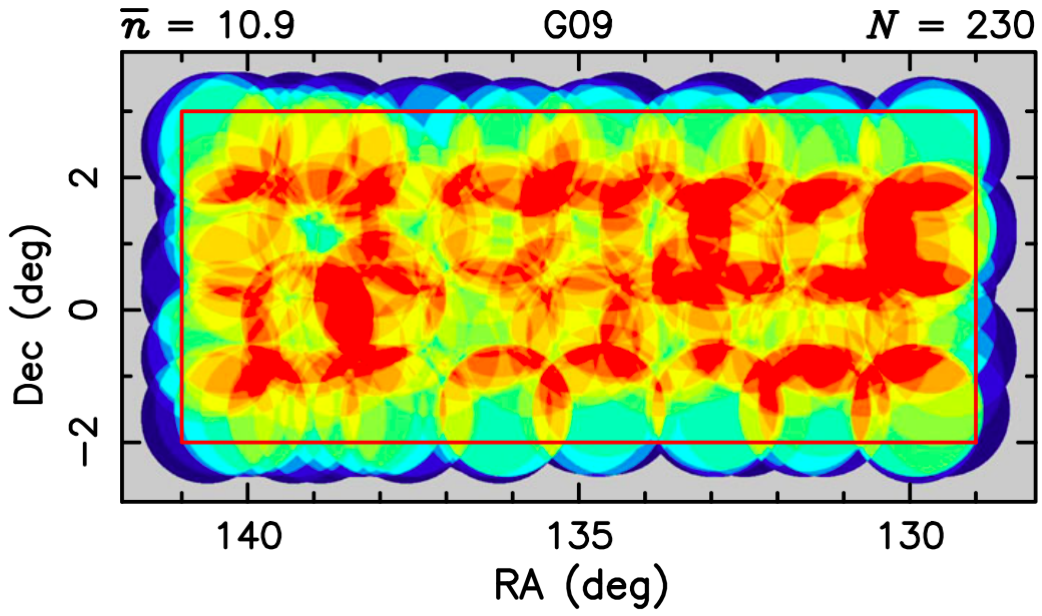

Figure 2.2. G09 region of the GAMA-II survey marked as a red rectangle overlaid on the observed fields from 2dF/AAOmega. The colour represents the number of fields covering a given position, from fewest (n = 1, shaded blue) to most (n = 15, shaded red). For G09, the average number of fields, $\overline{n}$, is 10.9, whilst the total number of fields, N, is 230 (Liske et al. 2015).

2.3 Sérsic modelling and bulge-disc decomposition

The following procedure applies to both the data set used in this thesis, and the new catalogue I created using the new SDSS-VIKING data which will soon be available for future work. Wherever images and figures are presented, these are from the SDSS-VIKING fits I performed.

- I use the entire GAMA G09 field (129 deg < RA < 141 deg and -1 deg < Dec < 3 deg). This area was cut out from the original GAMA SWARP mosaic, see Fig. 2.2.
- The point spread functions (PSFs) used are those obtained by Kelvin et al. 2012 (for the SDSS data) and Lange et al. 2015 (for the VIKING data, using the methods of Kelvin et al. 2012). GALAPAGOS chooses the closest PSF to the targeted object for the fit. I add a background pedestal so that GALFIT can construct correct sigma images, in order to determine the 'reliability' of flux in a given region. For each band, I

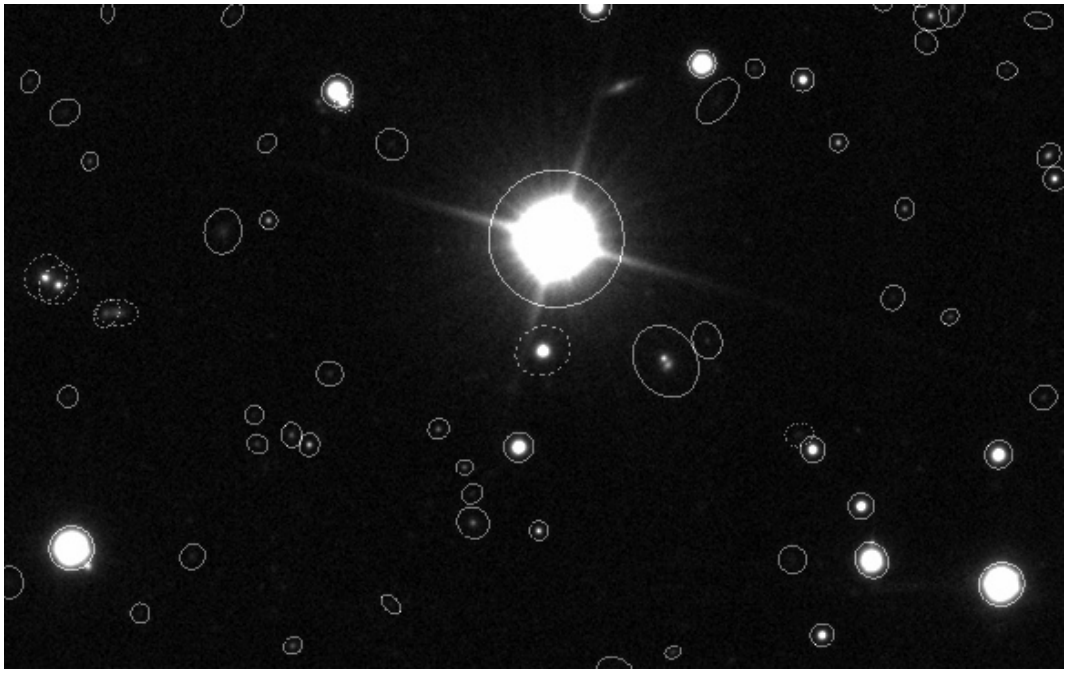

Figure 2.3. Ellipses showing the sources identified by the hot mode of SExtractor; this mode fits sources in more detail, and is able to pick out faint sources within the outskirts of brighter sources.

simply use a typical background value from the original SDSS imaging. I also cut the images into overlapping tiles, which makes the data easier to handle in GALAPAGOS.

- I then use SExtractor (Bertin & Arnouts 1996) to identify sources using a co-added image of all bands, in order to detect sources with extreme colours that would be missed if only one band were used for detection. This is a 2-stage (hot + cold) process, which allows SExtractor to distinguish between bright objects, and fainter objects which may be at risk of being lost in the outskirts of brighter objects. The hot mode is more able to separate out smaller clumps within a galaxy, or pick out faint galaxies from the outskirts of a nearby bright galaxy (see example in Fig. 2.3), whilst the cold mode takes broader strokes and lumps multiple clumps together as one single object (see example in Fig. 2.4). Fine-tuning both these modes to make sure that all galaxies are detected, without clumpy galaxies being detected as multiple sources, is key. A segmentation map (see example in Fig. 2.5) is also produced which shows which pixels are attributed to which object.

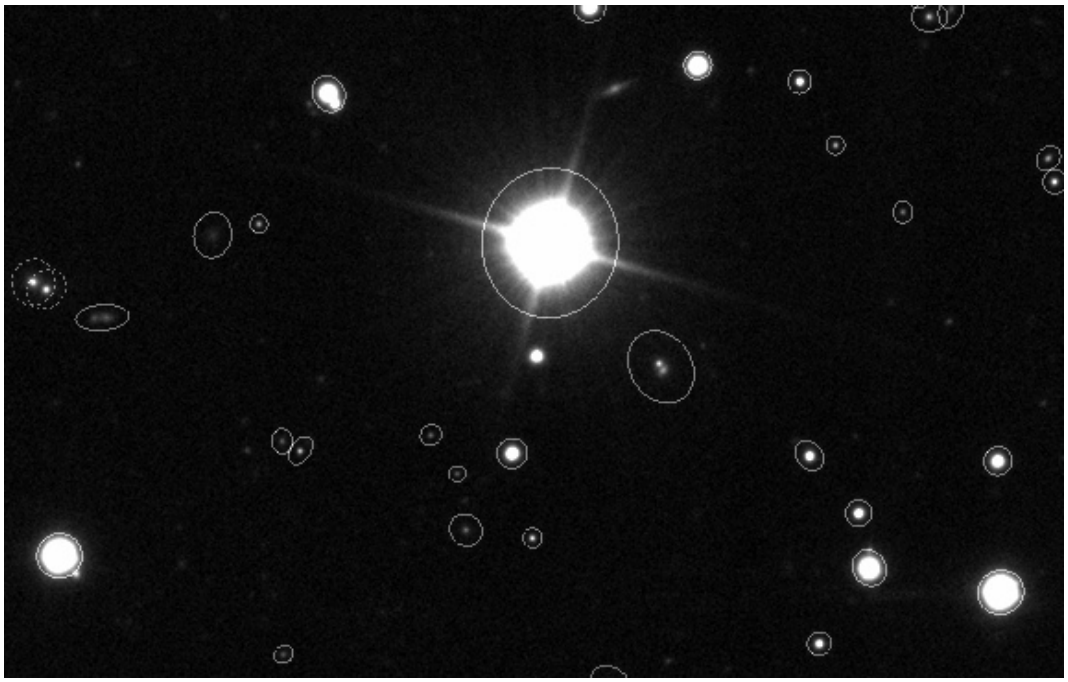

Figure 2.4. Ellipses showing the sources identified by the cold mode of SExtractor; this mode uses 'broad strokes' to identify sources, and avoids over-fitting lumpy objects

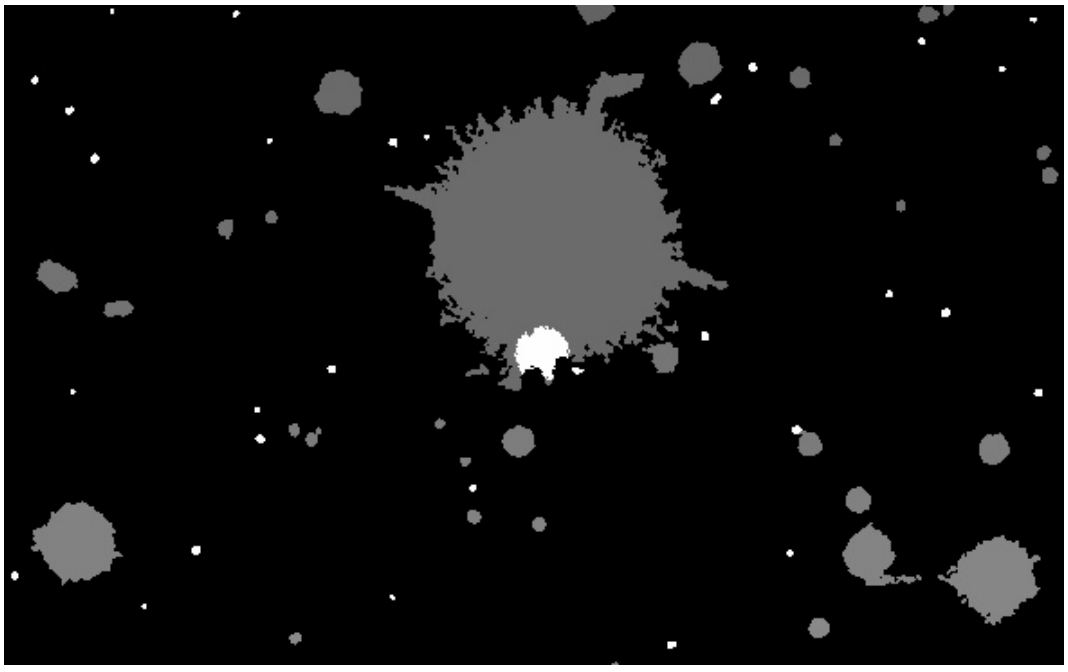

Figure 2.5. Example segmentation map from one tile of the GAMA G09 region. This shows which pixels have been attributed to each source. In the centre there are some pixels which contain light from two sources, so these have been flagged accordingly.

- A postage stamp is cut out around each object, to speed up the fitting process and to reduce the memory required at a given time. This also means that the fitting process can be parallelised, and multiple sources can be fitted simultaneously.

- A skymap is created, which estimates the local sky level around an object and excludes other nearby sources. This will later allow GALFIT to remove model profiles for nearby sources when fitting a given object.

- GALFIT allows various parameters to be constrained in a setup file for single-Sérsic fits; for this project we restrict the effective radius to be no larger than 400 pixels, and the Sérsic index should fall within the range $0.2 < n < 8$. I also constrain the wavelength dependence of certain parameters (x, y, mag, R_e, n, AR, PA) using Chebyshev polynomials, which are discussed in more detail in Section 2.2, and the minimum number of wavebands required for each fit, which in this case is six. An example of the image, model and residual in each band for a single-Sérsic fit is given in Fig. 2.6.

- While most of the setup for the bulge-disc decomposition is analogous to the single-Sérsic setup – e.g. I use the same postage stamps, masks, PSFs and deblending decisions and wavelengths to be given to GALFITM– some additional issues have to be considered when carrying out bulge/disc decompositions. Most importantly, the user is able to decide on the order of the polynomial used in the B/D decomposition and the starting values for the fit itself. Whilst in principle colour gradients could exist within individual components, we expect the colour differences between components as a whole to be greater. I therefore choose to initially allow no wavelength variation of n and R_e, whilst leaving the SEDs of the bulges and discs to vary as eighth-order polynomials. The Sérsic index of the discs are set to $n = 1$. Variation in bulge and discs structural parameters with wavelength will be tested and studied in future work. An example of the image, model and residual in each band for a bulge+disc fit is given in Fig. 2.7

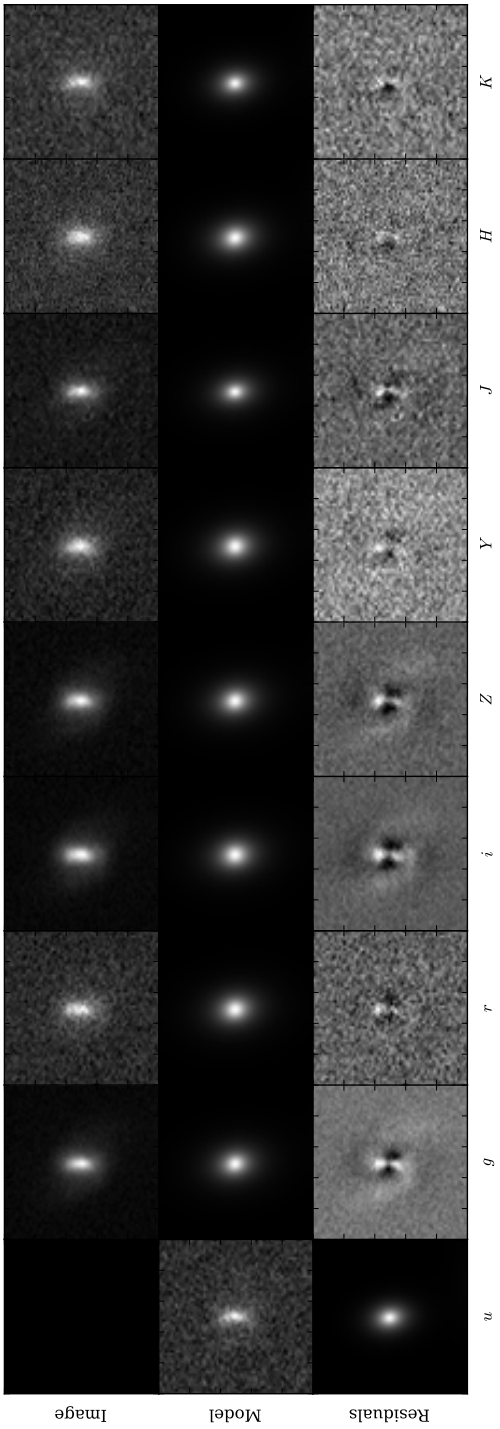

Figure 2.6. Image, model and residual in $ugriZYJHK$ bands for a single-Sérsic fit of an example galaxy. The data presented here is from SDSS and VIKING, however the data analysed in this thesis are from SDSS and UKIDSS.

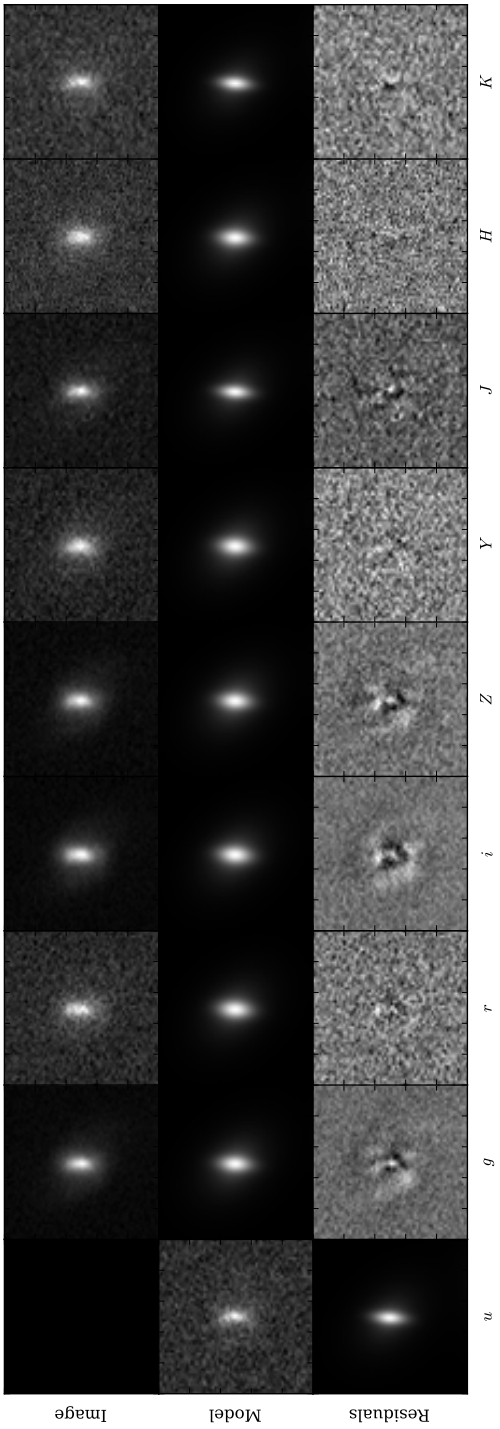

Figure 2.7. Image, model and residual in $ugriZYJHK$ bands for a bulge-disc fit of an example galaxy. The data presented here is from SDSS and VIKING, however the data analysed in this thesis are from SDSS and UKIDSS.

2.4 Data used in this thesis

The galaxy measurements used in this thesis have previously been presented in Häußler et al. (2013) (hereafter H13), and a subsample of these were studied in Vulcani et al. (2014) (hereafter V14). A detailed description of the selection criteria, robustness of fits and properties of the sample can be found in those papers; here, we only give a brief overview.

As in V14, the data we use in this chapter are limited to the G09 region of GAMA. I therefore only utilise approximately one-fifth of the area covered by GAMA II. For efficiency, we chose to focus on a single region for our initial exploration of multi-band fitting techniques with GAMA. The application of MegaMorph methods to the full GAMA dataset, with UKIDSS-LAS replaced by VISTA-VIKING data, are ongoing.

Restframe values of Sérsic index and effective radius for each wavelength have been obtained from the polynomials returned by GALFITM. For the magnitudes, k-corrections have been performed using InterRest (Taylor et al. 2009).

I take the GALAPAGOS-2 output catalogue; however not every fit was necessarily accurate or meaningful, so a number of cleaning criteria were applied to eliminate galaxies for which the fit has violated my criteria in one or more bands. These criteria are identical to those used in H13 and V14, with the exception of Sérsic index which is limited to $0.201 < n < 7.75$. I have reduced the upper limit on Sérsic index to avoid including suspected poor fits, with final parameters close to the fitting constraint (objects with very high n are typically poor fits, often to point sources, and are therefore removed). Note that the cleaning described above removes only 0.42 / 0.39 per cent of the V14 / low-redshift samples.

In this thesis I use two different volume-limited samples to avoid selection effects, which are illustrated in Fig. 2.8. For studying variation in galaxy properties with redshift, a first volume-limited sample of 13,871 galaxies is taken with $z < 0.3$, $M_r < -21.2$, in line with V14.

For studying variation in galaxy properties with absolute magnitude, M_r, a second volume-limited sample ($z < 0.15$, $M_r < -19.48$) of 5331 galaxies is used, allowing galaxies to be considered over a wider range of absolute magni-

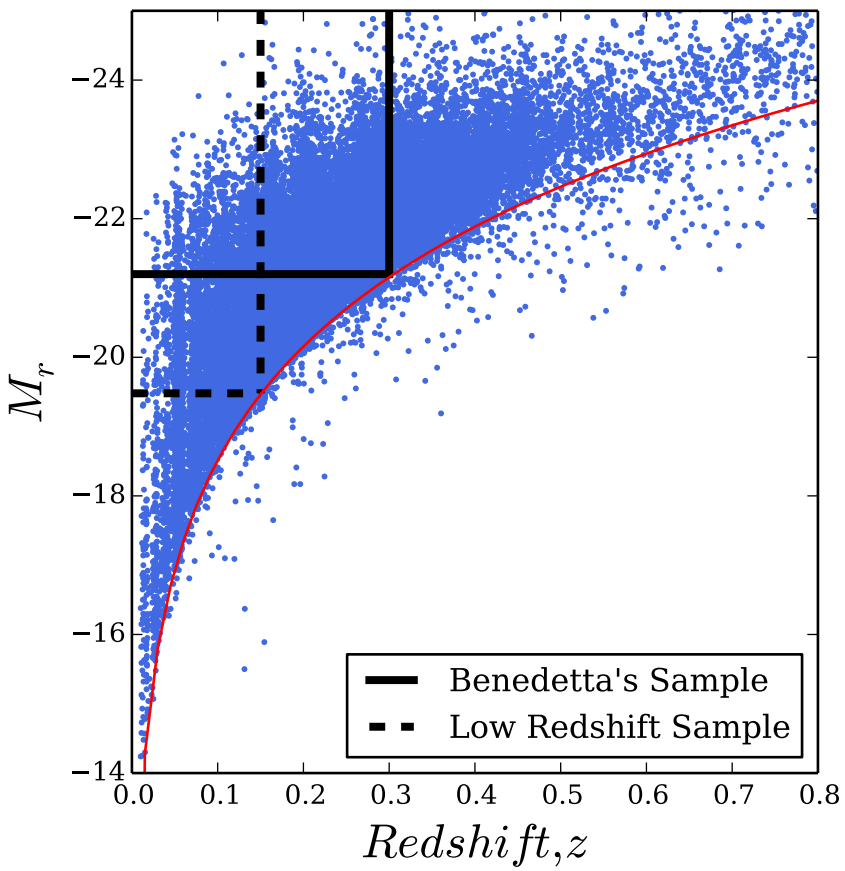

Figure 2.8. Absolute r-band magnitude versus redshift for my parent sample, with our volume-limited selection boxes overlaid. The red curved line indicates the primary apparent magnitude limit of the GAMA II redshift survey, $r < 19.8$. This corresponds to an absolute magnitude of $M_r = -21.2$ at $z = 0.3$ and $M_r = -19.48$ at $z = 0.15$.

tude.

One of the aims of this thesis is to study how galaxy properties vary as a function of wavelength. It is expected that different types of galaxies will behave in different ways, so I subdivide the samples by both colour and Sérsic index. The number of galaxies in each subsample are given in Tables 2.1 & 2.2 for both volume-limited samples, after basic cleaning has been applied.

Initially the samples are divided into 'red' and 'blue' at $(u - r) = 2.1$. I also want to separate the bluest galaxies, which may contain starbursts, so I further divide this 'blue' sample at $(u - r) = 1.6$ into 'green' and 'blue'. Note that the 'green' sample corresponds to the main population of star-forming galaxies, not the green valley. I have confirmed that altering these colour cuts does not

		$n_r < 2.5$		$n_r > 2.5$	
	Colour	no.	%	no.	%
Blue:	$(u-r) < 1.6$	1380	9.9	322	2.3
Green:	$1.6 < (u-r) < 2.1$	3311	23.9	1047	7.5
Red:	$2.1 < (u-r)$	2523	18.2	5288	38.1

Table 2.1. Number count and fraction of the $z < 0.3$, $M_r < -21.2$ volume-limited sample (total = 13871 galaxies), for different combinations of colour and Sérsic index.

		$n_r < 2.5$		$n_r > 2.5$	
	Colour	no.	%	no.	%
Blue:	$(u-r) < 1.6$	1323	24.8	134	2.5
Green:	$1.6 < (u-r) < 2.1$	1417	26.6	245	4.6
Red:	$2.1 < (u-r)$	994	18.6	1218	22.8

Table 2.2. Number count and fraction of the $z < 0.15$, $M_r < -19.48$ volume-limited sample (total = 5331 galaxies), for different combinations of colour and Sérsic index.

affect my results. The galaxy sample is also split by Sérsic index, in an attempt to separate discy galaxies from ellipticals, at $n_r = 2.5$. These divisions can be seen in Fig. 2.9.

The analysis has been carried out using a cosmology with $(\Omega_m, \Omega_\Lambda, h) = (0.3, 0.7, 0.7)$ and AB magnitudes.

2.4.1 Two-component fits

In addition to the single-Sérsic fits presented previously, two-component fits have also been performed by the MegaMorph project, comprising independent Sérsic and exponential (a Sérsic profile with $n = 1$) components (Häußler et al., in prep), the Sérsic index and effective radius of which is constant with wavelength. This fitting procedure followed the steps outlined in Section 2.2, which I have since performed on SDSS+VIKING data. Various tests have been performed to ensure that the fits consistently move away from their starting parameters, and converge on final solutions that are generally independent of these initial values. The robustness of these decompositions will be discussed in depth in Häußler et al. (in prep.). The two components are intended to model the bulge and disc structures seen in many galaxies, and I will often use these labels for convenience, although the interpretation of the two com-

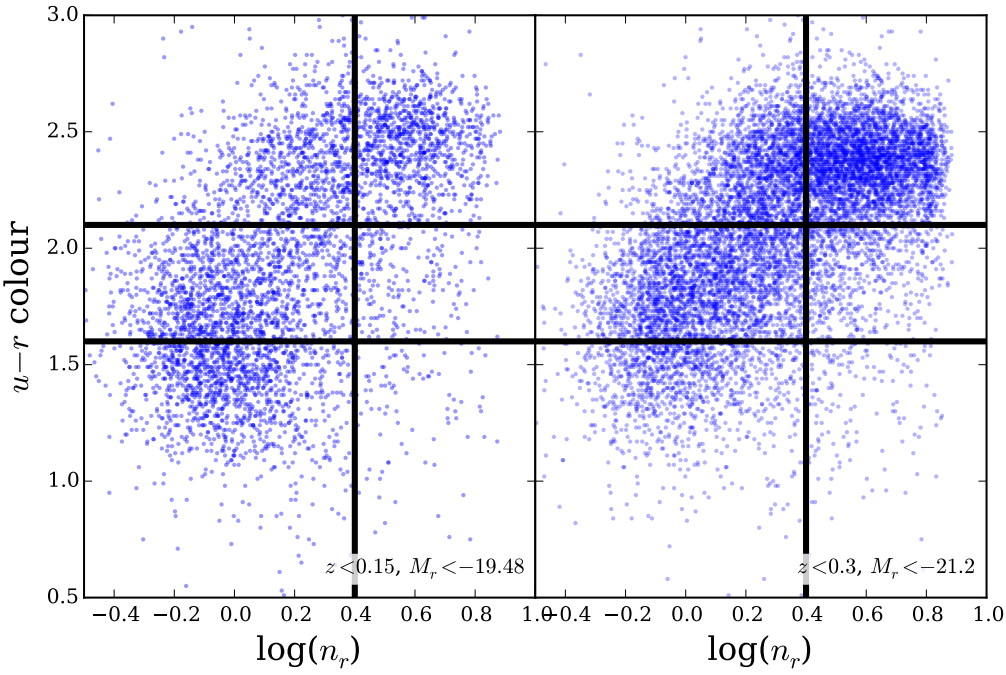

Figure 2.9. (u-r) rest frame colour vs. n_r for the galaxies in our two samples. Lines illustrate the cuts we apply to divide the galaxies by colour and Sérsic index.

ponents may vary for galaxies that do not correspond to this simple structural approximation.

I acknowledge that there may not be statistical evidence for choosing a 2-component fit over a single-Sérsic fit. However, one of the problems involved with choosing a 1- or 2-component model is that this builds a dichotomy into the data. One of the strengths of fitting every object with 2 components is that I give consistent treatment to the whole sample, and don't introduce a bias of deciding which fit is more appropriate on a case-by-case basis. Nowadays we know that the vast majority of galaxies are multi-component. Forcing them to be fit by a single component model introduces a bias. The distributions of component properties I find in Chapter 3 strongly support the assumption of multiple components. This is particularly true for the red galaxies; with single-band fits these can often be well-fit by single-component models, but these multi-band fits clearly indicate a preference for two components with different colours.

To obtain rest-frame colours for the bulge and disc components of both samples, K-corrections have been performed using the SED fitting code of Duncan

et al. (2014). Following a method similar to that of Blanton & Roweis (2007), stellar population synthesis models from Bruzual & Charlot (2003) are fit to the decomposed bulge and disc photometry and the rest-frame colours taken from the best-fit model for each component. The model stellar populations are drawn from a wide range of ages, star-formation histories and metallicities, with dust attenuation allowed to vary in the range $0 \leq A_V \leq 4$ assuming the Calzetti et al. (2000) attenuation law.

I then apply the following criteria to select reliable fits:

- $0.201 < n_B < 7.75$, to eliminate values that lie very close to the fitting boundaries.
- $0 < m_{B,D} < 40$ at all wavelengths, where $m_{B,D}$ is the total apparent magnitude in each band for the bulge and the disc, respectively.
- $m - 5 < m_{B,D} < m + 5$, where m is the starting value of the magnitude in each band. See Häußler et al. (2013) for more details.
- $0.301 < R_e(B, D) < 399$ pixels, which ensures bulge and disc sizes remain in a physically meaningful range.
- $0.001 < q_{B,D} \leq 1.0$, where $q_{B,D}$ is the axial ratio of the bulge and disc, respectively.
- Position (x, y); positions are constrained to lie within a box of size $0.5R_{\rm e}$ around the centre as defined by the single-Sérsic fit. Additionally, the position of the disc and the bulge are constrained to be the same.

Chapter 3

Understanding the wavelength dependence of galaxy structure

3.1 Overview

In this chapter I study how the sizes and radial profiles of galaxies vary with wavelength, by fitting Sérsic functions simultaneously to imaging in nine optical and near-infrared bands.

Ideally we would be able to decompose galaxies into all their constituent structures. However, with limited physical resolution and signal-to-noise, even bulge-disc decompositions can prove difficult to perform robustly. Although many galaxies comprise multiple components, fitting with a single Sérsic profile can provide valuable insights into their structure, providing sizes, axial ratios, rough morphological classifications and total photometry (e.g., Kelvin et al. 2012).

Fitting Sérsic models to galaxy images in different wavebands allows one to explore the dependence of galaxy structure on wavelength for large samples in a homogeneous manner. Variation in a galaxy's surface brightness profile parameters with wavelength is qualitatively equivalent to a radial trend in the colour of the galaxy. Such 'colour gradients' have been well-studied, usually by measuring the surface brightness in a series of elliptical annuli. This approach is usually limited by the seeing, and hence confined to relatively extended objects. The result is a colour profile for the galaxy, usually summarised as the

overall change in colour over some (logarithmic) radial range (e.g., Goudfrooij et al. 1994; deJong 1996; Saglia et al. 2000; den Brok et al. 2011), as described in Section 1.4.3.

The wavelength-dependence of Sérsic model parameters provides an alternative description. This is less detailed than a full colour profile, though more robustly determined in typical survey imaging. In addition, as the PSF can be easily accounted for when fitting the model, the results are not biased by seeing.

Considering the wavelength-dependence of Sérsic parameters is more efficient than dealing with empirical colour profiles, while providing significantly more general information than quoting a colour gradient over a single (or several) radial ranges. Furthermore, the ubiquity of the Sérsic profile in describing galaxy profiles, and the correlations between its parameters and other galaxy properties, suggests that the profile and its parameters have a physical significance. Expressing colour gradients in terms of the wavelength-dependence of effective (half-light) radius and Sérsic index naturally separates the proportions associated with changes in size and profile shape, which may have different physical drivers. However, the price of all this is the assumption of a particular functional form for the surface brightness profile. When this assumption is inappropriate (e.g., in merging galaxies, multi-component systems or potentially very high redshift), it may result in biases or misinterpretations.

Some studies have chosen a compromise between performing a parametric fit and directly measuring a colour profile. La Barbera & de Carvalho (2009) fit independent Sérsic models in various wavebands and then use elliptical annuli to measure colour profiles and gradients on the model images. This removes the effect of the PSF and reduces noise in the measurements.

Several groups have examined the trends of Sérsic model parameters with wavelength. For a sample of bright elliptical galaxies, La Barbera et al. (2010b) find that the mean effective radius decreases significantly with increasing wavelength from g to H, but that there is little variation in Sérsic index. Kelvin et al. (2012) find similar behaviour in data from the Galaxy And Mass Assembly survey (GAMA; Liske et al. 2015). They also consider late-types, finding a substantial increase in Sérsic index, and decrease in effective radius, across the same wavelength range. Metallicity gradients and dust attenuation are

proposed as reasons for these trends.

Lange et al. (2015) have recently extended the work of Kelvin et al. (2012), replacing the GAMA infrared UKIDSS LAS imaging (Lawrence et al. 2007) with deeper VISTA-VIKING data (Edge et al. 2013). They also separate the galaxy population into early- and late-types using a variety of dividers, including visual classification. Lange et al. find that their results are not sensitive to the chosen divider, but show that the bimodality of galaxy structure becomes less distinct at lower stellar masses. They confirm that galaxies appear more compact at redder wavelengths, although this appears less dramatic than in the previously mentioned studies. Lange et al. argue that these structural variations with wavelength may arise from the two-component nature of many galaxies, in which the bulge is observed in the redder wavebands whilst the disc is observed in the bluer wavebands (also see Driver et al. 2007a). However, they do not examine the dependence of Sérsic index on waveband.

The above studies fit the image in each filter-band independently. This model freedom can be seen as an advantage. However, such an approach does not utilise the expected strong correlations between structural parameters at neighbouring wavelengths. In data with low signal-to-noise or poor resolution, using these physical expectations can improve the reliability and precision of structural measurements. Furthermore, even in high-quality data, utilising available colour information can improve the performance of decompositions. To address these issues, the MegaMorph project (Bamford et al. 2012) has developed a technique which fits a single, wavelength-dependent model simultaneously to a set of imaging in different filter-bands. These developments have been implemented in an extended version of GALFIT (Peng et al. 2002; Peng et al. 2010) named GALFITM (H13, Vika et al. 2013, 2014). GALAPAGOS (Barden et al. 2012), a software package dedicated to running GALFIT on large surveys, has been similarly extended to become GALAPAGOS-2, which uses GALFITM (H13).

Using MegaMorph multi-band techniques to perform single-Sérsic fits, V14 studied the wavelength dependence of galaxy effective radius, $\mathcal{R}$, and Sérsic index, $\mathcal{N}$, (see Fig. 3.1). They confirmed the trends described above, and demonstrated that galaxies with contrasting total colours and Sérsic indices display strikingly different behavior in terms of the wavelength dependence of their effective radii and Sérsic indices.

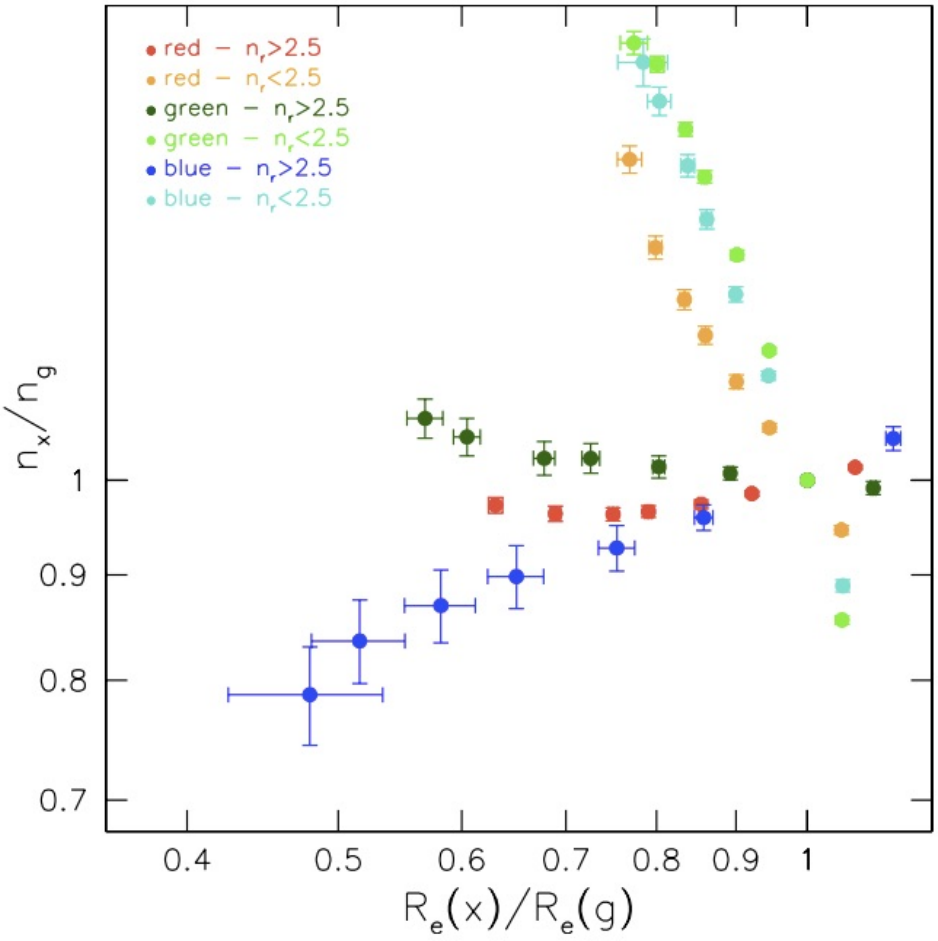

Figure 3.1. Median n_x/n_g versus median $R_e(x)/R_e(g)$ for galaxies in each colour/Sérsic index subsample, from Vulcani et al. 2014. Multiple points of the same symbol correspond to different wavebands, x. These consistently follow the wavelength sequence from H on the left to u on the right. All the g-band points lie at (1, 1) by definition.

V14 concluded that, regardless of overall $u-r$ colour, low-n galaxies display a very different behaviour to high-n galaxies, implying that both the wavelength dependence of n and R_e depend strongly on Sérsic index. They suggested that low-n discy (two-component) galaxies show a large change in Sérsic index with wavelength because in bluer wavebands the Sérsic index of the disc is being measured, whereas in redder wavebands the Sérsic index of the bulge dominates. High-n galaxies are, on the other hand, likely to be bulge-dominated (closer to one-component), so there is little change in Sérsic index with wavelength. There is, however, a large change in R_e with wavelength for high-n galaxies, which indicates that elliptical galaxies contain a number of different pressure-supported stellar populations with different extent, possibly resulting

from multiple minor merging events throughout a galaxy's lifetime.

In this chapter I aim to gain a greater confidence in, and deeper understanding of, the trends of galaxy structural parameters with wavelength as measured by the various studies described above. This work will advise the application of multi-band structural fitting to the full set of high-quality imaging currently being assembled by GAMA, and my subsequent analysis. I build on the results of V14, first ensuring they are robust to redshift effects.

For the first time, I examine the wavelength-dependence of galaxy structure as a function of luminosity. I also show that the measured trends persist for selections based on visually classified morphology, rather than morphological proxies. Next, I investigate the role of dust in driving the wavelength dependence of late-type galaxy structure. The chapter is concluded by discussing the various potential factors responsible for the variation of galaxy structural parameters with wavelength. By taking the novel approach of considering the joint wavelength dependence of Sérsic index and effective radius, I can begin to decouple the relationships between concentration, size and colour.

3.2 Data

The data used in this chapter is described in detail in Section 2.4. A summary is provided here.

In this chapter I use two different volume-limited samples to avoid selection effects, which are illustrated in Fig. 2.8. For studying variation in galaxy properties with redshift, a first volume-limited sample of 13,871 galaxies is taken with $z < 0.3$, $M_r < -21.2$, in line with V14. For studying variation in galaxy properties with absolute magnitude, M_r, a second volume-limited sample ($z < 0.15$, $M_r < -19.48$) of 5331 galaxies is used, allowing galaxies to be considered over a wider range of luminosities. Each galaxy has been fitted with a wavelength-dependent model; magnitudes are allowed to vary freely, whilst Sérsic index and effective radius are modelled as quadratic functions of wavelength.

Restframe values of Sérsic index and effective radius for each wavelength have been obtained from the polynomials returned by GALFITM. For the magni-

tudes, k-corrections have been performed using InterRest (Taylor et al. 2009).

I have divided each volume-limited sample by Sérsic index and colour to obtain six subsamples which aim to separate out different galaxy populations.

3.3 Results

V14 examined the variation of n and $R_{\rm e}$ with wavelength in order to reveal trends of internal structure, and therefore formation history, for galaxies in different subsamples (see Fig. 3.1). For consistency I continue to use the notation $\mathcal{N}_g^x = n(x)/n(g)$ and $\mathcal{R}_g^x = R_{\rm e}(x)/R_{\rm e}(g)$, which express the variation for a given waveband, x, versus that in the g-band. For simplicity, I will only consider the ratio of H-band to g-band in this chapter, as V14 shows that there is a consistent trend with wavelength and this pair has the longest robust wavelength baseline. I omit the band labels from $\mathcal{N}$ and $\mathcal{R}$ when discussing their general behaviour.

As will be shown in Chapter 4, if I convert my $\mathcal{N}$ and $\mathcal{R}$ trends to colour gradients I find good agreement with previous work, e.g. *red*, high-n galaxies show identical colour gradients to the passive, 'early-type' sample studied in La Barbera et al. (2010a). I also see the same behaviour of colour gradient with luminosity. However, here I focus on $\mathcal{N}$ and $\mathcal{R}$, which allows me to decouple variations in concentration and size with wavelength, which are combined in a measurement of colour gradient alone.

3.3.1 Redshift effects on galaxy structure

The sample used in V14 extends to $M_r < -21.2$, $z < 0.3$, so much of the sample is faint and of small angular size. This selection was partly chosen to demonstrate the power of multi-band fitting in this challenging regime. V14 showed that the measured $\mathcal{N}$ and $\mathcal{R}$ correspond to differences in the visual appearance of the galaxies. However, before exploring the luminosity dependence of these trends, I will further test the resilience of my $\mathcal{N}_g^H$ and $\mathcal{R}_g^H$ measurements versus redshift.

I split my bright volume-limited sample ($z < 0.3$, $M_r < -21.2$) into three

redshift bins: $0.0 \leq z < 0.15$, $0.15 \leq z < 0.25$ and $0.25 \leq z < 0.3$. These bins were chosen to span the redshift range of my volume-limited sample, while ensuring a similar number of galaxies in each bin to permit meaningful comparisons (see Table 2.1). The wavelength dependence of effective radius is shown in Fig. 3.2, for galaxies split by $u-r$ colour, n_r, and redshift. Galaxies of all colours and Sérsic indices are typically found to have $\mathcal{R}_g^H < 1$, indicating they are smaller at redder wavelengths, while $\mathcal{R}_g^H = 1$ (i.e. $\log \mathcal{R}_g^H = 0$) corresponds to no variation in size with wavelength. Here, $\mathcal{R}_g^H$ does not appear to change substantially with redshift in any subsample. Kolmogorov–Smirnov (KS) tests do indicate some significant differences between the $\mathcal{R}_g^H$ distributions in the different redshift samples. However, these differences are generally small, particularly in comparison with the width of each distribution and the offsets between the low- and high-n subsamples. To determine whether an offset between subsamples can be considered 'large' or 'small' I sum the standard deviations of the widest and narrowest distributions in quadrature. I then find the difference in the median value of $log(\mathcal{R}_g^H)$ in the highest and lowest redshift bins, as a fraction of the summed standard deviation. Here, the average offset is 15.5% of the distribution widths, which can be considered small.

What trends are present indicate that at lower redshift (higher S/N and better resolution) I measure $\mathcal{R}_g^H$ closer to unity for low-n galaxies. The departure of $\mathcal{R}_g^H$ from unity may therefore be slightly overestimated in V14. High-n systems appear unaffected, with perhaps the exception of blue, high-n galaxies. There are, however, very few galaxies in this subsample as blue spheroids are uncommon. I therefore consider my measurements of the wavelength dependence of effective radius to be robust out to $z = 0.3$.

$\mathcal{N}_g^H$ is studied in the same manner. The wavelength dependence of Sérsic index is shown in Fig. 3.3, for galaxies split by $u-r$ colour, n_r, and redshift bin. Again, some small trends are visible. Galaxies at lower-z tend to display $\mathcal{N}_g^H$ further from unity. This is most significant for low-n galaxies, and suggests that V14 may slightly underestimate the wavelength dependence of n for these systems. Apart from this small effect (approx. 18.5% offset in median values compared to the width of the distributions, as described previously), we can consider measurements of the wavelength dependence of Sérsic index to be robust out to $z = 0.3$.

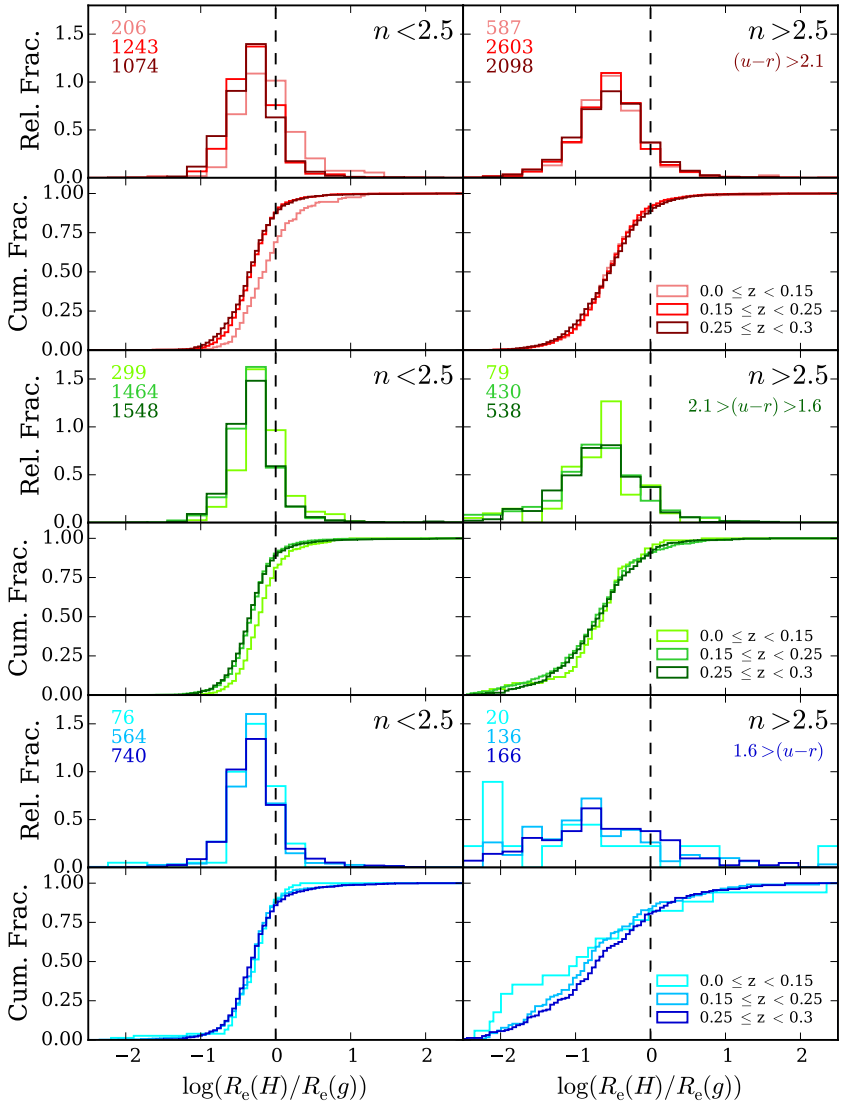

Figure 3.2. Effective radii of galaxies binned by redshift, for colour and Sérsic index subsamples. The left column shows low-n galaxies, the right column shows high-n galaxies. The top, middle and bottom groups of four panels contain *red*, *green* and *blue* samples, respectively. Within each group, the top panels show normalised histograms, whilst the bottom panels present corresponding cumulative histograms to better visualise subtle shifts in the distributions. In each panel lines in light colours show galaxies in the low redshift bin ($0 \leq z < 0.15$), mid-shades indicate the intermediate redshift bin ($0.15 \leq z < 0.25$), whilst the darkest colours show galaxies in the high redshift bin ($0.25 \leq z < 0.3$).

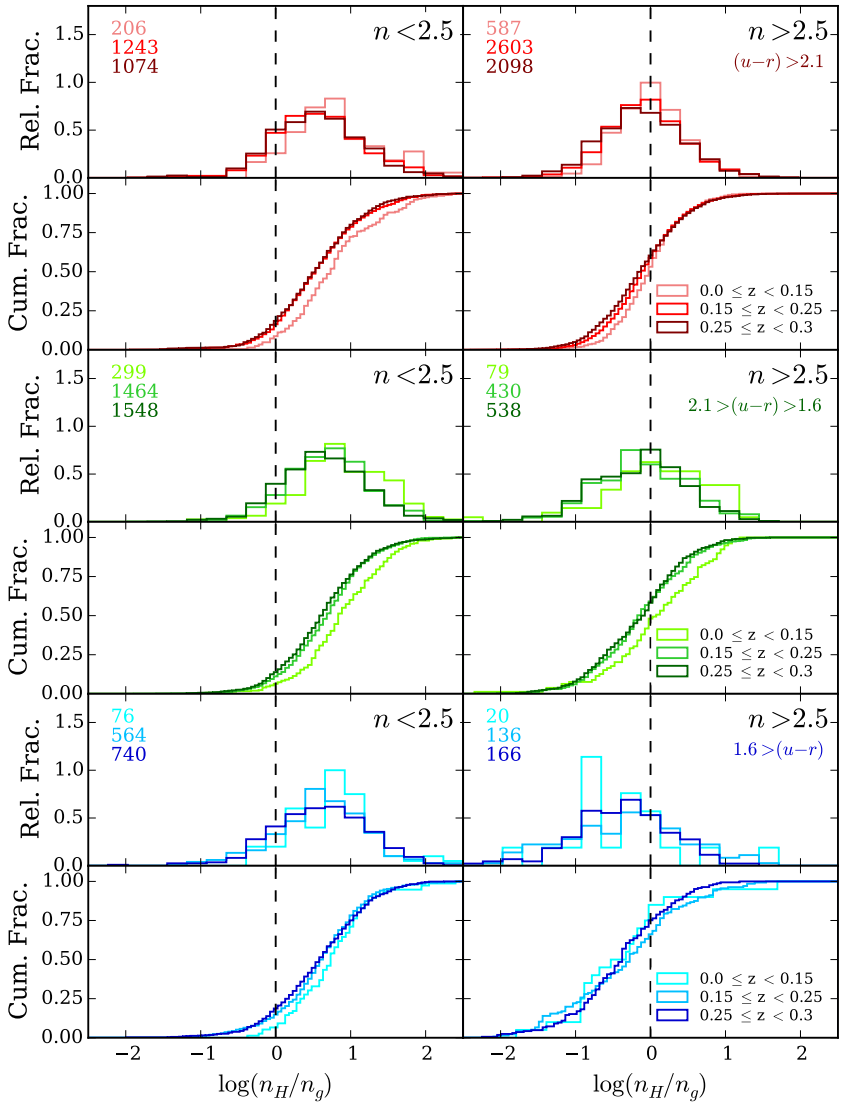

Figure 3.3. Sérsic indices of galaxies binned by redshift, for colour and Sérsic index subsamples. Panels and colours are chosen similar to Fig 3.2.

As in Fig. 17 of V14, I summarise the relationship between $\mathcal{N}_g^H$ and $\mathcal{R}_g^H$ for the three redshift bins in Fig. 3.4. The small trends with redshift, described above, are again evident in this figure. However, for each subsample, the redshift bins lie close to one another. In addition to observational effects, redshift trends may result from real changes in the galaxy population. However, given my volume-limited, colour-selected samples, and the narrow range of redshift, I do not expect evolution of the galaxy population to play a significant role in these trends. I have determined that the differences in $\mathcal{N}$ and $\mathcal{R}$ between redshift bins are small relative to the differences between galaxy types, and thus my results are robust to the sample selection I have used. In particular, the distinctions between high- and low-n systems are maintained independent of redshift. The conclusions of V14 are thus robust. With that established, I now move on to examining how the wavelength dependence of galaxy structure varies with luminosity.

3.3.2 Luminosity dependence of galaxy structure

V14 specifically chose a volume-limited sample of bright galaxies with $M_r < -21.2$. Here I investigate whether the conclusions drawn from their study apply to a wider range of galaxy luminosities.

My sample is divided into three magnitude bins: $-22.48 \leq M_r < -21.48$, $-21.48 \leq M_r < -20.48$ and $-20.48 \leq M_r < -19.48$. These intervals ensure similar numbers of galaxies in each bin, allowing for meaningful comparisons.

In Fig. 3.5 I present the wavelength dependence of effective radius for subsamples divided by $u - r$ colour, n_r and luminosity.

For high-n galaxies, there appears to be a consistent trend in the distribution of $\mathcal{R}_g^H$ with changing absolute magnitude. Fainter high-n galaxies have $\mathcal{R}_g^H$ closer to unity than brighter high-n galaxies. Their sizes therefore vary less as a function of wavelength. The most luminous galaxies, such as those studied by V14, display the strongest variation of their sizes with wavelength.

For the low-n samples, although K-S tests indicate some differences between the distributions in the luminosity bins, there is little obvious consistent variation. The *blue* sample displays similar trends to the high-n galaxies, while typical *green* galaxies show no luminosity dependence. *Red* galaxies hint at an

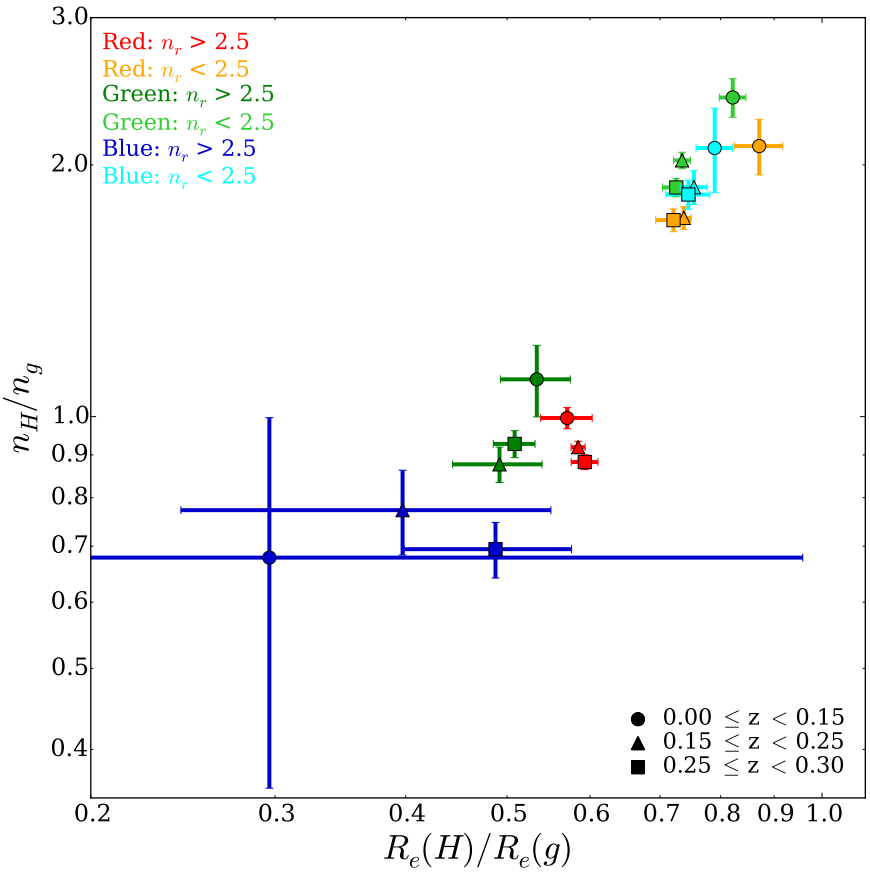

Figure 3.4. Median $\mathcal{N}_g^H$ versus median $\mathcal{R}_g^H$ for galaxies in each of my different subsamples divided by colour, Sérsic index and redshift bin. Colours are the same as in figure 17 of V14. Error bars show uncertainty on the median, estimated as $1.253\sigma/\sqrt{N}$, where σ is the standard deviation about the median and N is the number of galaxies in the sample. There are small trends with redshift due to observational biases. However, the distinction between the subsamples, particularly the contrast between low- and high-n, remains very clear.

opposing behaviour, such that the most luminous bin displays less variation in size with wavelength.

On average across all samples, the offset of the distributions with respect to the standard deviation of the distributions is 27%, calculated as before, for the redshift distributions.

I study $\mathcal{N}_g^H$ in the same manner; Fig. 3.6 shows the wavelength dependence of Sérsic index for the same subsamples as Fig. 3.5. There appears to be a consistent positive trend in the distribution of $\mathcal{N}_g^H$ with changing absolute magnitude for both low- and high-n galaxies, i.e. the brightest galaxies exhibit higher $\mathcal{N}_g^H$, with a 47% mean offset of the distributions, compared to the width of those distributions. In the high-n sample, distributions for all luminosity bins peak around one, supporting the conclusion of V14 that bulge-dominated (and likely one-component) systems show little change in Sérsic index with wavelength. Comparing cumulative distributions for the high-n samples, one can see that bluer and less luminous samples tend to have slightly lower values of $\mathcal{N}_g^H$, i.e. a decrease in n at longer wavelengths. Typical bright high-n galaxies have $\mathcal{N}_g^H$ very close to unity.

The low-n samples consistently display values of $\mathcal{N}_g^H$ above one, indicating an increase in Sérsic index with wavelength. This offset from unity strongly increases with luminosity, such that the brightest low-n galaxies display the greatest dependence of Sérsic index on wavelength.

In a similar manner to before, Fig. 3.7 shows the relationship between $\mathcal{N}_g^H$ and $\mathcal{R}_g^H$ for our three magnitude bins. High Sérsic index galaxies show a clear variation in effective radius with luminosity (brighter galaxies showing a greater decrease in R_e with wavelength). Low Sérsic index galaxies show a change in n with wavelength (brighter galaxies showing a greater increase in n with wavelength). The overall effect is that the differences between low- and high-n galaxies become more pronounced with increasing luminosity.

I have also performed all of the analysis in Sec. 3.3.1 and 3.3.2 using an optical baseline (u–z), although using the same fits as for the full u–K dataset. As one would expect, over this narrower wavelength range the differences between the samples narrow, though not in terms of significance, as the scatter shrinks roughly in proportion. All of the behaviour seen in the g versus H plots is qualitatively the same, and our inferences would be unchanged.

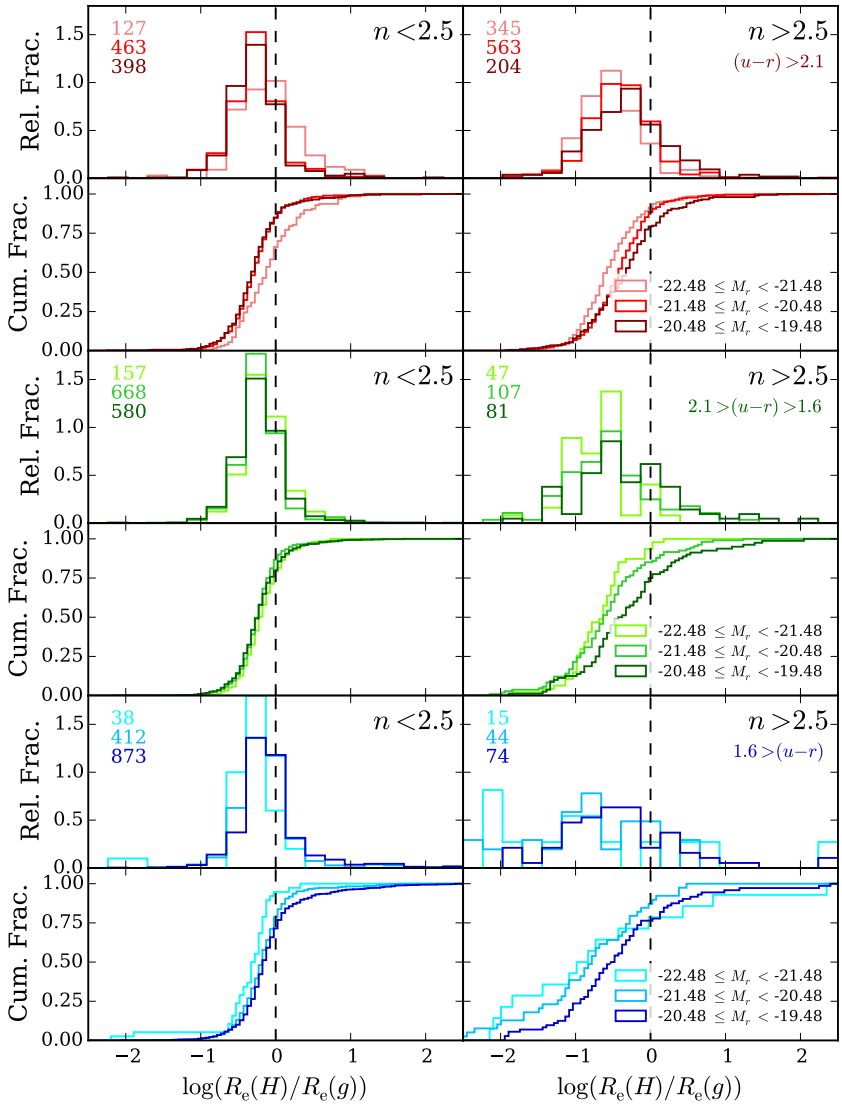

Figure 3.5. Effective radii of galaxies binned by absolute magnitude, for colour and Sérsic index subsamples. Panels and colours are chosen similar to Fig 3.2.

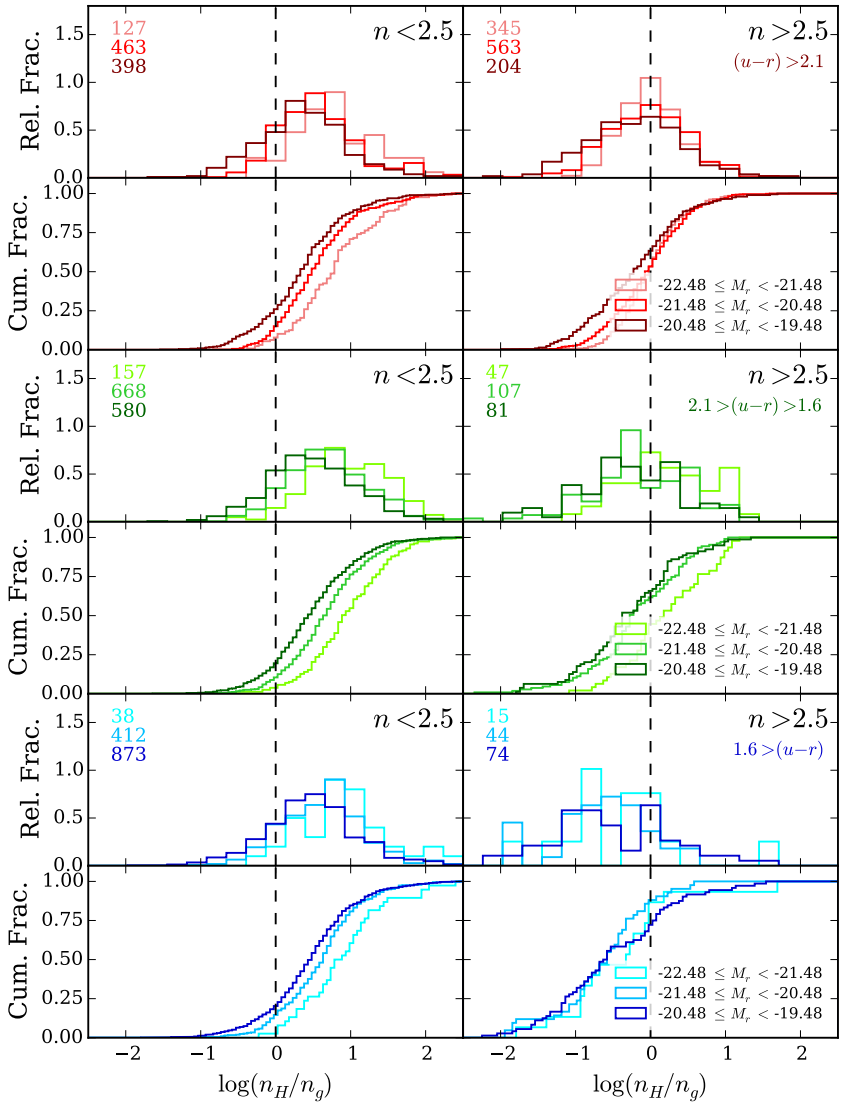

Figure 3.6. Sérsic index of galaxies binned by absolute magnitude, for colour and Sérsic index subsamples. Panels and colours are chosen similar to Fig 3.2.

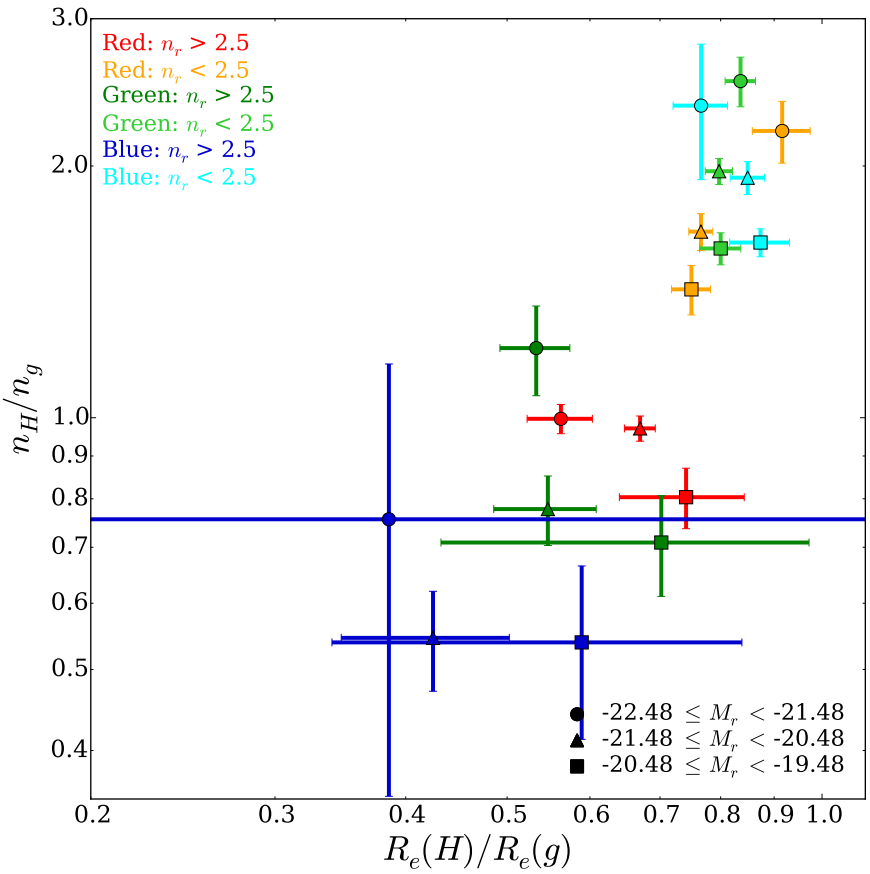

Figure 3.7. Median $\mathcal{N}_g^H$ versus median $\mathcal{R}_g^H$ for galaxies in each different subsample divided by colour, Sérsic index and luminosity. Colours are the same as in figure 17 of V14.

In terms of overall colour, concentration and size, early- and late-type galaxies become more similar with increasing luminosity. However, when one considers the joint distribution of these three properties, as in this chapter, one instead finds a divergence which widens with luminosity. The process by which late-type (low-n) galaxies grow must promote the variation of profile shape with wavelength. The growth of early-type (high-n) galaxies must also maintain a radial segregation of their stellar populations, but crucially in terms of size, not profile shape. Furthermore, any process which transforms late-types to early-types must do so in a manner that erases the wavelength-variation of profile shape, but enhances that of size. Realistic mechanisms for galaxy growth and transformation must reproduce the trends we observe.

3.3.3 Morphological classifications

The work of V14 assumes that one can perform a meaningful division of the galaxy population using Sérsic index as a proxy for structure or morphology. Typically $n_r < 2.5$ galaxies are associated with structures with prominent discs, whilst $n_r > 2.5$ galaxies are thought to be spheroid-dominated. To verify that my results do not strongly depend on this assumption, I now examine the distributions of $\mathcal{N}_g^H$ and $\mathcal{R}_g^H$ for samples selected by visual morphology. In Figs. 3.8 and 3.9 I show the wavelength dependence of n and R_e for galaxies separated by Hubble types from the GAMA Visual Morphology catalogue (Kelvin et al. 2014). Note that visual morphologies are only available for galaxies with $0.025 < z < 0.06$ and $M_r < -17.4$. Figure 3.8 shows only galaxies within the overlapping redshift and magnitude regions, i.e. $0.025 < z < 0.06$ & $M_r < -21.2$ (V14 sample) or $M_r < -19.48$ (low-z sample). Also plotted (as triangles) are the median locations of the high- and low-n populations, selected within the same redshift and absolute magnitude limits as the morphologically-classified points. Background contours show the distribution of galaxies in each of our volume-limited samples for which we do not have a visual morphological classification.

Despite the severe limitation in sample size that the visual morphological classifications impose, they confirm the behaviour of our high- and low-n galaxy samples. In both volume-limited samples one can see that the median location of the high-n galaxies lies very close to the median point of the elliptical sample, whilst the median of the low-n galaxies lies close to that of the Sab-Scd galaxies. Vika et al. (2015) see identical behaviour for a sample of very low-redshift galaxies, and show that this is robust against artificial redshifting.

Note that the offset between the late-type/low-n points at low-redshift and the contoured distribution at higher redshifts appears to confirm the (small) biases inferred in Section 3.3.1. At lower-redshift (i.e. in better quality data) we measure slightly higher $\mathcal{R}_g^H$ and $\mathcal{N}_g^H$ for low-n galaxies. Previous results therefore somewhat underestimate the difference between the two galaxy populations. However, even at $z = 0.3$ the contrast between their behaviour is such that my conclusions are unaffected.

The finer distinctions between the Hubble types reveal some further details

in the $\mathcal{N}_g^H$–$\mathcal{R}_g^H$ figures. Ellipticals and Sab-cd galaxies form the opposite extrema of the distributions. S0-Sa galaxies are intermediate between the two, but closer to the ellipticals. Perhaps surprisingly, late-type discs, Sd-Irr, occupy the same intermediate region. This may be a result of their similar one-component natures, with higher values of $\mathcal{N}_g^H$ indicative of system with comparable bulge and disc components. Note that $\mathcal{R}$ and $\mathcal{N}$ may be noisier for systems that depart greatly from an elliptical Sérsic, and more difficult to interpret physically. Nevertheless, measuring these properties still gives insight into their structure and allows us to make qualitative comparisons. So, in Fig. 3.9 we see that, on average, Sd-Irr galaxies display properties similar to late-spirals, but with less peakiness at longer wavelengths. It is also worth noting that the presence of a bar does not appear to greatly alter the measured wavelength dependence of galaxy structure.

3.3.4 The effects of dust

Late-type galaxies contain significant quantities of dust, which can strongly affect their measured properties (e.g., Popescu et al. 2002; Pierini et al. 2004; Holwerda et al. 2005, 2009; Möllenhoff, Popescu & Tuffs 2006). The effects vary with the amount and distribution of dust within the galaxy, as well as the observed inclination and wavelength.

A wide range of observations, together with detailed modelling (Popescu et al. 2000), have helped to establish a typical geometry for the distribution of dust in the discs of star-forming galaxies (Tuffs et al. 2004). When accounting for attenuation, this dust model can be parametrised by a single dominant parameter: the central face-on optical depth in the B-band, τ, while remaining widely applicable, at least to relatively massive spiral galaxies. It should, however, be noted that in lower-mass galaxies the dust distribution may be significantly different (Holwerda et al. 2012; Hinz et al. 2007). The Tuffs et al. (2004) model has been used to quantify, and potentially correct for, the effect of dust on galaxy structural parameters (Möllenhoff, Popescu & Tuffs 2006; Pastrav et al. 2013a,b).

Figure 3.10 shows the effect of dust on $\mathcal{N}_g^H$ and $\mathcal{R}_g^H$ for pure discs fit with a single-Sérsic profile, as determined by Pastrav et al. (2013a). Their results are

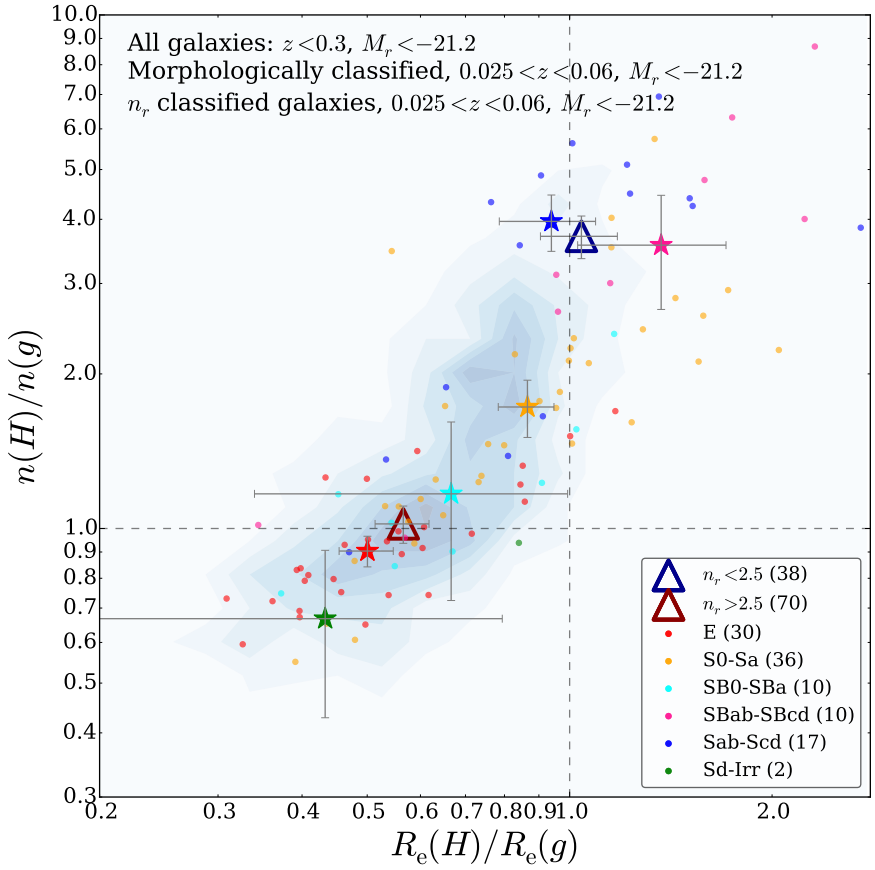

Figure 3.8. $\mathcal{N}_g^H$ versus $\mathcal{R}_g^H$ for galaxies in my high-luminosity volume-limited sample with Hubble type classifications in the GAMA visual morphology catalogue. Median points for each Hubble type bin are plotted as stars, with associated error bars (estimated as $1.253\sigma/\sqrt{N}$). Morphological classifications are only available for a low-redshift subset of galaxies. For comparison, the median values for galaxy samples with the same redshift limits, but separated by n_r, are plotted as triangles. The distribution of the full volume-limited sample (to the same luminosity limit, but extending out further in redshift) is plotted as contours.

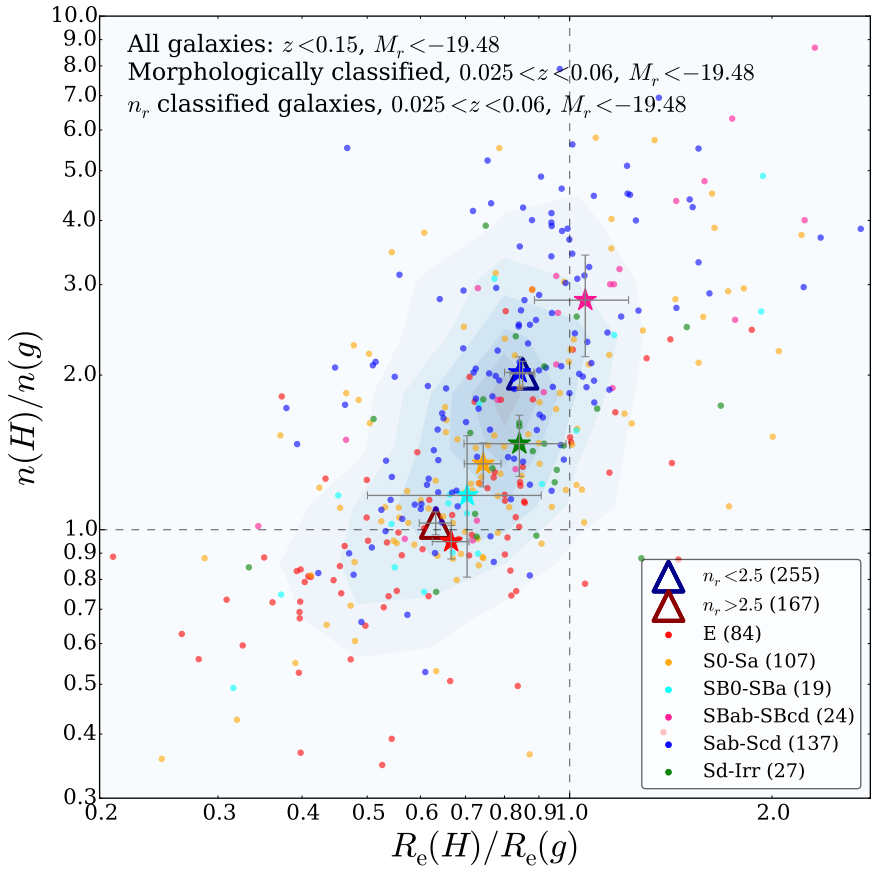

Figure 3.9. $\mathcal{N}_g^H$ versus $\mathcal{R}_g^H$ for galaxies in the lower-luminosity volume-limited sample. Points and shading are as described for Fig. 3.8

shown for a range of inclinations along loci corresponding to a wide variety of central dust opacities. Typical spiral galaxies have $\tau \sim 2$–4 (Keel & White III 2001; Holwerda et al. 2005; Driver et al. 2007b; Masters et al. 2010). Projection effects, as defined and predicted in Pastrav et al. (2013a,b), are not considered here, as their contribution is minimal compared to dust effects. As the purpose of this figure is illustrative, I have simply taken the published B and K-band dust effects from Pastrav et al. (2013a), without attempting the small interpolation to the g- and H-bands. These dust effects are shown as applied to a nominal 'galaxy' with $(\mathcal{N}_g^H, \mathcal{R}_g^H) = (1, 1)$, and for each τ value I show how $\mathcal{N}_g^H$ & $\mathcal{R}_g^H$ change with inclination. Fig. 3.10 shows that dust always acts to decrease $\mathcal{R}_g^H$, i.e. increase effective radius more at shorter wavelengths. It also tends to increase $\mathcal{N}_g^H$, i.e. raise the Sérsic index with increasing wavelength, except for at high opacities and close to edge-on inclinations.

Note that the stellar disc emitting in the optical bands in the Tuffs et al. (2004) model actually has an intrinsic stellar population gradient, such that the scale length of the old stellar disc decreases by ∼30 percent from the B to K bands, corresponding to $\mathcal{R}_g^H \sim 0.7$. Including this intrinsic $\mathcal{R}_g^H$ would make the loci overlap with the observed distribution in Fig. 3.10. One can see that for a population of pure discs with a variety of opacities and inclinations, a correlation in $\mathcal{N}_g^H$–$\mathcal{R}_g^H$ would arise from their variation with inclination, while a scatter about that correlation would be associated with variations in opacity. However, as one would expect, dust effects alone cannot account for the full observed $\mathcal{N}_g^H$–$\mathcal{R}_g^H$ distribution. Late-types extend to substantially greater $\mathcal{N}_g^H$ than can be attributed to dust, presumably as a result of the presence of a central bulge that becomes more dominant at longer wavelengths. However, there remains the possibility that more varied dust models may have more success in reproducing this observed dependence of $\mathcal{N}$ and $\mathcal{R}$. For example, the dust within lower-mass galaxies is more likely to be vertically distributed throughout the stellar disc, rather than concentrated in the central plane (Holwerda et al. 2012). On the other hand, early-types, which generally contain little dust, must have stronger intrinsic stellar population gradients than those in the discs.

3.4 Discussion

In this chapter I have studied how the wavelength dependence (from rest-frame u- to H- bands) of galaxy structure varies for samples selected in a variety of ways. As in V14, galaxy properties have been measured using MegaMorph techniques to fit consistent, wavelength-dependent, two-dimensional Sérsic profiles in multiple wavebands simultaneously. My results are summarised in terms of the fractional variation in Sérsic index and effective radius between the g- and H-bands, which I denote $\mathcal{N}_g^H$ and $\mathcal{R}_g^H$.

3.4.1 The physical meaning of $\mathcal{R}$ and $\mathcal{N}$

Before discussing the implications of our results, and comparing to other studies, I first review the meaning of these quantities in terms of the appearance

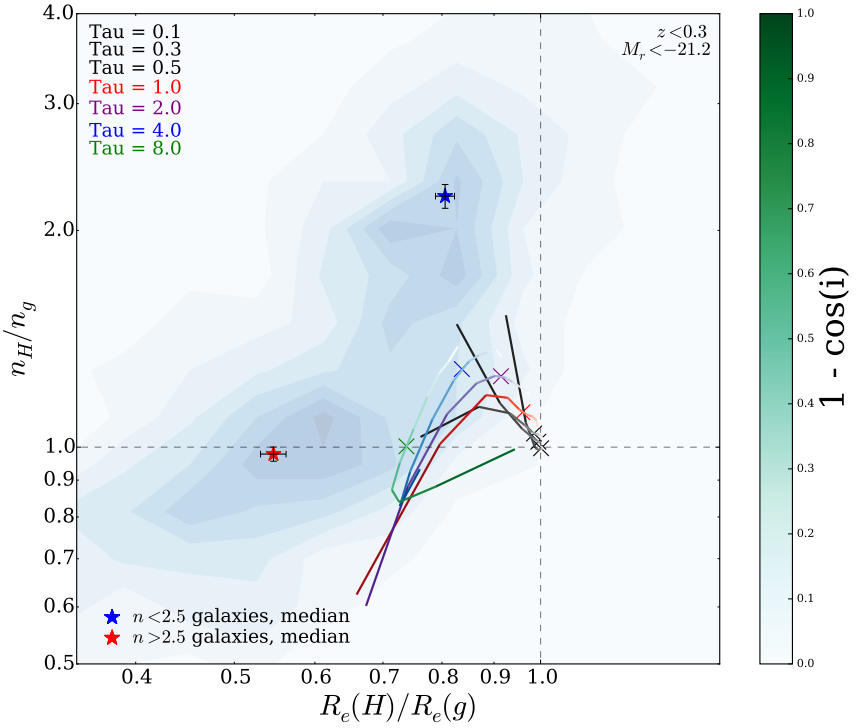

Figure 3.10. The effect of dust on $\mathcal{N}_g^H$ vs $\mathcal{R}_g^H$ for discs. Underlayed are contours for all galaxies in the V14 sample, as in Fig. 3.8. Overplotted are the mean locations of low- and high-n galaxies within the V14 volume limited sample. Black lines show model tracks for optically thin discs having a nominal value ($\mathcal{N}_g^H$,$\mathcal{R}_g^H$)=(1,1), whilst coloured lines correspond to model tracks for optically thick discs The intensity of the colour in each line shows the inclination of the galaxy. Crosses indicate the point at which $(1 - \cos i) = 0.5$.

and physical structure of a galaxy. A value around unity, for either quantity, indicates that that particular aspect of structure does not vary with wavelength. $\mathcal{R}$ gives the variation in galaxy size (R_e) with wavelength. The vast majority of galaxies are found to have $\mathcal{R} < 1$, indicating that they are larger in the blue. These galaxies therefore display redder colours in their centres, and become bluer at larger radii. In the rarer case, $\mathcal{R} > 1$, galaxies are larger in the red, and hence bluer in the centre, becoming redder with increasing radius.

$\mathcal{N}$ indicates how a galaxy's profile shape (n), or equivalently its central concentration, depends on wavelength. Galaxies with $\mathcal{N} > 1$ have a high-n profile in redder bands. They are therefore 'peakier' in their centres and have more significant surface brightness at large radii. Galaxies with $\mathcal{N} > 1$ are thus expected to be redder in the centre and in their outskirts, and bluer at intermediate radii ($\sim R_e$). In practice, the outermost red regions may be too faint

to been seen in normal depth imaging, and so the visible outskirts of such a galaxy may appear blue. However, the difference with respect to $\mathcal{R} < 1$ is that the colour gradient should become shallower with radius. Galaxies with $\mathcal{N} < 1$ obviously show the opposite trend, appearing more strongly peaked at bluer wavelengths.

Of course, both $\mathcal{N}$ and $\mathcal{R}$ may both depart from unity at the same time, indicating variations in both size and profile shape with wavelength. In that case, the resulting colour profile is a combination of the two behaviours. These may, to a degree, counteract (if $\mathcal{N}$ and $\mathcal{R}$ are correlated) or reinforce (if anti-correlated) one another. Indeed, some of the correlation in the $\mathcal{N}$–$\mathcal{R}$ plane, within subsets of the galaxy population, may be a result of this degeneracy.

I study the effect of redshift on my ability to measure $\mathcal{N}_g^H$ and $\mathcal{R}_g^H$ in Section 3.3.1. For low-n (i.e. typically late-type) galaxies I find a bias of $\mathcal{R}_g^H$ and $\mathcal{N}_g^H$ to lower values ($\mathcal{R}_g^H$ away from unity, $\mathcal{N}_g^H$ toward unity) at higher redshifts. However, these observed biases are significantly smaller than the differences between the galaxy subsamples, particularly for low- versus high-n galaxies. The conclusions of V14 therefore are not significantly affected by the generous redshift limit adopted in that study. The quantitative results of V14 are also relatively robust and may be compared to other studies of comparable galaxy populations in similar quality imaging. However, when comparing to much lower redshift samples of late-types, e.g. in Fig. 3.9, one must bear in mind the redshift bias.

In Section 3.3.2, the wavelength-dependence of both R_e and n are found to depend on luminosity, with brighter galaxies generally showing stronger trends with increasing wavelength: to smaller sizes (especially for early-type galaxies) and higher-n (especially late-type galaxies). The contrast between the behaviour of high- and low-n galaxies lessens with decreasing luminosity, suggesting greater structural similarity between (Sérsic index selected) early- and late-type galaxies at lower luminosities.

3.4.2 Comparison of observed trends of $\mathcal{R}$ and $\mathcal{N}$ with other studies

My work is consistent with that of La Barbera et al. (2010b). I find an extremely similar decrease in effective radius for red, $n > 2.5$ galaxies at the same luminosities. Furthermore, I have shown that this is robust to redshift effects and the use of visual morphology, rather than Sérsic index, to select early-types. My results also agree with those of Kelvin et al. (2012) and Ko & Im (2005), both of which find a nearly 40 per cent decrease in $R_{\rm e}$ over the corresponding wavelength range.

The existence of negative colour gradients in elliptical galaxies, particularly strong in optical-NIR colours, has been known for a long time (e.g., Peletier, Valentijn & Jameson 1990). La Barbera et al. (2010a) use their Sérsic models, independently fit to each wavelength, to determine colour gradients for their sample of early-type galaxies. They find that more optically-luminous galaxies display stronger (negative) NIR-optical colour gradients. This agrees with our finding that $R_{\rm e}$ depends on wavelength more strongly for more luminous high-n galaxies. However, La Barbera et al. (2010a) see little variation in colour gradients with NIR luminosity or stellar mass. This is consistent with the bluer stellar population being located at larger radii, and this feature being more prominent in more luminous galaxies.

La Barbera et al. (2012) show that, compared to optical-NIR measurements, colour gradients based only on optical bands are weaker. They are nevertheless widely observed (e.g., Gonzalez-Perez, Castander & Kauffmann 2011). Optical gradients also do not show as much variation with luminosity, being strongest for intermediate luminosities (La Barbera et al. 2012; Roche, Bernardi & Hyde 2010). Using stacked optical (SDSS) images, D'Souza et al. (2014) find strong evidence for the presence of blue (in $g-r$) halo components in various galaxy populations. This extended component can account for around half of the light of a galaxy, being more prominent in higher-n and more luminous galaxies. Even the majority of massive early-type galaxies at $z \sim 1.5$ are found to display negative colour gradients (Gargiulo et al. 2012).

A small subset of local early-type galaxies display positive optical colour gradients, due to the presence of blue cores associated with recent star-formation

(Suh et al. 2010). These become more prevalent at higher redshifts (Ferreras et al. 2005). Such galaxies correspond to my high-n, very blue, selection. These galaxies display $\mathcal{R}_g^H < 1$, like other early-types, implying they are more compact in the red. However, in contrast to my other subsamples, this is combined with $\mathcal{N}_g^H < 1$, implying their profiles are more strongly peaked in the blue. The intermediate and outer gradients of these galaxies are therefore apparently like other ellipticals, but they must display a blue excess in their cores.

Typical spirals (Sab-Scd) show less R_e variation with wavelength, compared to early-types, but it is still significant: a ~ 20 per cent decrease from g to H. This value has little dependence on galaxy luminosity, at least over the range we probe here. However, note that the wavelength variation of R_e for late-types is somewhat susceptible to being overestimated in lower-quality data. Both early-discs (S0-Sa) and very late-types (Sd-Irr) display behaviour intermediate between ellipticals and spirals.

In terms of Sérsic index, I find that early-type (high-n) galaxies show little variation in n, while late-types substantially increase in n with increasing wavelength. Again, early-discs (S0-Sa) and very late-types (Sd-Irr) fall between the two behaviours. My results for disc galaxies agree well with those of Kelvin et al. (2012), who find that Sérsic indices almost double from u to K, although most of the change occurs over the optical range.

Various studies have found the Sérsic indices of early-type galaxies to be generally unchanged with wavelength (Kelvin et al. 2012; La Barbera et al. 2010a, 2012), perhaps with a slight increase in n with wavelength. The estimated changes in n and R_e with wavelength for these, and other, studies are displayed in Table 3.1. I do not generally see such an increase, rather a small decrease is more common in my early-type samples. However, redshift appears to have an effect, as does luminosity. In my lowest-redshift, brightest samples I find Sérsic indices that are constant, or slightly rising, with wavelength. Visually-classified ellipticals also have $\mathcal{N}_g^H$ very close to unity. On the other hand, fainter and bluer high-n galaxies tend to display Sérsic indices that decrease with wavelength, by several tens of per cent. La Barbera et al. (2012) find that larger (and hence typically more luminous) early-type galaxies show stronger trends of n increasing wavelength, matching the form of behaviour I

	'Early type'		'Late type'		Notes
	n	R_e	n	R_e	
LB10	1*↑	28 ↓	-	-	5080 bright spheroids from SPIDER, g- to K-band. (La Barbera et al. 2010a)
Kel12	30 ↑	38 ↓	52 ↑	25 ↓	167,600 galaxies from GAMA, g- to K-band. (Kelvin et al. 2012)
V14	1*↑	45 ↓	38*↑	25 ↓	14,274 galaxies from GAMA-II G09 region, $M_r < -21.2, z < 0.3$, u- to H-band.
L15: $10^9 M_\odot$	-	-	-	16 ↓	8399 galaxies from GAMA-II, $0.01 < z < 0.1$, g- to K_s-band. (Lange et al. 2015)
L15: $10^{10} M_\odot$	-	13 ↓	-	13 ↓	As above.
L15: $10^{11} M_\odot$	-	11 ↓	-	-	As above.
K15: $M_r \sim -20$	12 ↓	23 ↓	29 ↑	13 ↓	5331 galaxies from GAMA-II G09 region, $z < 0.15$, g- to H-band (this study).
K15: $M_r \sim -21$	5 ↑	25 ↓	40 ↑	15 ↓	As above
K15: $M_r \sim -22$	5 ↑	33 ↓	55 ↑	12 ↓	As above

Table 3.1. Comparison of results from previous studies. Each number shows the percentage change in n and R_e between the wavebands given under 'notes'. ↑ = increase; ↓ = decrease; * = value has been calculated from information given in the paper; - = no data available...

see here.

The redshift biases and luminosity trends I have found allow me to, at least partly, reconcile the dramatic wavelength-dependence reported by V14 with the more modest behaviour seen by some other recent studies. Kelvin et al. (2012) find slightly weaker trends than V14, but they use a magnitude-limited sample, dominated by somewhat less luminous galaxies. When I adopt the same selection, my results are in excellent agreement.

Lange et al. (2015) find a substantially weaker dependence of R_e on wavelength, though it is still significant. I have shown that dividing galaxies by visual morphology (as in Kelvin et al. 2014) confirms the behaviour inferred from selections based on colour and Sérsic index, but severely limits the usable sample size.

For late-type galaxies, my results are actually in good agreement with Lange

et al. (2015). If I consider my low redshift sample, I find a similar ~ 15 per cent decrease in size. At higher redshifts I appear to slightly overestimate the strength of the size decrease compared with Lange et al. (2015). However, for early-types, there is a larger discrepancy, although the qualitative behaviour is the same. Redshift (i.e. data-quality) appears to have little effect on my results. Considering my $M_r \sim -20$ ($\log M_\star \sim 10$) selection I still find a ~ 25 per cent decrease in the effective radii of red high-n galaxies. This is not reduced if I limit my analysis to visually-classified ellipticals. The wavelength-dependence results featured by Lange et al. (2015) are based on linear fits to the R_e–$M_\star$ relation, and hence galaxies with relatively low masses, $\log M_\star \sim 10$, exert a strong influence. These different analyses may have something to do with our disagreement. However, it may also be that the difference in depth between the UKIDSS LAS and VIKING VISTA NIR imaging is responsible, as suggested by Lange et al. (2015). Many, but not all, of the studies that also find strong trends for early-type galaxies, as mentioned above, are also based on SDSS and UKIDSS LAS data and hence may be similarly affected. In the near future I will have the results of this methodology applied to the same SDSS plus VIKING data set, so will be better placed to evaluate this issue.

3.5 Summary

The variation of galaxy structure with wavelength reveals the connections between the stellar populations within a galaxy and their spatial distributions. Specifically, I consider the change in Sérsic index and effective radius from g- to H-band, which I denote $\mathcal{N}$ and $\mathcal{R}$. As shown by V14, the majority of early-type (high-n) galaxies show little variation in their Sérsic index with wavelength ($\mathcal{N} \sim 1$), but are significantly smaller at longer wavelengths ($\mathcal{R} < 1$). This behaviour is suggestive of a structure formed by similar (violent) mechanisms being apparent at all wavelengths, but with a scale that strongly depends on the colour of the stellar population. On the other hand, late-type galaxies (low-n) display a substantial increase in Sérsic index with wavelength ($\mathcal{N} > 1$), suggesting a variation in the type of structure dominating the light at different wavelengths, but less variation in size ($\mathcal{R} \lesssim 1$). Very blue, high-n, galaxies present an interesting contrast, having significantly higher Sérsic indices in the

blue, indicating the presence of a peaky blue component.

In this chapter I have used optical-NIR imaging and redshifts from the GAMA survey (Driver et al. 2009), with multi-band single-Sérsic fits performed using tools developed by the MegaMorph project (Bamford et al. 2012), in order to study four further aspects of the wavelength-dependence of galaxy structure. I consider the distributions of $\mathcal{N}$ and $\mathcal{R}$ for a variety of volume-limited samples subdivided by $u-r$ colour, Sérsic index and morphology. The main conclusions from my analysis are:

- I have verified that my measurements of $\mathcal{N}$ and $\mathcal{R}$ are robust to the effects of redshift, strengthening the earlier results of V14. Early- and and late-type galaxies (selected using Sérsic index) present strongly contrasting behaviour in terms of the wavelength-dependence of their structure. Out to $z \sim 0.3$ I see no substantial changes in $\mathcal{R}$ or $\mathcal{N}$, particularly when compared to the striking differences between galaxy subsamples. What small biases are present, suggest that at higher redshift (lower S/N and poorer resolution) we may be slightly overestimating the offset of $\mathcal{R}$ from unity, and underestimating the offset of $\mathcal{N}$ from unity, for low-n galaxies. Both of these effects act to reduce the apparent difference between the high- and low-n populations. The estimated contrast is therefore even more pronounced than that determined by V14.

- The strengths of $\mathcal{N}$ and $\mathcal{R}$ depend on galaxy luminosity:

  - High-n galaxies with lower luminosities have $\mathcal{R}$ closer to unity than their brighter counterparts. Most high-n galaxies have $\mathcal{N}$ around unity for all luminosities, supporting the suggestion of V14 that these are single-component objects.

  - Low-n galaxies display weaker, more mixed trends in $\mathcal{R}$ compared to high-n galaxies. There is a striking trend in the $\mathcal{N}$ distributions of low-n galaxies with luminosity: brighter objects display $\mathcal{N}$ further from unity, for all colour subsamples.

- The interpretations of V14 are supported by visual morphological classifications of a low-redshift subset of our sample from Kelvin et al. (2014); my low-n samples share the same part of the $\mathcal{N}$–$\mathcal{R}$ diagram as Sab/Scd

galaxies, whilst the high-n samples follow the distribution of elliptical galaxies. Both early- and late- disc galaxies occupy intermediate regions of the $\mathcal{N}$–$\mathcal{R}$ plane, confirming that the extreme values for intermediate types are related to their two-component nature.

- Results from fitting dusty galaxy models (Pastrav et al. 2013a) indicate that some of the wavelength-dependence of disc galaxy structure may be attributable to dust. The natural distribution of disc inclinations may account for the trend seen in the $\mathcal{N}$–$\mathcal{R}$ plane, while varying central dust opacities may account for the scatter in this relation. However, pure dusty discs cannot reach the values of $\mathcal{N}$ observed for intermediate-type spirals.

Further improving our understanding of the wavelength-dependence of galaxy structure requires more detailed consideration of the two-component nature of galaxies. These results are the subject of Chapter 5.

Chapter 4

Internal colour gradients of galaxies

4.1 Overview

The wavelength dependence of structure that I measured in Chapter 3, i.e. $\mathcal{N}$ and $\mathcal{R}$, must be driven by radial variations in stellar populations and/or dust extinction. For early-type galaxies, many studies have found that colour gradients are caused by negative metallicity gradients. Age is generally fairly constant with radius, or even slightly increasing, and hence acting against the metallicity trend. The outskirts of massive early-type galaxies (ETGs) are therefore typically more metal poor and older than their cores, with weaker gradients for lower mass ETGs. (e.g., La Barbera et al. 2012, and references therein).

Metallicity gradients are expected in models of monolithic collapse (Worthey, Trager & Faber 1995), and this mechanism may be responsible for the gradients in the centres of today's galaxies. However, most massive galaxies are expected to have experienced a major merger since their formation, which will have partly erased these initial gradients. It has been discovered that early-type galaxies must at least double in effective radius between $z \sim 2$ and today (e.g. van der Wel et al. 2014). Although various processes have been proposed, the dominant mechanism appears to be minor mergers (Hopkins et al. 2009; Lackner & Gunn 2012). The stellar material accreted in such mergers tends

to contribute most significantly to the outskirts of the more massive galaxy, building up an outer envelope (Huang et al. 2013). The effect is to increase effective radius over time and produce stellar population gradients.

The increase I have measured in effective radius toward shorter wavelengths, which is stronger for more luminous systems, ($\mathcal{R}_g^H \sim 0.55$–$0.75$ from $M_r \sim -22$–-20), is consistent with observations of negative colour gradients and extended blue components (La Barbera et al. 2012). The lack of variation in Sérsic index with wavelength ($\mathcal{N} \sim 1$) suggests that the extended profile of the stellar populations seen in the blue is structurally consistent with the profile traced by those stellar populations dominating at red wavelengths, possibly indicative of a similar origin. Together, these observations are consistent with a gradual build-up of massive early-type galaxies through accretion of low-mass galaxies.

Lower-luminosity, and bluer, early-type (high-n) galaxies tend to show slightly peakier profiles in the blue, which may be an indication of an additional blue stellar component in their centres, possibly as a result of recent central star-formation.

Dust in early-type galaxies is generally not expected to be present in sufficient quantities to have a significant effect on their observed structure. However, Rowlands et al. (2012) do find that ~ 5 per cent of luminous early-type galaxies are detected in the far-infrared, implying that they must contain significant fractions of dust (also see Bendo et al. 2006). It is uncertain how this dust impacts upon their measured structural parameters, but it may be responsible for some of the scatter we see in $\mathcal{N}$ and $\mathcal{R}$ for my early-type samples.

In late-type galaxies, dust is likely to play a more dominant role. The apparent differences in optical structure in disc galaxies across the Hubble sequence is largely determined by the presence of young stars and dust. The old stellar discs of spiral galaxies, as seen in the NIR, are very similar at all Hubble types (Block et al. 1999).

Modern studies of the opacity of spiral discs find that they suffer from substantial face-on and inclination-dependent extinction (e.g. Holwerda et al. 2005; Masters et al. 2010). Testing the model of Tuffs et al. (2004) with a large galaxy sample, Driver et al. (2007b) find good agreement and infer that bulges and the central regions of discs suffer from substantial attenuation of their

optical light. This has a significant impact on measurements of their structural parameters (Möllenhoff, Popescu & Tuffs 2006; Pastrav et al. 2013a,b). However, as I have shown in Section 3.3.4, dust alone cannot explain the observed wavelength trends. It seems obvious that the two-component, bulge-disc, nature of late-type galaxies, with their contrasting stellar populations and structures, must have at least some impact on the wavelength-dependence of their overall structure. I will investigate this further in Chapter 5.

In Chapter 3 I studied the wavelength dependence of galaxy structure to reveal the connections between the stellar populations within a galaxy and their spatial distributions. I found evidence for multi-component structure in many galaxies, even those visually classified as elliptical (see Chapter 5). This suggests that considering structural variations with wavelength may provide fundamental insights into galaxy formation. Nevertheless, studying internal colour gradients is a complementary and widely-used approach, and thus it is important to understand how our results on the wavelength-dependence of structure relate to more traditional colour gradients. In this chapter I study how colour gradient varies with wavelength (from ∇_{g-r} to ∇_{g-H}) for six subsamples split by overall Sérsic index and galaxy colour, and then consider the luminosity dependence of these colour gradients.

4.2 Data

As in Chapter 3, the sample used in this chapter comes from the G09 region of GAMA II (Driver et al. 2009, 2011; Liske et al. 2015). It is volume-limited to $M_r < -19.48$ mag and $z < 0.15$ when studying trends with luminosity, which gives a larger luminosity range but smaller sample of 5317 galaxies, with a stellar mass limit of $\sim 10^9 M_\odot$. The sample is volume-limited to $M_r < -21.2$ mag and $z < 0.3$ elsewhere, which gives a larger sample of 13825 galaxies at the expense of a smaller luminosity range with a stellar mass limit of $\sim 10^{10} M_\odot$. GALFITM (Häußler et al. 2013; Vika et al. 2013) has been used to fit a single-Sérsic wavelength-dependent model to all bands simultaneously, and returns (amongst other parameters) magnitude (m), Sérsic index (n), and effective radius (R_e). For more information on the data used here, see Chapter 2.

As described in section 2.4 I divide my sample into high- and low-Sérsic index

at $n_r = 2.5$, and separate *red* and blue galaxies using a $u - r = 2.1$ colour cut. I then separate the blue galaxies into *green* and *blue* at $u - r = 1.6$ in an attempt to separate out the bluest, potentially starburst, population. Note that the *green* population corresponds to the main population of star-forming galaxies, not specifically the green valley.

In the previous chapter I measured the wavelength dependence of Sérsic index, $\mathcal{N} = n(H)/n(g)$, and effective radius, $\mathcal{R} = R_{\rm e}(H)/R_{\rm e}(g)$ between the H- and g-bands. I saw that there is a striking difference in the behavior of high-n ($n_r > 2.5$) and low-n ($n_r < 2.5$) galaxies; high-n galaxies show a large change in $R_{\rm e}$ ($\mathcal{R} < 1$) but little change in n ($\mathcal{N} \sim 1$), whereas in low-n galaxies show little change in $R_{\rm e}$ with wavelength but a large change in n with wavelength. Although $\mathcal{N}$ and $\mathcal{R}$ are useful for considering the dependence of structure on wavelength, they are hard to compare to the literature. Here I therefore convert these measurements into more traditional colour gradients which describe a change in stellar population or dust with radius, rather than a change in radial profile with wavelength.

The colour profile for each galaxy is computed over a range of radii using the Sérsic formula, as seen in Fig. 4.1, for our six subsamples. The $g - H$ colour profiles of high- and low-n galaxies are shown as dashed and solid lines respectively for *red*, *green* and *blue* galaxies, which are coloured accordingly. In agreement with the literature, one can qualitatively see in Fig. 4.1 that the majority of galaxies are redder in the centre than the outskirts. Note that the blue, high-n subsample contains less than 3% of the full population.

I derive my colour gradients from these radial colour profiles using the logarithmic slope of a galaxy's radial colour profile between $0.1R_{\rm e}$ and $1R_{\rm e}$,

$$\nabla_{g-x} = \frac{d(g-x)}{d(log\rho)} \tag{4.1}$$

where g is the SDSS g-band, $x = rizYJH$, and ρ is the distance to the galaxy centre, taking $R_{\rm e}$ as the effective radius in the r-band (see e.g. Peletier, Valentijn & Jameson 1990; La Barbera et al. 2010a).

Recall that both the Sérsic index and effective radius of a galaxy are allowed to vary quadratically with wavelength during the two-dimensional Sérsic model fit. As the colour gradient is measured over a radial range defined in a single

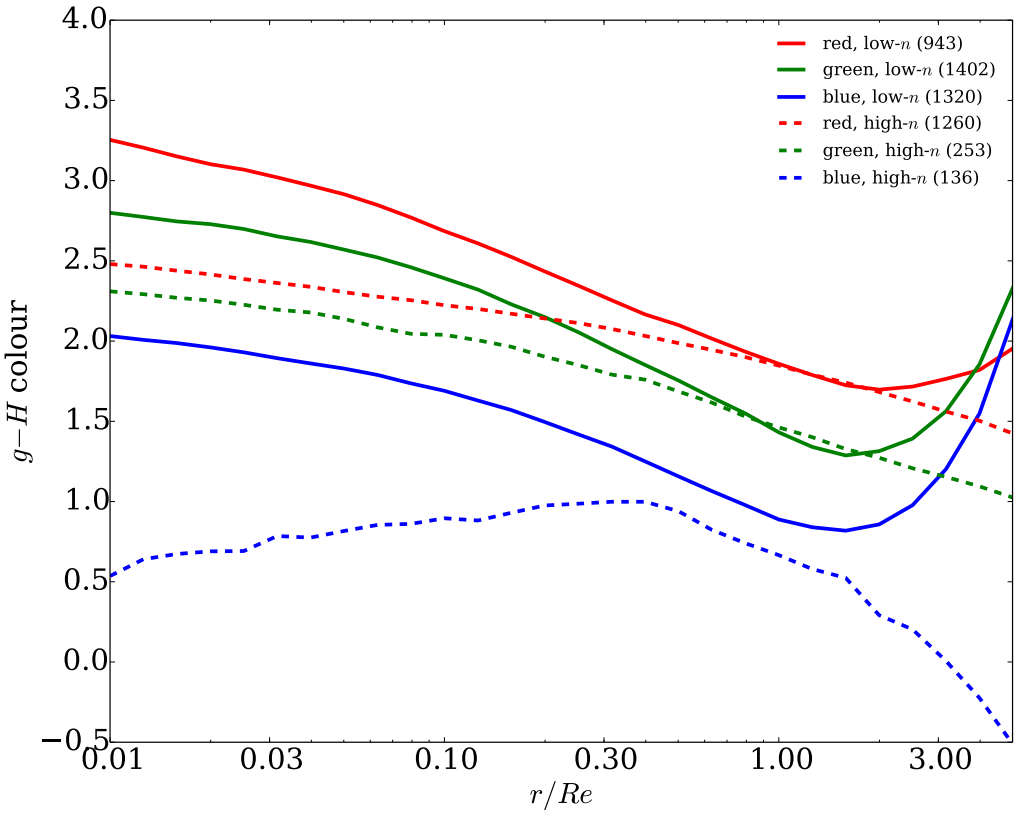

Figure 4.1. Median $g - H$ colour profiles of high- and low-n galaxies (dashed and solid lines respectively) for *red*, *green* and *blue* galaxies, which are coloured accordingly. The number of galaxies in each subsample is given on the plot. The colour profile for each galaxy is computed from $0.1R_e$ to $4R_e$ using the Sérsic formula, and the median is shown here. The colour profiles presented here diverge in the outskirts of each galaxy because the fit only constrains parameters to $1R_e$. Orthogonal regression can then be used to convert these colour profiles into colour gradients.

band (the r-band), both the variations of n and R_e with wavelength contribute to the measured colour gradients. I then use orthogonal regression to find ∇_{g-x}, the gradient of the best-fitting profile where $x = rizYJH$.

My large sample size allows me to study both early- and late-type galaxies in 7 wavebands. I can therefore provide a more complete picture of how colour gradients - and hence stellar mass growth channels - vary across the galaxy population. I am also able to extend the work in Chapter 3 to study in detail the luminosity dependent colour gradients for my subsamples of galaxies.

4.3 Results

4.3.1 Variation in colour gradient with wavelength

The variation in colour gradient with wavelength is summarised in Fig. 4.2; it can be seen that the majority of colour gradients are negative, i.e. appear bluer at larger radii. I have also examined the redshift dependence of these colour gradients in a similar manner to section 3.3.2, and find that they do not change significantly. As one would expect, colour gradients are stronger for more widely spaced waveband pairs. We can see a distinct difference in the colour gradients of low- and high-n galaxies, regardless of overall galaxy colour. The low-n samples consistently have the strongest colour gradients. In Chapter 5 I find these low-n samples to contain galaxies with more significant disc components (i.e. a lower bulge/total flux ratio) than their high-n counterparts, which is in agreement with Gonzalez-Perez, Castander & Kauffmann (2011) who find that steep negative gradients are more likely to be found in late-types. We can also see that the *red* subsamples consistently have shallower colour gradients than the *blue* and *green* subsamples; once again I am in agreement with the conclusion of Gonzalez-Perez, Castander & Kauffmann (2011) that the redder a galaxy, the shallower its colour gradient. The red, high-n sample is a reasonable proxy for early-type galaxies, and the mean colour gradients I find (given in Table 4.1 for all subsamples) agree well with the colour gradients found in La Barbera et al. (2010a) for their sample of ETGs over the same range of wavebands. These values are shown later, in Fig. 4.4. Within the uncertainties, the mean colour gradients of the low-n

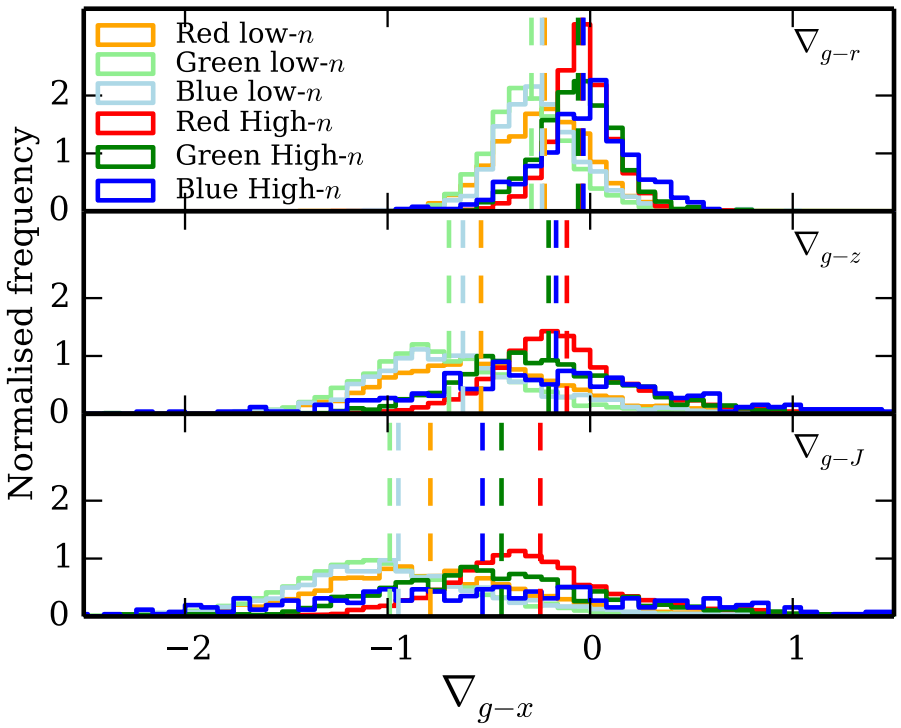

Figure 4.2. Distributions of ∇_{g-x} for galaxies in each of the colour/Sérsic index subsamples (see section 4.2 for more details), normalised to unit integral. Each panel shows the distribution for a different pair of bands. The median of each distribution is indicated by a vertical dashed line. These median values, and their uncertainties, can be found in Table 4.1. A bimodality in colour gradients for high- and low-n galaxies can be seen in all wavebands.

samples also agree with those of Taylor et al. (2005) for 'mid-type' (Sc) spiral galaxies, and Gonzalez-Perez, Castander & Kauffmann (2011) for late-type galaxies in a similar magnitude range.

4.3.2 Luminosity dependence of colour gradients

I now proceed to examine how colour gradients depend on galaxy luminosity. Fig. 4.3 shows the median colour gradients, ∇_{g-x}, where $x = rizYJH$, of the entire low redshift sample as a function of r-band absolute magnitude. In all wavebands we observe shallower colour gradients for the brightest and faintest galaxies, with the strongest colour gradients at around $M_r \sim -21.25$. One must be mindful, however, that we are looking at many different galaxy populations here, as my only selections are volume-limiting the sample, and excluding the $\sim 0.4\%$ of objects for which the GALAPAGOS fits fail (H13, V14).

	Red, low-n		Green, low-n		Blue, low-n		max. err.
	μ	σ	μ	σ	μ	σ	on μ
∇_{g-r}	-0.22	0.24	-0.29	0.21	-0.24	0.23	0.01
∇_{g-i}	-0.39	0.40	-0.51	0.35	-0.44	0.38	0.03
∇_{g-z}	-0.54	0.50	-0.70	0.45	-0.63	0.51	0.04
∇_{g-Y}	-0.64	0.54	-0.82	0.50	-0.76	0.57	0.05
∇_{g-J}	-0.79	0.58	-0.99	0.54	-0.95	0.62	0.07
∇_{g-H}	-0.95	0.61	-1.12	0.55	-1.11	0.68	0.08
	Red, high-n		Green, high-n		Blue, high-n		max. err.
	μ	σ	μ	σ	μ	σ	on μ
∇_{g-r}	-0.04	0.16	-0.06	0.19	-0.03	0.25	0.01
∇_{g-i}	-0.07	0.28	-0.12	0.35	-0.07	0.45	0.03
∇_{g-z}	-0.12	0.40	-0.21	0.51	-0.17	0.72	0.04
∇_{g-Y}	-0.16	0.46	-0.28	0.60	-0.29	0.92	0.05
∇_{g-J}	-0.25	0.52	-0.44	0.71	-0.53	1.20	0.07
∇_{g-H}	-0.40	0.52	-0.67	0.80	-0.79	1.44	0.08

Table 4.1. Mean colour gradients, μ, and standard deviations, σ, for each of our colour/Sérsic index subsamples. The final column gives the maximum uncertainty on the mean values ($\sigma/\sqrt{N}$), corresponding to the smallest subsample, blue high-n. For the larger subsamples, this uncertainty is up to an order of magnitude smaller.

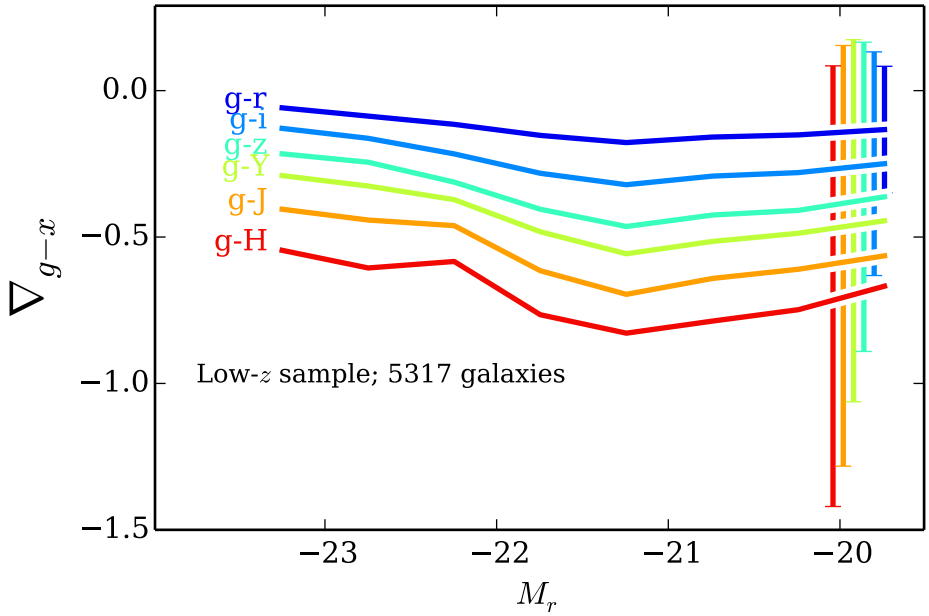

Figure 4.3. Median colour gradient, ∇_{g-x}, where $x = rizYJH$, as a function of r-band absolute magnitude, M_r, for the low redshift sample. Different colours correspond to different wavebands, with $g-r$ at the top to $g-H$ at the bottom, as indicated by the label to the left of each line. The standard deviation of each distribution (as shown by error bars on the faintest luminosity bin) is largely constant with luminosity, and is comparable to the standard deviations given in Table 4.1. Particularly at longer wavelengths we see a double-valued behaviour with the shallowest colour gradients occurring at the brightest and faintest ends. This appears to be due to the contribution of different galaxy populations, which is studied further in Fig. 4.4.

4.3.3 Origin of bimodality in luminosity dependence of colour gradient

As seen in Fig. 4.2, different galaxy types (in this context, different n and colours) display contrasting colour gradients. I therefore show in Fig. 4.4 how colour gradients, ∇_{g-x} where $x = rizYJH$, change with luminosity depending on a galaxy's overall $u-r$ colour and Sérsic index. I perform this analysis over two radial ranges: $0.1R_{\rm e}$ - $R_{\rm e}$, and $0.1R_{\rm e}$ - $2R_{\rm e}$.

The variety of trends seen in each panel of Fig. 4.4 shows that the overall trends seen in Fig. 4.3 are actually the result of a number of different populations. Red, high-n galaxies dominate at bright magnitudes (i.e. there are only red, high-n galaxies brighter than $M_r \sim -22.5$) whilst low-n galaxies dominate at faint magnitudes. Note that colour gradients in high-n galaxies do not change when measuring over a wider radius range (as previously found by La Barbera & de Carvalho (2009) for ETGs, and shown as dashed lines in Fig. 4.4). Low-n galaxies do show slightly flatter colour gradients between $0.1R_{\rm e}$–$2R_{\rm e}$ which suggests that bright, low-n galaxies have stronger colour gradients towards their centres. This is consistent with the presence of a bulge within a relatively homogeneous outer disc, with the bulge being more significant in brighter galaxies.

La Barbera et al. (2010a) find a 'double-valued' behavior in the ∇_{g-r} colour gradient with luminosity for their early-type galaxies. One can see in Fig. 4.4 that this double-valued behavior can actually be considered a combination of the trends seen in the low- and high-n *red* populations. The colour gradients seen in a population are sensitive to the selection criteria used to define that population.

The *red*, high-n sample shows little change in colour gradient with luminosity in optical wavebands, but at longer wavelengths the faintest galaxies have the shallowest colour gradients. den Brok et al. (2011) study a sample of 142 ETGs and find that the colour gradients of elliptical galaxies (shown in Chapter 5 to be analagous to the red, high-n population) become shallower at fainter magnitudes, which is consistent with my results. Note that only the red, high-n population has a significant number of galaxies brighter than $M_r \sim -22.5$ mag, so in Fig. 4.3 these galaxies dominate the brightest end of the sample.

Tortora et al. (2010) use ∇_{g-i} as a measure of colour gradient for a large sample of SDSS galaxies, and find that colour gradients decrease with mass; i.e. more massive, and therefore more luminous, systems have the weakest colour gradients. This is consistent with my assumption that the high-n populations contain elliptical galaxies, which tend to be larger and more massive than spirals and S0s (Kelvin et al. 2012; Moffett et al. 2016).

On the whole, the low-n subsamples show little change in colour gradient vs. luminosity with wavelength (i.e. lines are approximately parallel to one another). However, in the high-n subsamples the faintest galaxies show very similar colour gradients, whilst the brightest objects show a larger change in colour gradient with wavelength.

La Barbera et al. (2010a) find that the behavior of colour gradients with luminosity depends on both the wavebands in which the colour gradient was calculated, and the waveband in which the luminosity was determined.

Overplotted in grey in Fig. 4.4 are the colour gradients for samples from some previous studies, in the panel to which their sample is most closely related. In the red high-n panel I show ∇_{g-r} for the La Barbera et al. (2005) sample of luminous ETGs in clusters, which lies within the standard deviation (not shown here, but can be inferred from Table 4.1) of the faint end of our ∇_{g-r} line. In this panel I also show, with open circles, ∇_{g-r} for a larger sample of ETGs with $ugrizYJHK$ photometry from La Barbera et al. (2010a). The ∇_{g-r} luminosity dependence agrees well with my red, high-n sample, but sits a little lower at intermediate magnitudes. This is likely due to the ETG sample in La Barbera et al. (2010a) also containing galaxies which lie in my red, low-n sample, which have stronger colour gradients than their high-n counterparts at $M_r \sim -22$. The ∇_{g-i} colour gradient for the Gonzalez-Perez, Castander & Kauffmann (2011) ETG sample lies directly on my ∇_{g-i} line at that r-band magnitude, whilst in the red, low-n panel I plot the Gonzalez-Perez, Castander & Kauffmann (2011) ∇_{g-i} for their brightest late-type sample which again agrees with my ∇_{g-i} for more discy objects.

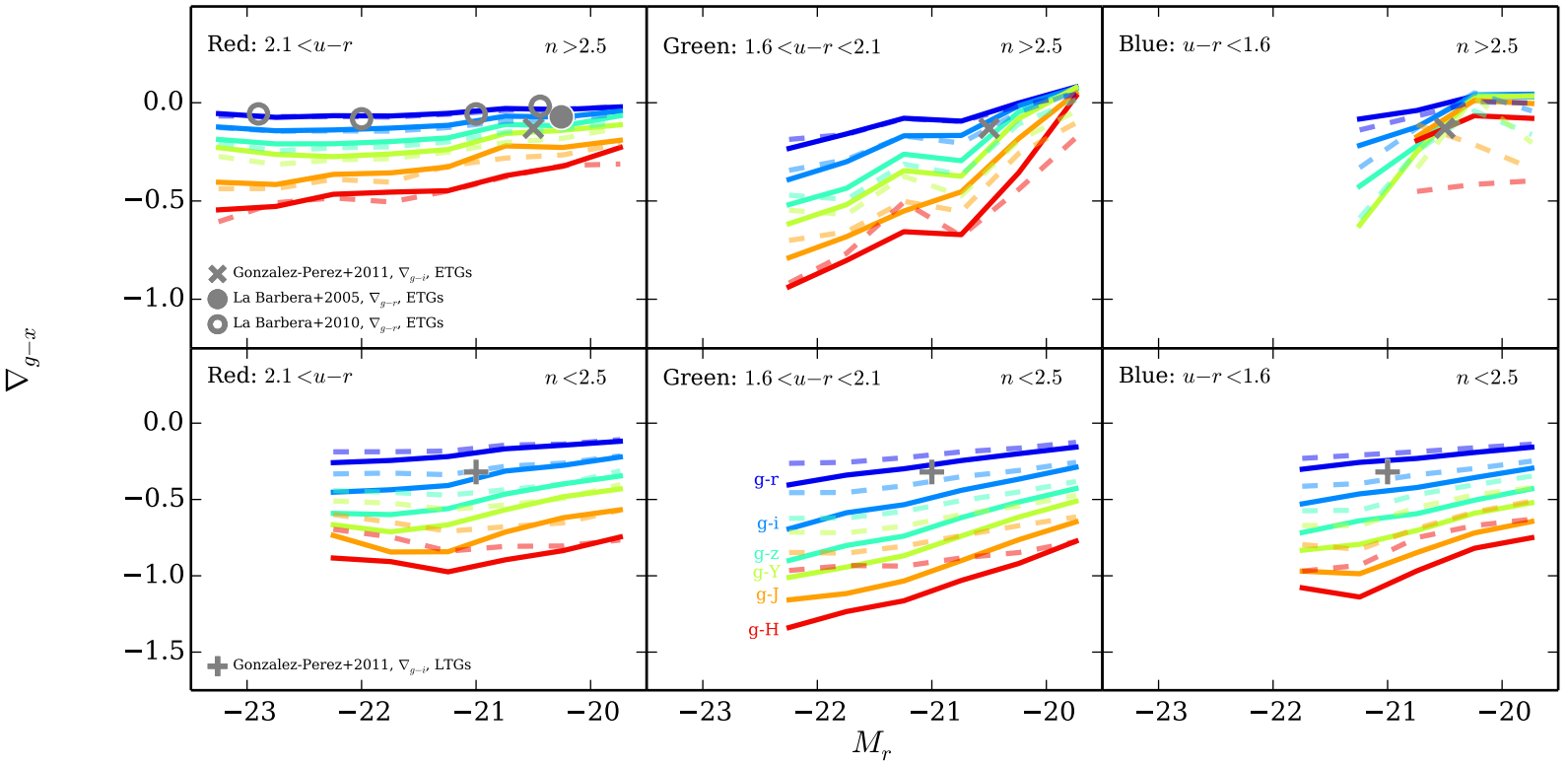

Figure 4.4. Median colour gradient, ∇_{g-x}, where $x = rizYJH$, as a function of r-band absolute magnitude, M_r, in each of my colour/Sérsic index subsamples. Solid and dashed lines show colour gradients over the radius ranges $0.1R_e$–$1R_e$, and $0.1R_e$–$2R_e$, respectively. Lines are limited to magnitude bins containing at least 10 objects. They are therefore only shown where each subsample makes up a significant fraction ($\gtrsim$1%) of the galaxy population. Different colours correspond to different wavebands, with $g-r$ at the top to $g-H$ at the bottom, as indicated. Results of previous studies are overlaid in the panels which most closely match the subsample of that study (see legends). We see that only the red, high-n population has galaxies brighter than $M_r \sim -22.5$, so these galaxies dominate at the bright end.

4.3.4 Relationship between colour gradients and wavelength dependence of n and R_e

As discussed in Section 4.1, measuring both colour gradients and the wavelength dependence of n and R_e provide valuable insights into a galaxy's stellar populations. Whilst colour gradients provide a widely-used non-parametric measure, measuring $\mathcal{N}$ and $\mathcal{R}$ allows us to separate the contributions of changes in size and shape, which may have different physical drivers. In order to draw meaningful conclusions between different studies it is important to consider the relationship between traditional colour gradients and their parametric counterparts.

In Figure 4.5 I plot the median colour gradient, ∇_{g-x}, as a function of $\mathcal{N}_g^H$ for the V14 sample. The strongest colour gradients are seen in galaxies with the highest $\mathcal{N}$; in Chapter 3 and V14 these were generally found to be low-n galaxies. This is consistent with what can be seen in Fig. 4.4, which shows that low-n galaxies have steeper colour gradients than high-n galaxies. Over the majority of the range of $\mathcal{N}$ this is consistent regardless of the bands in which colour gradient is measured. However, at $\mathcal{N} \sim 0.7$, galaxies exhibit little or no colour gradient regardless of the band in which the colour gradient is observed. It is also interesting to note that galaxies at $\mathcal{N} \sim 1$, showing no wavelength dependence of Sérsic index, nevertheless have measurable colour gradients. This is due to their wavelength dependence of effective radius, which drives the colour gradients in these galaxies.

In Figure 4.6 I plot the median colour gradient, ∇_{g-x}, as a function of $\mathcal{R}_g^H$ for my low redshift sample. One may have expected the low-n population to exhibit stronger colour gradients and $\mathcal{R}$ closer to unity than the high-n population (see Fig. 3.1). We *actually* see that colour gradient appears to be largely constant with $\mathcal{R}$, with double-valued behaviour, particularly at longer wavelengths. This may, however, be due to the smaller numbers of galaxies at the extremes of $\mathcal{R}$. In any case, it is clear that there is a significant colour gradient associated with $\mathcal{R}$, since colour gradients at $\mathcal{N} \sim 1$ are non-zero. This colour gradient associated with $\mathcal{R}$ is similar for all galaxies, so any deviation from this standard must be driven by $\mathcal{N}$.

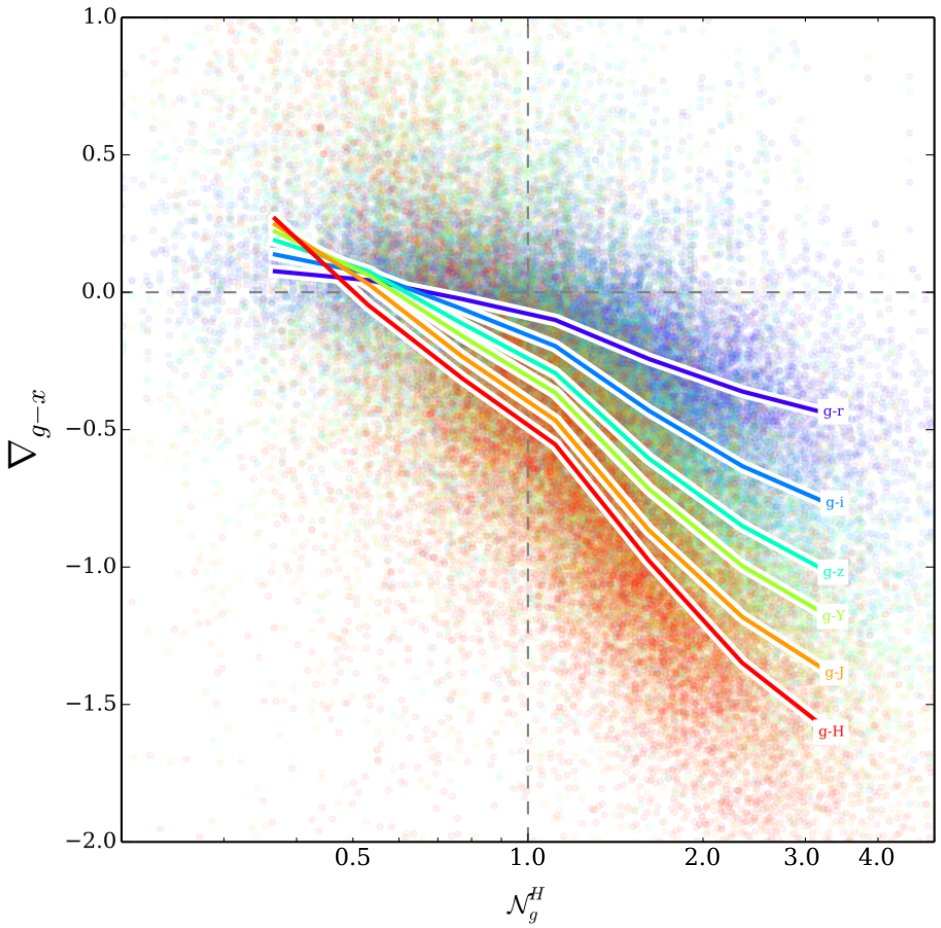

Figure 4.5. Median colour gradient, ∇_{g-x}, where $x = rizYJH$, as a function of the wavelength dependence of Sérsic index between the $H-$ and $g-$bands, $\mathcal{N}_g^H$ for my V14 sample. Different colours correspond to different wavebands, with $g - r$ at the top to $g - H$ at the bottom, as indicated by the label to the right of each line. Individual galaxies are plotted as scatter points under the median lines. The strongest colour gradients are seen in galaxies with the highest $\mathcal{N}$.

4.4 Discussion

I have measured radial gradients in six colours using multi-wavelength single-Sérsic model fits to galaxies in the GAMA survey. These complement previous studies (V14 and Chapter 3 of this thesis) on the variation of structural parameters with wavelength ($\mathcal{N}$ and $\mathcal{R}$). My measurements correspond well to those in the literature, supporting the reliability of my methods and earlier conclusions regarding the wavelength-dependence of galaxy structure.

I find that galaxies with differing Sérsic index and total colour display contrasting behaviour in terms of both the distributions and luminosity dependence of

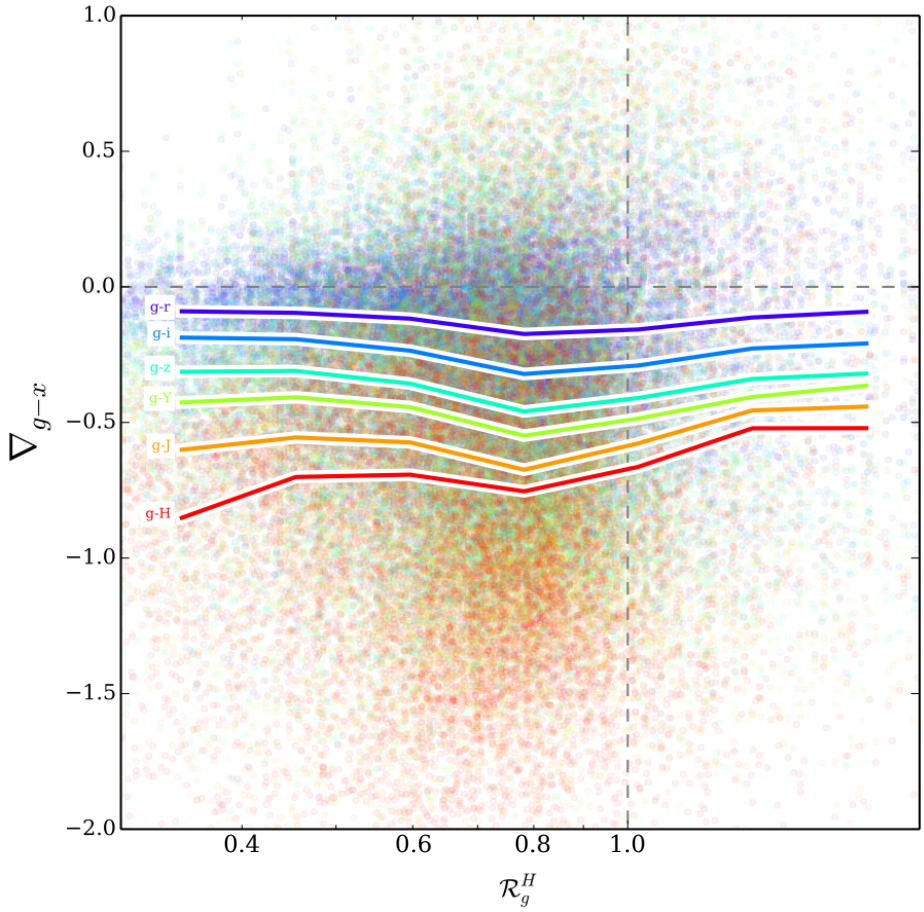

Figure 4.6. Median colour gradient, ∇_{g-x}, where $x = rizYJH$, as a function of the wavelength dependence of effective radius between the $H-$ and $g-$bands, $\mathcal{R}_g^H$ for my V14 sample. Different colours correspond to different wavebands, with $g-r$ at the top to $g-H$ at the bottom, as indicated by the label to the left of each line. Individual galaxies are plotted as scatter points under the median lines. There does not appear to be a strong dependence of colour gradient on $\mathcal{R}$.

their colour gradients. This means that care must be taken when comparing results for different sample selections.

The ubiquitous negative gradients that I find are indicative of stellar populations becoming younger and/or lower metallicity as one progresses from the centres to the outskirts of galaxies. While this is consistent with simple models of galaxy formation via early dissipative collapse (e.g. Pipino et al. 2010), in our ΛCDM Universe we expect the colour gradients of most galaxies to reflect their long-term hierarchical growth.

Strong negative gradients in low-n systems are consistent with inside-out disc formation via gradual accretion of gas to their outskirts, via smooth flows or (gas-rich) minor mergers (e.g. Lemonias et al. 2011; Wang et al. 2011). Such

gradients are present in blue, low-luminosity galaxies, which typically have little in the way of bulge component (also see Chapter 5); they must therefore arise from stellar population and/or dust gradients within the discs themselves. Nevertheless, the presence of a substantially redder bulge in more luminous disc galaxies (Chapter 5), appears to further enhance colour gradients, particularly within $1R_{\rm e}$.

The presence of gradients, even if weak, in bright, high-n systems argues against these galaxies being the direct result of major mergers, since such violent interactions should flatten colour gradients (see Kim & Im 2013 and references therein). Instead, their gradients may either result from the fading of bluer and/or lower-n galaxies (e.g. Bell et al. 2006), or from a reintroduction of metal-poor and/or younger stellar populations in the outskirts of these galaxies, for example via dry minor mergers (Eliche-Moral et al. 2013). The latter can also account for the rapid size evolution of passive galaxies (Oser et al. 2010).

In contrast, lower-luminosity high-n galaxies with bluer colours display very flat, or even slightly positive, colour gradients, especially in the optical. I infer that this population is experiencing a period of central star-formation. These galaxies account for 2.4% of my sample, which corresponds well with the local major merger fraction: also $\sim 2\%$ across a wide range of galaxy masses (see Khochfar & Burkert 2001; Keenan et al. 2014 and references therein). At the luminosities of interest, major mergers are mostly mixed elliptical-spiral interactions, and hence gas-rich (see e.g. Khochfar & Burkert 2003; Darg et al. 2010). With regards to the timescale of these events, Xu et al. 2012 find a dynamical merger timescale of around 0.3 Gyr for low mass galaxies, so a major merger driven starburst would only have to last a few hundred Myr to maintain the size of the population we see in our blue low-n sample. I therefore associate the blue high-n population with dissipative major mergers. However, less violent causes of central star formation, such as bar instabilities and minor mergers (see e.g. Kormendy & Kennicutt 2004 and references therein), may also contribute. The rarity of these examples suggests their descendants will re-acquire negative colour gradients, via fading of the central star-formation and subsequent accretion.

The colour profiles of most galaxies therefore result from continued accretion,

with the ratio of gas to stars in the incoming material varying from high: in the case of lower-luminosity, lower-n and bluer galaxies; to low: for higher-luminosity, higher-n and redder galaxies.

Possible applications for my colour gradient measurements include multi- wavelength strong lensing (information about the likely internal colour gradient of a galaxy will allow tighter constraints on mass models), and comparison with galaxy simulations (colour gradients provide more information with which to challenge models). My future work will use decomposed bulge and disc properties to further study the relationships between stellar populations and galaxy structure. In particular, I will expand upon the present study by using multi-band method to measuring colour gradients for individual galaxy components, e.g. bulges and discs, separately. This is discussed further in Chapter 7.

Chapter 5

Understanding the wavelength dependence of galaxy structure with bulge-disc decompositions

5.1 Overview

In Chapter 3 we followed V14 in examining the variation of Sérsic index (n) and effective radius ($R_{\rm e}$) with wavelength in order to reveal the internal structure, and therefore the formation history, of galaxies in their sample. As in Chapter 3, I continue to use the notation $\mathcal{N}_g^H = n(H)/n(g)$ and $\mathcal{R}_g^H = R_{\rm e}(H)/R_{\rm e}(g)$ to denote the ratio between the H- and g-bands. I omit the waveband labels from $\mathcal{N}$ and $\mathcal{R}$ when discussing their general behavior. V14 speculates that the variation in $\mathcal{N}$ reflects whether a system has one or two components; in a high-$\mathcal{N}$ system we are observing the Sérsic index of a disc in bluer wavelengths and a bulge in redder wavelengths. Conversely, V14 suggests that for one-component systems we see $\mathcal{N}$ closer to unity because we are measuring the Sérsic index of just one component at all wavelengths, e.g. in the case of elliptical galaxies. There is, however, a large change in $R_{\rm e}$ with wavelength for high-n galaxies, and corresponding colour gradients (see Chapter 4), which shows that elliptical galaxies contain a radial progression of different stellar populations, possibly resulting from multiple minor merging events throughout the galaxy's lifetime.

Vika et al. (2015) found that by combining $\mathcal{N}$ with the colour information of the galaxy we can separate elliptical galaxies from S0s more reliably than other photometric classification methods.

V14 and Vika et al. (2015) suggest that inferences about a galaxy's bulge-disc nature can be made from single-Sérsic fits. In this chapter I use a large sample of low-redshift galaxies to study whether there is a connection between bulge-disc properties and single-Sérsic results. Using multi-wavelength bulge−disc decompositions I also study the relationship between bulge and disc properties in order to uncover information about the developmental histories of these galaxies. As in Chapter 3 I first ensure that the recovered properties of my bulges and discs are robust with redshift (Section 5.2.2), before studying the wavelength dependence of n and $R_{\rm e}$ as a function of bulge:total (B/T) flux ratio, in order to determine whether V14's inferences from single-Sérsic fits are consistent with bulge-disc decompositions (Section 5.3.1). I go on to look at the relative colours of bulges and discs for six subsamples (as defined in V14), and what they (and their single-Sérsic colours) can tell us about their likely formation histories (Section 5.3.2). I then explore the relative colours of these components in the context of visual morphological type (Section 5.3.3), before examining trends in physical properties as a function of luminosity (Section 5.3.4).

5.2 Data

As in previous chapters, I use two different volume-limited samples (see Fig. 2.8), which are determined by the the apparent magnitude limit of the GAMA II redshift survey, $r < 19.8$ mag, at two different redshifts. When studying variation in galaxy properties with redshift, a volume-limited sample is taken with $z < 0.3$, $M_r < -21.2$ mag. When studying variation in galaxy properties with absolute magnitude, M_r, a $z < 0.15$, $M_r < -19.48$ mag volume-limited sample is taken. I also use a sample of morphologically classified galaxies from Kelvin et al. (2014) with $M_r < -17.4$ mag and $0.025 < z < 0.06$. The number of objects, and 'strong' bulge and disc components (See section 5.2.1 for my definition of 'strong'), in each sample are given in Table 5.1.

I subdivide my sample by colour and Sérsic index as described in Section 2.4,

	Pre-cleaning	*Strong* bulges	*Strong* discs	*Strong* bulge & *strong* discs
V14	10491	5459	4456	1836
Low-z	4109	2342	1945	966
Vis. Morph.	1013	634	472	264

Table 5.1. Table showing the number of galaxies in each volume-limited sample. V14 sample: $z < 0.3$, $M_r < -21.2$ mag; Low-z sample: $z < 0.15$, $M_r < -19.48$ mag; Vis. Morphology sample: $0.025 < z < 0.06$, $M_r < -17.4$ mag. Cleaning is applied in all bands simultaneously. The *strong* bulge category contains only bulges which are no more than 3 magnitudes fainter than their corresponding disc (and vice versa for the *strong* disc category). '*Strong* bulge & *strong* disc' contains galaxies which have both a bulge and disc within three magnitudes of one another, and are therefore a subset of the previous two categories.

in concordance with Fig. 2.9 of this thesis.

5.2.1 Component selection

In this study I take a liberal attitude to what constitutes a 'bulge', not least because the central component of many of our galaxies is not well resolved. Thus, bars, lenses, pseudo bulges, classical bulges, and their superpositions, are all swept up in this term. My primary aim is to distinguish the extended, thin disc from more centrally concentrated stellar structures. I postulate that the relative properties of these two components are responsible for much of the observed variation in galaxy properties, particularly that correlated with environment. I aim to test this claim in detail in this and future works.

Two-component models have been fit to all galaxies in my sample, regardless of whether they are best modeled as one- or two-component systems. This raises the issue that one of the components may be negligible, in respect of the luminosity or structure of a galaxy. For example, a small fraction of the light from a one-component elliptical galaxy may be attributed to a disc with poorly-constrained properties, without affecting the resulting model image. A further issue is the potential for one component, or both, to be used to fit some features of a galaxy that they are not intended to model; a false disc may help reduce the residuals caused by an isophotal twist in a pure elliptical galaxy, or a false bulge or a bar may attempt to fit to the arms in a spiral galaxy. To avoid considering the properties of insignificant or incorrect components, I have applied a cleaning process. Several cleaning methods are employed in the

literature, including using a logical filter (e.g. Allen et al. 2006), visual inspection (e.g. Kelvin et al. 2012) and likelihood-ratio tests (e.g. Simard et al. 2011). While useful, each of these approaches have their difficulties: visual inspection is subjective and insensitive in certain circumstances, whereas goodness-of-fit tests are often unable to eliminate physically meaningless fits.

In this thesis I take an extremely simple approach and consider the distributions of component properties at face-value. I make no special attempt to remove the objects for which a two-component fit is inappropriate, nor do I substitute single-component measurements in any case. However, I do clean my catalogue of galaxies that may be affected by the constraints imposed on the fit, and hence for which Sérsic profile measurements are unlikely to be meaningful. These criteria are similar to those used in Chapter 3.

I do not consider the poorly-constrained properties of components that make a negligible contribution to the luminosity of their galaxy. From an examination of the fitting results, I choose to ignore components that are more than three magnitudes fainter than their counterpart (i.e. bulges must have at least 6% of the luminosity of the corresponding disc to be considered a trustworthy, and therefore '*strong*' bulge, and vice versa), as in Vika et al. (2014). See Table 5.1 for the number of galaxies deemed to have a *strong* bulge, *strong* disc, or both a *strong* bulge and *strong* disc.

When I use the term 'bulges' throughout this chapter I am referring to all bulges which are no more than 3 magnitudes fainter than their corresponding disc (i.e. this includes lone bulges/ellipticals AND the bulge components of 2-component galaxies). When I use the term 'only *strong* bulges' I am referring to bulges which do not have a significant disc. I similarly use the terms 'disc' and 'only *strong* disc' throughout the chapter.

5.2.2 Robustness of structural properties

In Figures 5.1 and 5.2 I present three-colour (Hzg) images, models and residuals for typical galaxies in my six subsamples to show how well they are fit by single-Sérsic and bulge-disc models respectively. By visually comparing the residuals of Fig. 5.1 with Fig. 5.2 one can see that the bluer objects (particularly the '*green*' high-n and '*blue*' low-n) are slightly better fit by a bulge

and a disc than by a single-Sérsic profile, which indicates that, as expected, these galaxies can generally be thought of as two-component objects. The '*red*' galaxies are well fit by either a single- or two-component model, but adding a second component does improve the residuals. Although the residuals do not all visibly improve in the cases shown, overall the two component fits better represent most galaxies in all subsamples, as indicated by the consistent and contrasting sizes, Sérsic indices and colours of the two components, as shown in this Chapter.

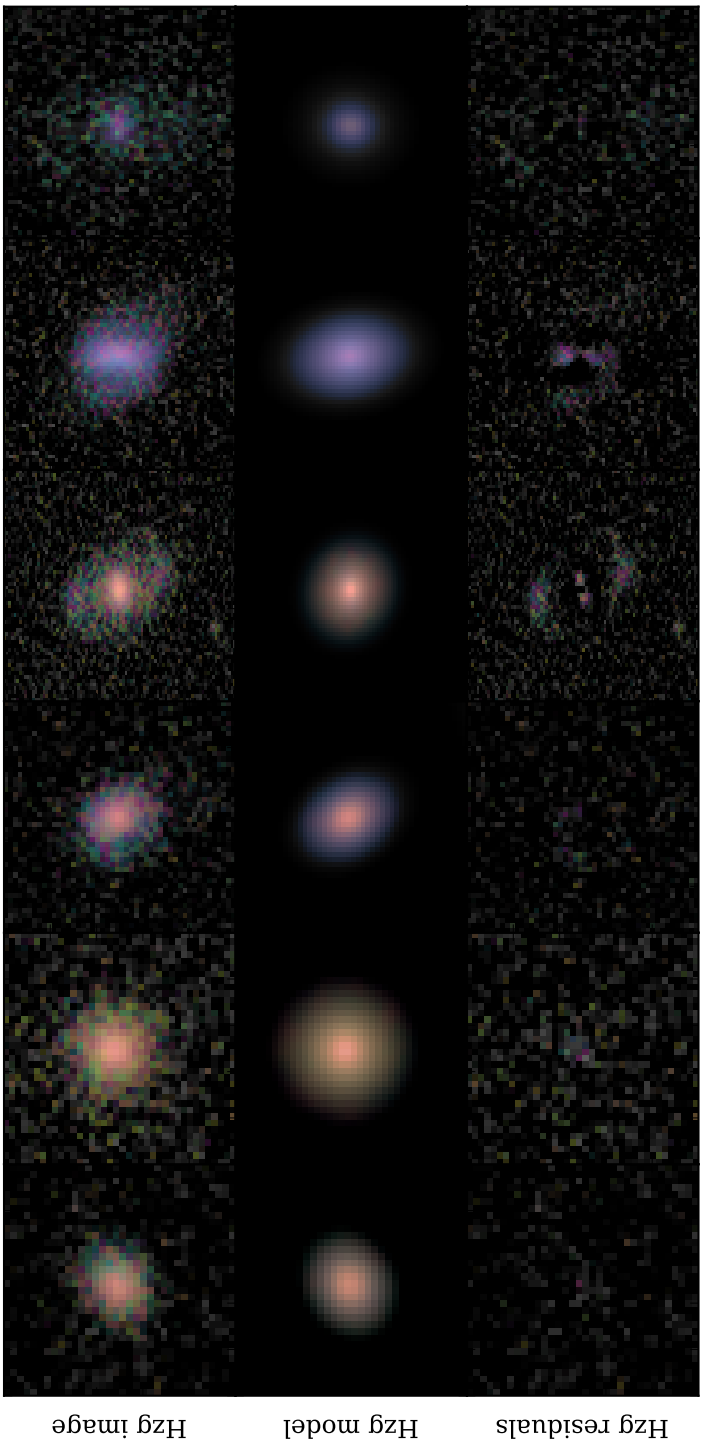

Figure 5.1. *Hzg* image, single-Sérsic model and residuals for an example galaxy in each of my colour/Sérsic index subsamples.

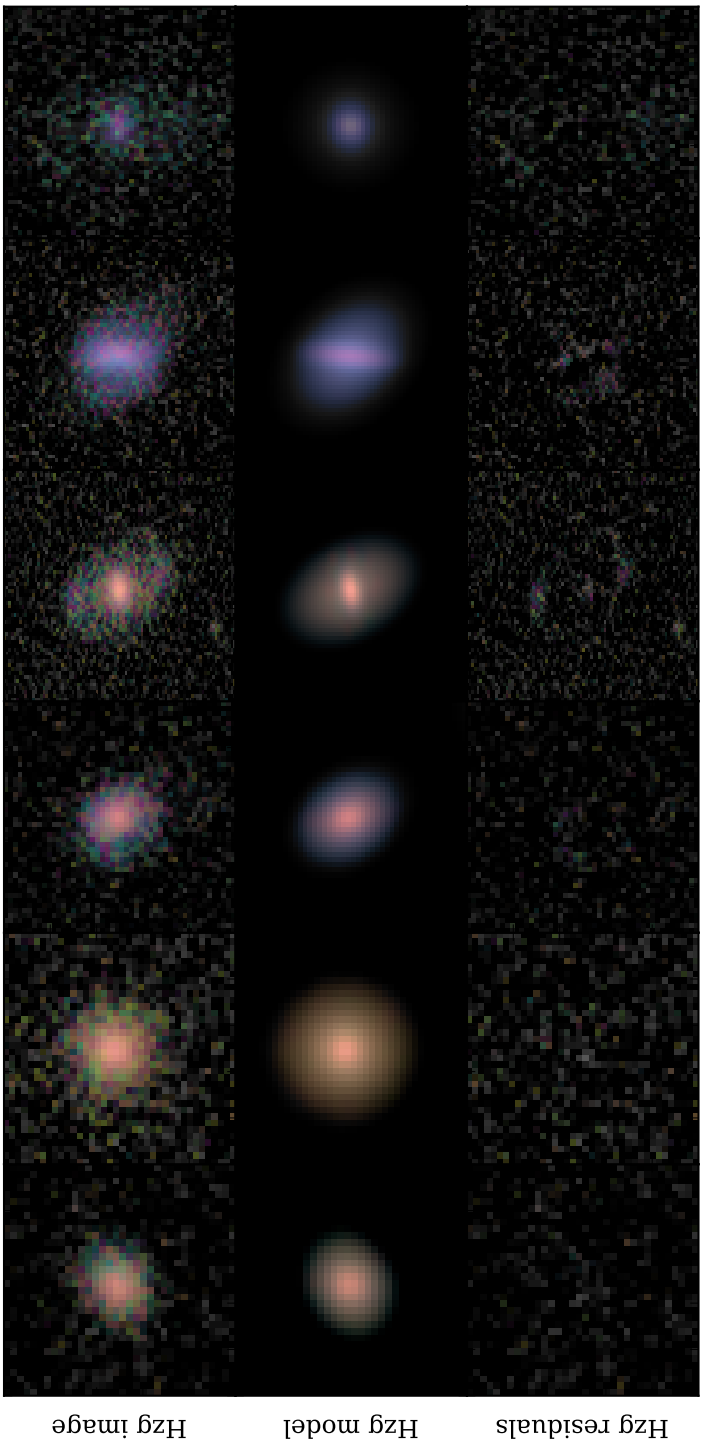

Figure 5.2. *Hzg* image, bulge+disc model and residuals for an example galaxy in each of my colour/Sérsic index subsamples.

Previous tests (Häußler et al., in prep.) have demonstrated that the multi-band fitting used by MegaMorph allows the SEDs of individual bulge and disc components of simulated galaxies to be recovered for even faint objects ($m_r < 20$ mag in the GAMA data). Whereas single-band fitting is prone to recovering the same SED for both the bulge and disc of a given galaxy, MegaMorph's multi-band fitting shows bulges and discs to have different SEDs, even for faint galaxies.

In Chapter 3 I tested the single-Sérsic measurements in my volume-limited samples for trends with redshift, which may arise due to biases with worsening resolution or signal-to-noise ratios. Although I measured small changes in $\mathcal{N}$ and $\mathcal{R}$ with redshift, I found that these were negligible compared to the differences between galaxy samples. Therefore, my results, including the strikingly different behaviour of high- and low-n galaxies, are robust to redshift effects. Here I similarly test the resilience of bulge and disc properties considered in this chapter.

Figure 5.3 demonstrates the redshift dependence of bulge and disc $u-r$ colours. The bulge and disc distributions are distinct in all redshift bins, with bulges typically found to be redder than discs by 0.65 mag. At lower redshifts the colours of bulges and discs become very slightly redder by ~ 0.1 mag, likely due to aging stellar populations and declining star-formation rates over this 2 Gyr timescale. Kolmogorov–Smirnov (KS) tests indicate a significant difference between the colour distribution of both bulges and discs between redshift samples, but these differences can be considered small compared with the width of the distributions. As in Chapter 3, to determine whether an offset between redshift bins can be considered 'small' I sum the standard deviations of the widest and narrowest distributions in quadrature. I then find the difference in the median value of $u - r$ colour in the highest and lowest redshift bins, as a fraction of the summed standard deviation. The offset is 17.5% of the distribution widths, which can be considered small. Furthermore, the colour separation between bulges and discs (shown by a black dashed line) is maintained, strongly supporting the consistency of the decompositions over a wide range of signal-to-noise and resolution. This is remarkable given that the bulges are unresolved for many of the high-z objects (see Fig. 5.5).

I also test the dependence of B/T flux ratio on redshift. Normalised histograms

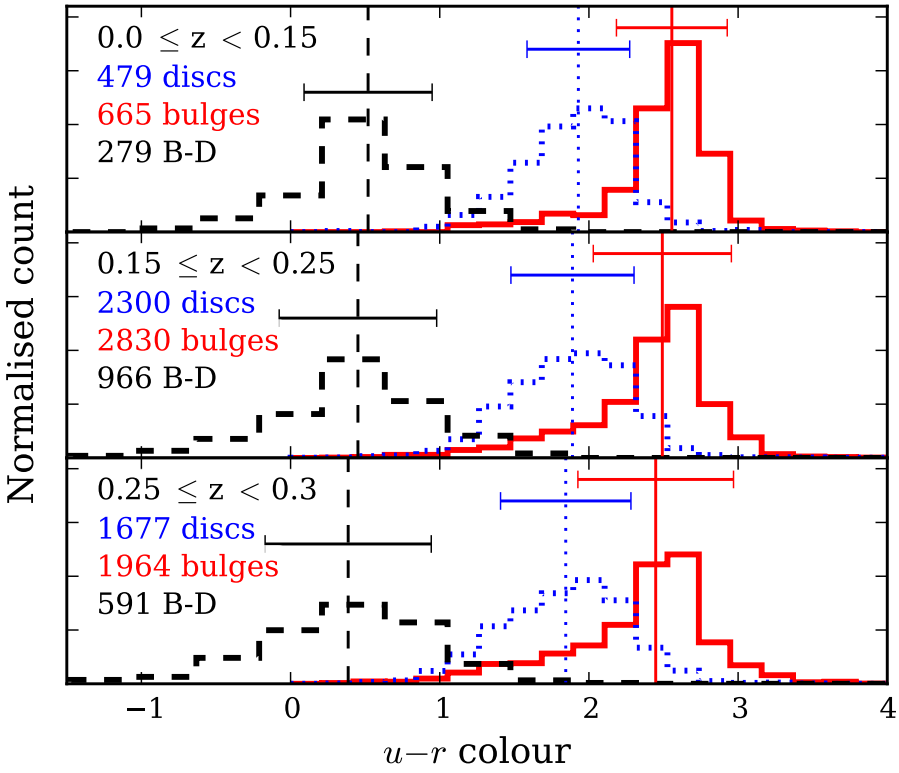

Figure 5.3. The distributions of $u-r$ colour for bulges (red, solid lines) and discs (blue, dotted lines) in the cleaned V14 catalogue. Black dashed lines show $B-D$ colours, i.e. the difference between the $u-r$ colour of the bulge and the $u-r$ colour of the disc in a given galaxy. Each panel is restricted to $M_r < -21.2$ and different redshift ranges, as labelled. Median $u-r$ colours for each distribution are indicated by vertical lines, with standard deviations marked as error bars. Overall, one can see that the difference between bulge and disc colours remains constant regardless of redshift.

can be seen in the upper panels of Fig. 5.4, showing the distribution of B/T for high- and low-n galaxies in three redshift bins. As seen in Chapter 3 for the redshift dependence of galaxy properties, the two highest redshift bins exhibit almost identical trends, whilst the lowest redshift bin shows slightly different behaviour, with more low-n galaxies exhibiting $B/T \sim 0.1$ flux ratios than the $z > 0.15$ samples. It should also be noted that these low-z bins contain far fewer galaxies than the high-z bins.

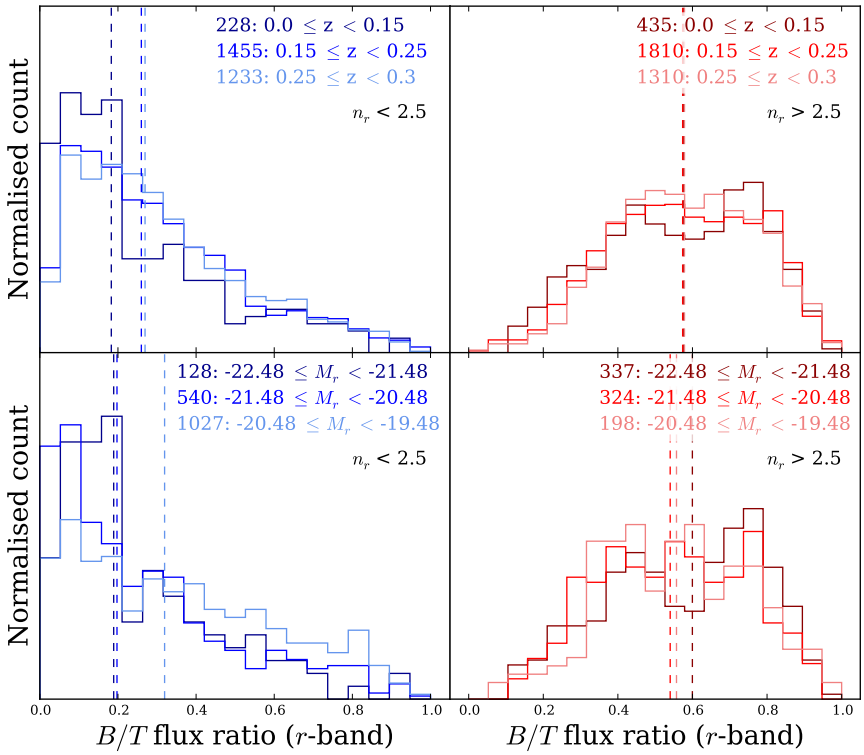

Figure 5.4. Redshift and luminosity dependence of B/T ratio for high- and low-n galaxies. All galaxies which meet my basic cleaning criteria are shown here; this includes discs with very faint bulges, and vice versa, to give an accurate impression of the range of B/T ratios exhibited by the sample. For the majority of galaxies the overall distribution of B/T flux ratios is similar at different redshifts. The B/T flux ratio of high-n galaxies show no significant dependence on luminosity, whereas the brighter the low-n galaxy, the lower its B/T flux ratio.

5.3 Results

To illustrate that the components from my bulge-disc decompositions generally do correspond to the usual notion of 'bulges' and 'discs' I show their n and R_e distributions in Fig. 5.5. By definition the discs have a Sérsic index of 1, whilst bulges adopt a much wider range of Sérsic indices. A large proportion (32%) of the bulges in my low-redshift sample have lower Sérsic indices than discs. This could be due to the largest, brightest galaxies being 'over-fit', or galaxies with faint bulges being wrongly fitted (i.e. some disc light being attributed to the bulge). The presence of bars could also be a factor here; I do not correct for the possible presence of bars in my sample cleaning, which

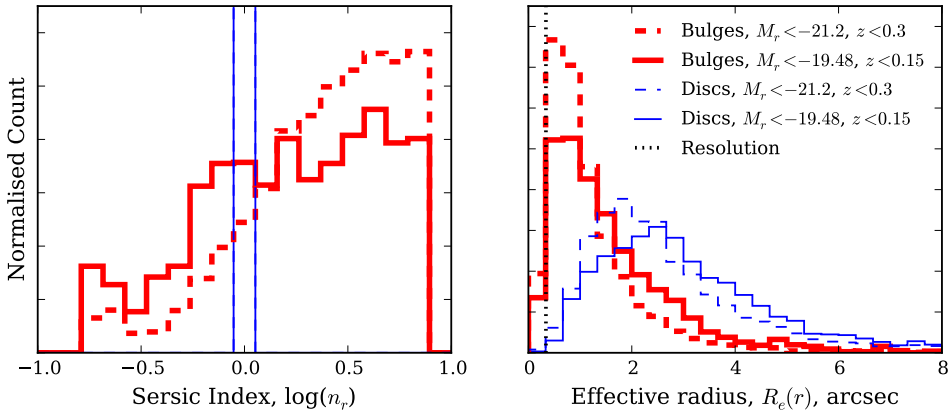

Figure 5.5. n_{galaxy} and $R_{\rm e}(galaxy)$ distributions for bulges (red) and discs (blue) in my 'low-redshift' sample (solid lines) and the V14 sample (dashed lines). The resolution ($R_{\rm e} \gtrsim 1.5$ pixels or 0.339 arcsec) is represented as a vertical dotted line in the right-hand panel.

could have Sérsic indices as low as ~ 0.5 (Aguerri et al. 2005; Laurikainen et al. 2007; Gadotti 2011). Different distributions for the V14 and low-redshift samples are expected, since the two samples cover different magnitude ranges and distances. The behaviour seen in this work does not change significantly depending on the sample used.

The bulges and discs also cover the expected relative values of effective radius; there are few small discs, but many that extend out to large radii, whilst bulges generally have smaller effective radii (in $\sim 90\%$ of cases) and none extend as far out as the largest discs.

To ascertain whether my subsample of $n > 2.5$ galaxies corresponds to bulge-dominated galaxies (i.e. $B/T > 0.5$), I show in Fig. 5.6 the relationship between Sérsic index and B/T flux ratio. Although there is a large scatter, it can be seen that there is a positive correlation between the two properties, implying that we can, to a certain extent, think of high-n galaxies as generally being bulge-dominated, and vice versa.

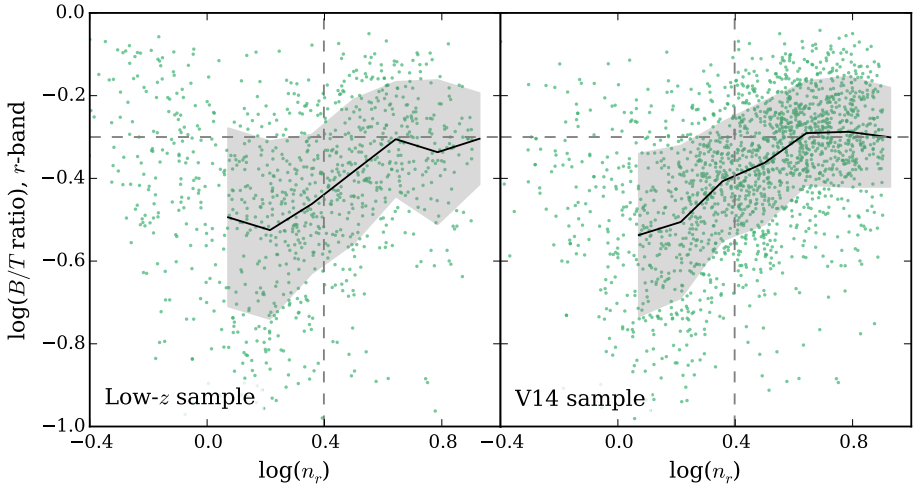

Figure 5.6. The relationship between $n_r(galaxy)$ and B/T for two-component galaxies in the low-z sample (left-hand panel) and the V14 sample (right-hand panel). Overplotted as grey dashed lines are the low-/high-n cut at $n_r = 2.5$, and the division between disc-/bulge-dominated galaxies at $B/T = 0.5$. Solid black lines show the median fitted values whilst the shaded areas show the 1σ dispersion. One can see a positive correlation between B/T and Sérsic index, implying that we can generally think of high-n galaxies as being bulge-dominated, and vice versa.

5.3.1 The wavelength dependence of single-Sérsic models

In this section I compare the general structural parameters of my galaxy sample in order to determine whether the trends seen in V14 and Chapter 3 are supported by bulge-disc decompositions. V14 observed a change in single-Sérsic index with wavelength for low-n galaxies, and suggested that this may be due to the lower Sérsic index of a galaxy's disc being observed in bluer wavebands, and the higher Sérsic index of its bulge being observed in redder wavebands. Similarly, V14 postulates that the small change in $\mathcal{N}$ seen for high-n galaxies may be due to the one-component nature of these objects, while the change in $\mathcal{R}$ seen for this subsample could be due to a number of different stellar populations superimposed on one another, each with a different effective radius.

The wavelength dependence of Sérsic index and effective radius ($\mathcal{N}$ & $\mathcal{R}$) vs. B/T

In Fig. 5.7 I show the relationships between $\mathcal{N}$ and $\mathcal{R}$ versus the relative luminosity, colour and size of the bulge and disc. Galaxies for which I have *strong* measurements of both the bulge and disc (grey points) are distinguished from those with only a *strong* disc (blue points) or only a *strong* bulge (red points). See Section 5.2.1 for more details on this selection of '*strong*' galaxy components. In Fig. 5.7(a) I show the relationship between $\mathcal{N}$ and r-band bulge-to-total ratio, B/T. From the arguments in V14 one would expect that galaxies with a high B/T (and particularly bulge-only galaxies) will display $\mathcal{N} \sim 1$, as they are dominated by a single component, containing one population of stars. Panel (a) confirms that galaxies with $B/T \gg 0.5$ exhibit $\mathcal{N} \sim 1$, albeit with some scatter. Furthermore, V14 anticipate that galaxies with two roughly equal components, corresponding to $B/T \sim 0.5$, should have $\mathcal{N} > 1$, as a result of the higher Sérsic index bulge becoming more dominant at redder wavelengths. This is also supported by bulge-disc decompositions. However, a deviation from the predictions of V14 comes with disc-dominated systems (with low B/T). Such galaxies were expected to exhibit $\mathcal{N} \sim 1$, because they are dominated by a single component. However, on the contrary, they consistently display high values of $\mathcal{N}$. The wavelength dependence of Sérsic index appears to depend not on whether a system has one or two components, but whether or not a significant disc is present.

Note that there are some galaxies with only a *strong disc* which appear to have high B/T flux ratios, and some galaxies with only *strong* bulges which have low B/T flux ratios. Such cases arise when the second component is rejected due to the cleaning criteria in section 2.1. The classification of a *strong* component requires a disc to be no more than three magnitudes fainter than its corresponding bulge, or vice versa. This translates to the luminosity of that disc being no less than 6% of the luminosity of the corresponding bulge. Hence, it is possible to have galaxies containing *strong* bulges with $B/T > 0.06$, or *strong* discs with $B/T < 0.94$, but which do not contain two strong components due to the other being discarded where a component has been discarded due to cleaning criteria detailed in section 5.2.1.

Similarly, the relationship between $\mathcal{R}$ and B/T ratio can be seen in panel

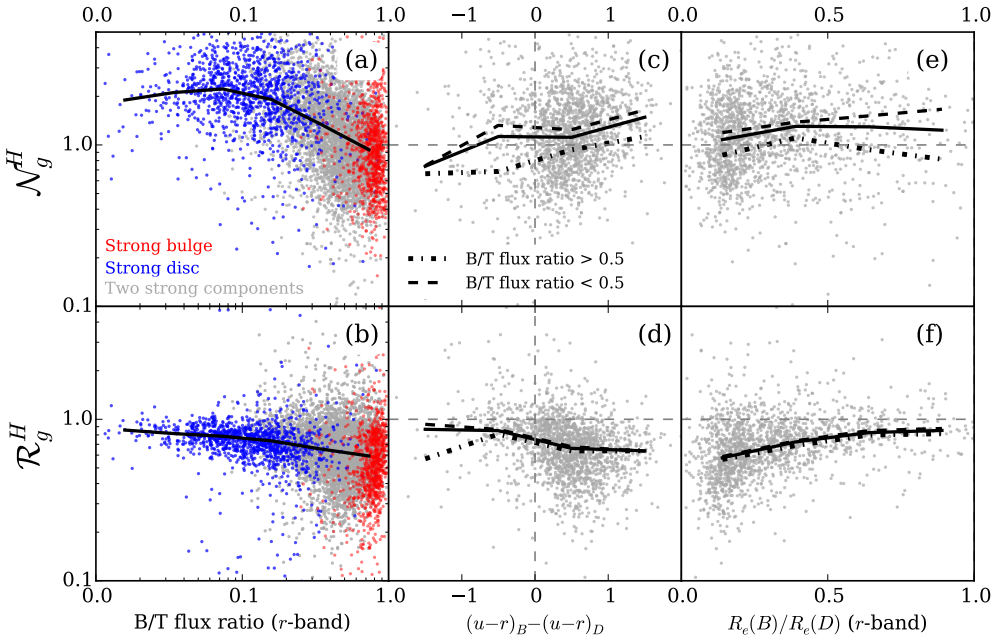

Figure 5.7. Upper panels show variation in Sérsic index with wavelength; lower panels show variation in effective radius with wavelength, for the V14 volume-limited sample. Overlaid in black on each panel is the median $\mathcal{N}$ or $\mathcal{R}$ trend for the whole sample. Panels (a) & (b) show the relationship between $\mathcal{N}$ and $\mathcal{R}$ vs B/T flux ratio in the r-band; grey points show galaxies that exhibit both a bulge and disc of similar magnitudes; red points show galaxies that have only *strong* bulges; blue points show galaxies that have only *strong* discs (see section 5.2.1 for more on this definition). See section 5.3.1 for an explanation of why there are some '*strong* bulge' galaxies with low B/T and vice versa. Panels (c) & (d) show $B-D$ colour difference, whilst panels (e) & (f) show the bulge:disc size ratio. The dashed lines in these panels show the median for galaxies with a B/T flux ratio > 0.5, whilst the dot-dash lines show the median for galaxies with a B/T flux ratio < 0.5. The wavelength dependence of n gives a more reliable indication of a galaxy's internal structure than $\mathcal{R}$, and galaxies with similarly coloured components exhibit a weaker dependence on $\mathcal{R}$ than galaxies in which the bulge is redder than its corresponding disc. Also note that there appears to be little dependence of $\mathcal{N}$ on B/D size ratio, however there is a stronger correlation with $\mathcal{R}$; as expected, the smaller the size ratio, the stronger the wavelength dependence of $R_{\rm e}$.

(b) of Fig. 5.7. As seen in Chapter 3, most galaxies display $\mathcal{R} < 1$, such that they appear smaller in the H-band than the g-band. Bulge-dominated systems exhibit the largest departures from unity, but also the largest scatter. This corresponds with the results for high-n galaxies from V14. Galaxies with a $B/T \lesssim 0.2$ are disc-dominated and are likely to correspond to V14's low-n galaxy samples. Panel (b) of Figure 5.7 shows that these galaxies, as in V14, have $\mathcal{R}$ closer to one than their high B/T counterparts; their radii change less with wavelength.

From these trends we are able to estimate the likelihood of a galaxy having a bulge and/or disc at a given value of $\mathcal{N}$. In Fig. 5.8 I show the percentage of galaxies at a given $\mathcal{N}$ which have $B/T < 0.25$, $0.25 < B/T < 0.75$ or $B/T > 0.75$. Although galaxies with $B/T > 0.25$ can be present at all values of $\mathcal{N}$, one can see that galaxies with prominent discs (i.e. $B/T < 0.25$) account for more than half the population at $\mathcal{N} \gtrsim 2$, while less than 10% of the population beyond $\mathcal{N} \sim 2$ have $B/T > 0.75$. I have included in the lower panel of Fig. 5.8 a black dashed line showing the percentage of $B/T < 0.5$ galaxies in the sample over the range of $\mathcal{N}$. It can be seen that at $\mathcal{N} \gtrsim 0.9$ ($\gtrsim 2$) we expect 50% (80%) of our population to be disc-dominated. One can therefore use $\mathcal{N}$ to determine how likely it is that a given galaxy has a prominent disc, although selecting galaxies in combination with the Sérsic index in a single band would be most effective (see Vika et al. 2015).

$\mathcal{N}$ & $\mathcal{R}$ vs B-D colour difference and B/D size ratio

In addition to their relative luminosity, one would expect other aspects of the bulge and disc to influence the overall wavelength dependence of galaxy structure. If the two components have strongly contrasting colours, then the relative dominance of overall structural parameters should vary dramatically with wavelength. In cases where a galaxy's Sérsic index is larger in redder wavelengths we will see $\mathcal{N} > 1$, and vice versa. Similarly, $\mathcal{R} > 1$ means a galaxy appears smaller at redder wavelengths. Panels (c) and (d) of Fig. 5.7 shows $\mathcal{N}$ and $\mathcal{R}$ versus the difference between the $u - r$ colours of bulge and disc, where both components are well-constrained. As the colour difference widens (in the typical sense of the bulge being redder than the disc), $\mathcal{N}$ and $\mathcal{R}$ do depart further from unity: galaxies exhibit peakier (higher-n) and smaller

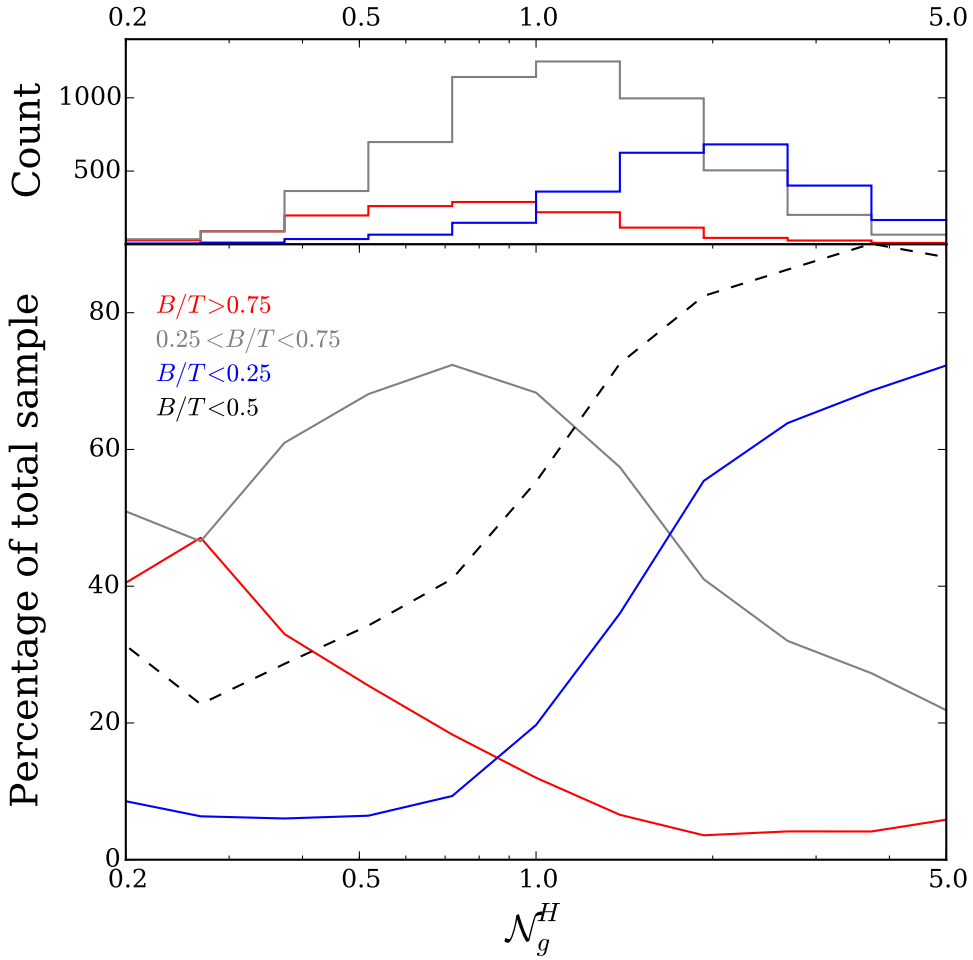

Figure 5.8. Upper panel shows blue, grey and red histograms giving the number of $B/T < 0.25$, $0.25 < B/T < 0.75$ and $B/T > 0.75$ galaxies respectively, for bins of $\mathcal{N}$. The lower panel shows what percentage of the whole population lies in each B/T subsample at a given value of $\mathcal{N}$. We also show with a black dashed line the percentage for $B/T < 0.5$ galaxies over the range of $\mathcal{N}$. The corresponding $B/T > 0.5$ line would be a mirror image of this, and has therefore been omitted from this plot. One can see that although it would be difficult to determine whether a galaxy has a prominent bulge using $\mathcal{N}$, we can see that above $\mathcal{N}_g^H \sim 1$ more than half the galaxies have prominent discs, or $B/T < 0.25$.

profiles at longer wavelengths.

Similarly, the relative sizes of the bulge and disc should affect the structural behaviour. Panels (e) and (f) of Fig. 5.7 demonstrate the relationship between $\mathcal{N}$ and $\mathcal{R}$ versus the ratio of bulge and disc size, $R_{\rm e}(B)/R_{\rm e}(D)$, in the r-band. In panel (e) one can see that the relative size of bulge and disc has little or no effect on $\mathcal{N}$.

There is, however, a positive correlation in panel (f); galaxies with smaller $R_e(B)/R_e(D)$ display a stronger wavelength dependence of single-Sérsic effective radius. This appears to meet expectations: the more pronounced the difference in the size of the bulge and disc, the greater the overall decrease in size from blue to red.

There are two particularly interesting aspects of these results. Firstly, the trends of $\mathcal{N}$ versus $B-D$ colour difference and size ratio are offset for different B/T, while for $\mathcal{R}$ they are very similar. Thus, $\mathcal{N}$ is dominated by the effect of B/T, while $\mathcal{R}$ appears to be driven by the relative size and colour of an extended 'disc' component, irrespective of its relative luminosity.

Secondly, bulge-only systems lie at values of $\mathcal{R}$ associated with the largest bulge−disc colour contrast. This is consistent with trends in overall colour: galaxies with larger bulge−disc colour difference or larger B/T tend to be redder in overall colour (see Fig. 5.9). This matches the findings of V14, in that red, high-n galaxies display a dependence of size on wavelength that is stronger than bluer, more disc-like galaxies. Drawing on the literature, V14 postulate that this behaviour is the result of accretion, preferentially to the galaxy outskirts via minor mergers, of younger or more metal-poor stars. In the case of our bulge-disc decompositions, the blue outskirts implied by the single-Sérsic fits of red, high-n galaxies are either too faint to be constrained or modelled by an extended blue disc. For most cases where a disc is significantly detected, it must be associated with the usual thin disc of spiral galaxies. However, fascinatingly, the same trends in $\mathcal{R}$ and $\mathcal{N}$ continue to galaxies where the disc is no longer discernible.

	μ_B	σ_B	μ_D	σ_D	μ_{B-D}	σ_{B-D}
Red, low-n	2.56	0.46	1.94	0.29	0.54	0.53
Red, high-n	2.54	0.27	2.05	0.38	0.46	0.42
Green, low-n	1.84	0.54	1.54	0.27	0.35	0.68
Green, high-n	1.94	0.49	1.61	0.42	0.34	0.63
Blue, low-n	1.44	0.54	1.25	0.30	-0.01	0.72
Blue, high-n	1.30	0.61	1.45	0.82	-0.24	0.79

Table 5.2. The median colour of bulges (μ_B) and discs (μ_D) in Fig. 5.9, the median $B-D$ colour difference (μ_{B-D}), and the standard deviations on these values (σ_B, σ_D, σ_{B-D}).

5.3.2 Colour distributions for bulges and discs

I have previously presented the colour distributions for bulges and discs in Fig. 5.3. As anticipated, these two components display distinct colour distributions. To draw more meaningful conclusions from the bulge and disc $u-r$ colours of galaxies in my sample, and to allow meaningful comparison with the single-Sérsic work presented in V14, we must study the same subsamples with the added detail of our bulge-disc decompositions. Figure 5.9 shows the $u-r$ bulge and disc colours, and the colour difference of the two components ($B-D=(u-r)_b-(u-r)_d$), for galaxies divided by Sérsic index and colour. Median colours are overlaid as dashed lines, and are given in Table 5.2. As the overall galaxy $u-r$ colour moves from red-green-blue, bulges and discs become closer in colour. For red, low Sérsic index galaxies there is a narrower peak of blue discs compared to the wider distribution of redder bulges. For blue galaxies, the peaks of the bulge and disc distributions overlap, although the relative widths of the distributions are consistent with those of red and green galaxies.

The $B-D$ colours, plotted in black, show that the redder the overall galaxy, the greater the difference between the colour of the disc and the bulge. Blue galaxies show a wider distribution of $B-D$ colours, but the peak is very close to 0, showing that these blue galaxies tend to have bulges and discs with similar colours.

The bulges and discs of high Sérsic index galaxies have distributions with similar widths to one another. The bulges and discs also follow the low Sérsic index trend of becoming closer in colour the bluer the overall galaxy is.

The observation that bulges are consistently redder than their associated discs for the majority of our sample could imply that the formation histories of these two components are linked; rather than all bulges being intrinsically red and all discs being intrinsically blue, we see a colour difference within a given galaxy.

To assess whether the trends seen here could be due to dust, I show in Figure 5.10 the colour distribution of bulges and discs for face-on ($q_r > 0.9$) galaxies and edge-on galaxies ($q_r < 0.35$) alongside the whole population. One can see that the trends seen here are also present in Figure 5.9, which suggests that whilst the inclination effects of dust act to redden the components of edge-on galaxies, this is not driving the B-D trends.

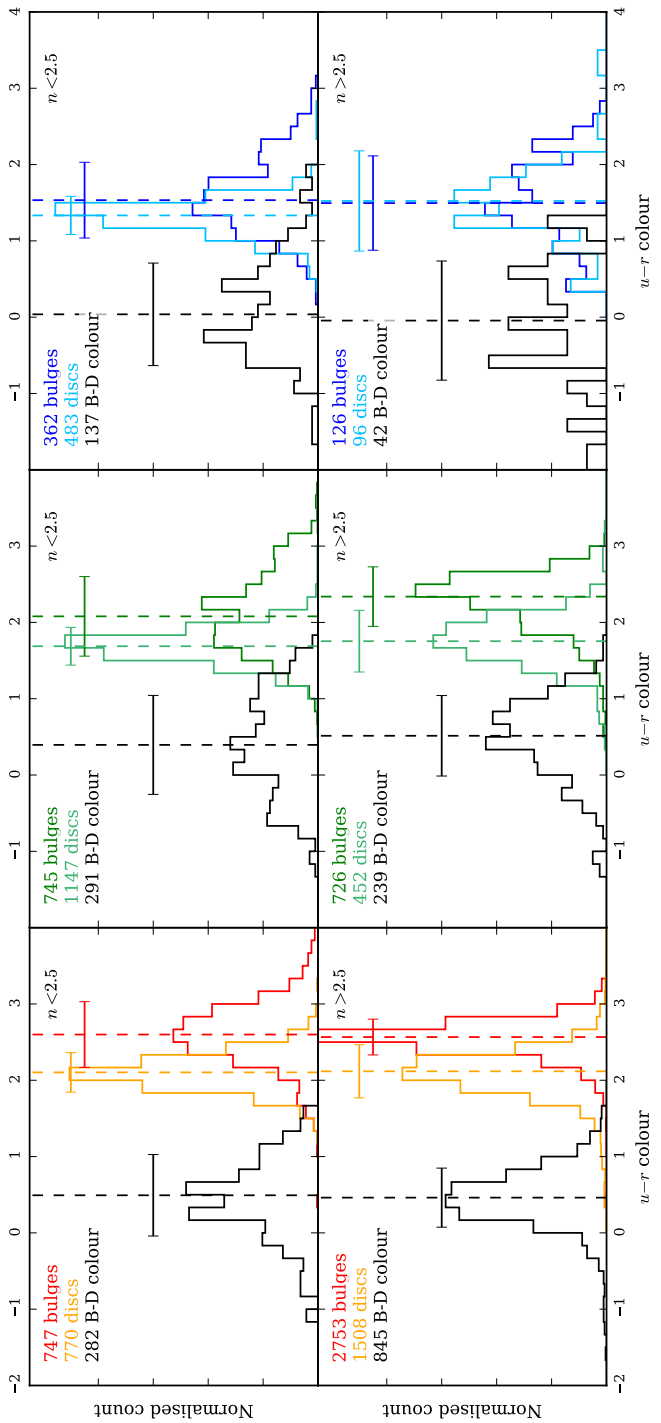

Figure 5.9. Normalised histogram showing the relative colour distributions of the bulges and discs of a volume-limited sample of $M_r < -21.2$, $z < 0.3$ galaxies, binned by single Sérsic index and overall galaxy colour, defined as follows: $u-r > 2.1 = red$, $1.6 < u-r < 2.1 = green$, $u-r < 1.6 = blue$. The $B-D$ colour (i.e. the difference between the $u-r$ colour of the bulge and the $u-r$ colour of the disc within a given galaxy) is plotted in black, with negative values indicating a redder disc than bulge, and positive values indicating a redder bulge than disc. The median $B-D$ colour is plotted as a vertical black dashed line, and the standard deviation of each sample is plotted in the corresponding colour. See Table 5.2 for exact values. Bulges are generally redder than their overall discs, and this colour difference correlates with the overall colour of the galaxy; the bluer the galaxy, the closer the colours of these two components.

5.3.3 Bulge and disc colour distributions with galaxy type

In the analysis of Fig. 5.9 I made assumptions about the connection between the populations seen in these figures and the subsamples used in V14 (i.e. that red, high-n galaxies correspond to our usual notion of elliptical galaxies, whilst we think of the 'green' low-n population as late-types). To assess how robust my assumptions are, in Fig. 5.11 I plot the $u - r$ colour of galaxies binned according to their morphological classifications for the low-z sample. These classifications are presented in Kelvin et al. (2014), and are a sample of 3727 galaxies with $M_r < -17.4$ and in the redshift range $0.025 < z < 0.06$, taken from the GAMA survey and visually classified into E, S0-Sa, SB0-SBa, Sab-Scd, SBab-SBcd, Sd-Irr and 'little blue spheroid' classes.

Elliptical galaxies have a similar $u - r$ colour difference to red galaxies of both low- and high-n (as expected). Barred galaxies tend to show a smaller B-D colour difference than comparable non-barred galaxies. This trend has been studied by papers that do bulge-disc-bar decomposition (Barazza, Jogee & Marinova 2008; Weinzirl et al. 2009; Masters et al. 2010). It most likely appears because the free Sérsic function that is supposed to fit the bulge is fitting both the bulge and the bar (De Geyter et al. 2014); consequently the stellar population of the bulge appears to be more blue that it actually is (Peng et al. 2002; Sánchez-Blázquez et al. 2011). It is also interesting to note that, when naïvely fitting a bulge and a disc to all galaxies in my sample, even galaxies that have been visually classified as 'elliptical' appear to contain both a *strong* bulge and disc. This phenomenon has been seen before; Naab & Burkert (2001) show that most ellipticals have evidence of a disc component containing $\sim$ 10-20% of the luminosity of the elliptical component. Huang et al. (2012) show that bright, nearby elliptical galaxies can be well-fitted with three exponential components of different sizes, whilst Krajnovic et al. (2013) find kinematic evidence for discs in early-type galaxies.

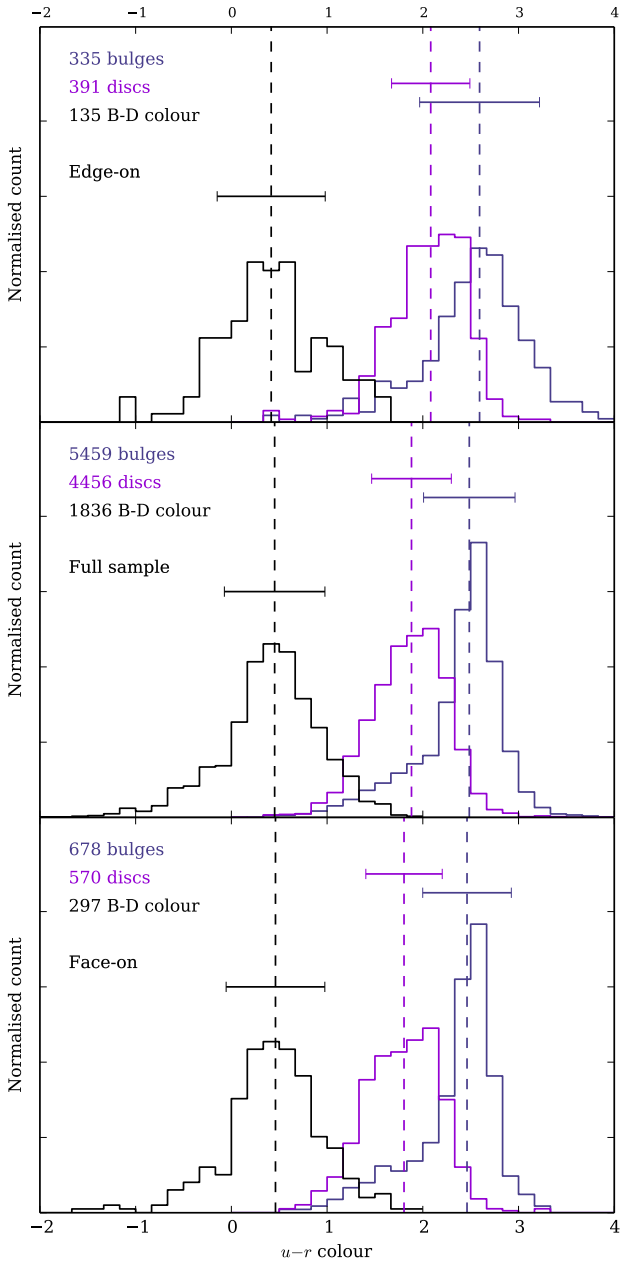

Figure 5.10. Face-on only ($q_r > 0.9$), edge-on only ($q_r < 0.35$): Normalised histograms showing the relative colour distributions of the bulges and discs of a volume-limited sample of $M_r < -21.2, z < 0.3$ galaxies, for edge-on galaxies (top panel), face-on galaxies (bottom panel) and the whole sample (middle panel). The trends seen here are also present in Figure 5.9, which suggests that whilst the inclination effects of dust act to redden the components of edge-on galaxies, this is not driving the B-D trends.

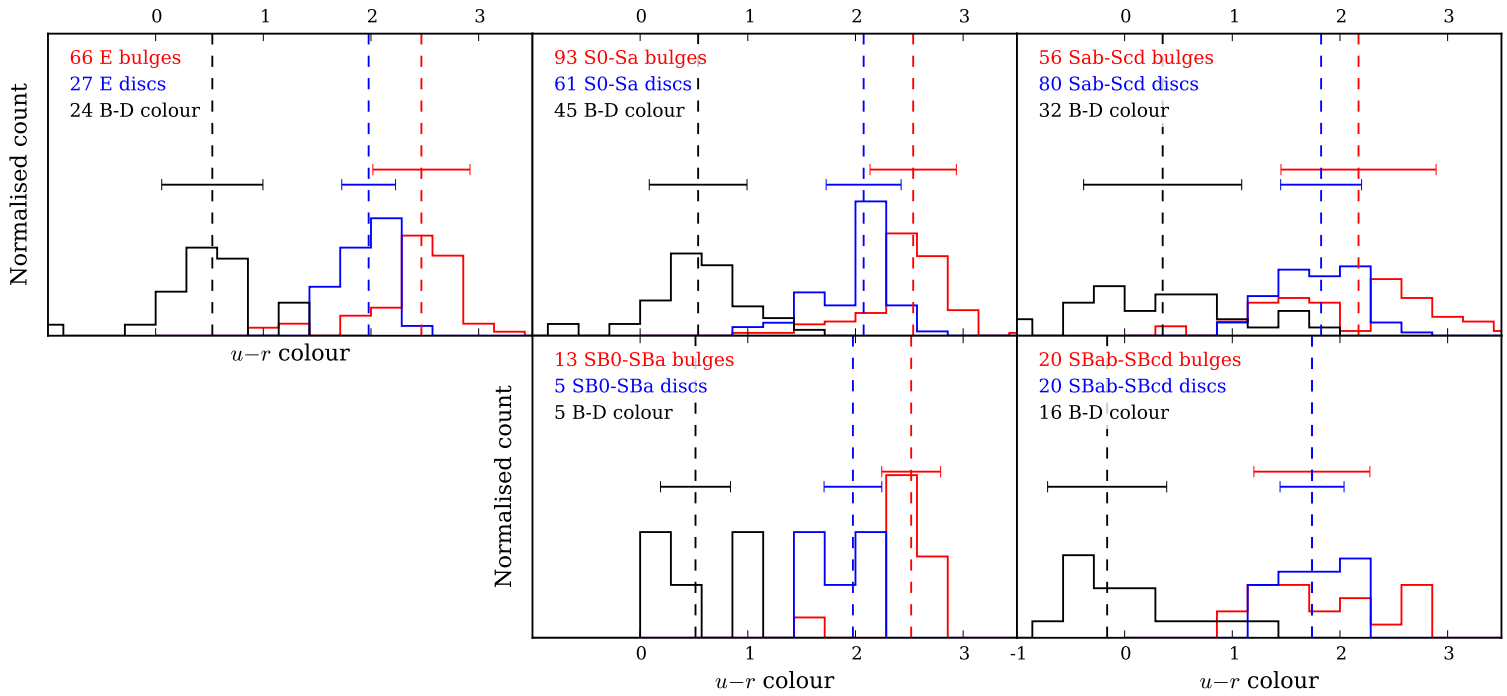

Figure 5.11. Normalised histogram showing the relative colour distributions of the bulges and discs of a volume-limited sample of $M_r < -19.48, z < 0.15$ galaxies, binned by visual morphology (visually classified by Kelvin et al. 2014). The $B - D$ colour is plotted in black, with negative values indicating a redder disc than bulge, and positive values indicating a redder bulge than disc. The median $B - D$ colour is plotted as a vertical black dashed line. The majority of galaxies have a bulge which is redder than its corresponding disc, irrespective of visual morphology. Even galaxies which have been visually classified as elliptical can show this $B - D$ colour difference.

5.3.4 Luminosity dependence of bulge and disc properties

Studying the luminosity dependence of bulge & disc colours and flux ratios gives us insight into the physical properties of our sample. The lower panels of Fig. 5.4 show normalised histograms of B/T flux ratio for my three magnitudes bins. For $n_r > 2.5$ I do not see a significant difference in the B/T flux ratio distribution with magnitude. In the $n_r < 2.5$ panel, however, we see a change in shape of the distribution with magnitude; the distribution of the brightest galaxies appears slightly 'peakier' around $B/T \sim 0.1$ than for fainter galaxies. The observation that the brighter galaxies are more disc-dominated is not necessarily surprising, as we could be seeing proportionally more star formation; bright low-n galaxies are predominantly discy, whereas the faint low-n population can include low-mass spheroids.

Figure 5.12 shows the luminosity dependence of bulge and disc $u - r$ colours for high- and low-n samples. Low-n systems experience a change in bulge and disc colour with luminosity; the fainter the galaxy, the closer in colour the bulge and disc appear, and the bluer the galaxy overall. High-n galaxies see a similar, although less pronounced, trend. It is interesting to note that in all populations the colours of the discs are comparatively unchanged by luminosity, whereas the bulges get significantly bluer (by up to 0.7 mag, in the case of low-n galaxies). A certain amount of the trends seen for fainter galaxies may be influenced by the fitting process; because the galaxies are so faint, the components cannot be as easily separated and therefore some properties of the bulge may be interpreted as that of the disc and vice versa. This will be explored further in Häußler et al. (in prep.).

5.4 Discussion

In this chapter I have presented multi-band bulge-disc decompositions for a sample of 10491 galaxies and tested that key quantities (B/T and colours of bulge and disc) are robust to the effects of redshift. These decompositions have been used to study how bulge and disc properties relate to the structural behavior measured using wavelength-dependent single-Sérsic models. I have

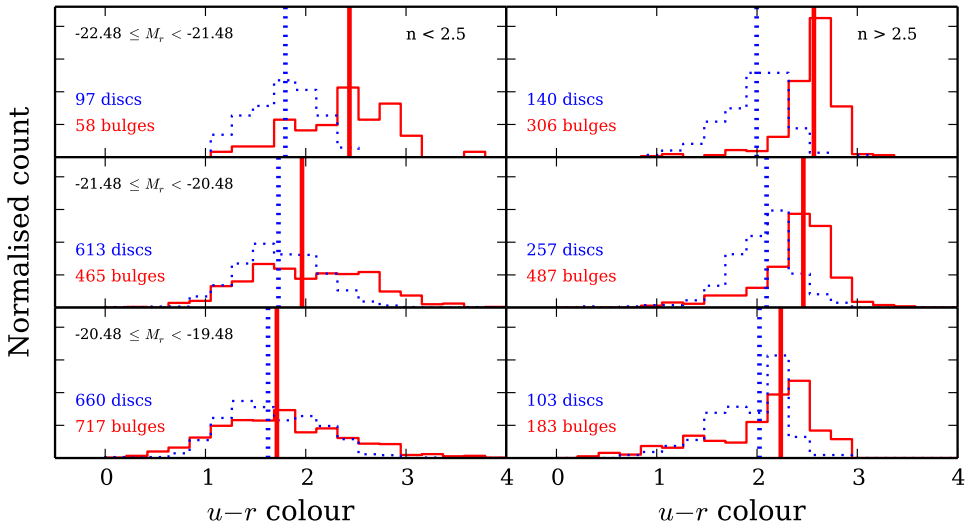

Figure 5.12. Luminosity dependence of bulge and disc colours, plotted as red solid lines and blue dotted lines respectively. Median $u-r$ colours for each sample are overlaid as thicker vertical lines. Left- and right-hand panels show low- and high-n galaxies respectively. Both the high- and low-n populations show a trend of fainter galaxies appearing to be bluer in overall colour.

then focused on how the relative colours of bulges and discs vary with overall galaxy properties.

5.4.1 Comparison of observed trends of $\mathcal{R}$ and $\mathcal{N}$ with other studies

The wavelength dependence of single-Sérsic structure was measured by V14, and summarised in terms of the fractional variation in Sérsic index and effective radius between the g- and H-bands, which I denote $\mathcal{N}_g^H$ and $\mathcal{R}_g^H$.

To recap, a value of unity for $\mathcal{R}$ and $\mathcal{N}$ means that a galaxy appears to be the same size, and has the same Sérsic index, between g- and H- wavebands. If $\mathcal{R} < 1$, as in the majority of galaxies, that object will appear larger in bluer wavebands. Conversely, in the more unlikely case in which $\mathcal{R} > 1$, a galaxy would appear bluer in the centre and redder at larger radii. The variation in Sérsic index with effective radius, $\mathcal{N}$, is greater than unity in cases where a galaxy's Sérsic index is larger (more 'peaky') in redder wavelengths, and smaller ('flatter') in bluer wavelengths. The reverse is true for $\mathcal{N} < 1$ galaxies.

I find that the different $\mathcal{N}$ and $\mathcal{R}$ distributions of high- and low-n galaxies can

be attributed to specific trends in the relative luminosity, colour and size of their constituent bulges and discs. Members of the high-n galaxy population are generally more bulge-dominated, and have $\mathcal{N}$ closer to unity. However, while these galaxies are often considered uniformly-red, single-component systems, I find they display $\mathcal{R}$ substantially below unity: their effective radii are much smaller at longer wavelengths. The decompositions attribute this to the presence of an extended, bluer, component, at least reasonably described by an exponential profile. Dullo & Graham (2013) and Graham, Dullo & Savorgnan (2015) have revealed that many local, massive galaxies are in fact lenticular galaxies with large 2D discs rather than spheroids with large 3D envelopes. In some cases the presence of a disc, including spiral features, may be visually confirmed. In the remaining cases, the extended component may be a faint disc or more spherically distributed material, although the trends in the properties of this component, as well as $\mathcal{N}$ and $\mathcal{R}$, with B/T suggest some continuity in its origin. The properties of these discs are consistent with what is seen in studies of kinematics (e.g. Emsellem et al. 2011; Krajnović et al. 2011 and references therein).

The low-n galaxy population is dominated by discs, i.e. low B/T, which we have found to be consistently associated with $\mathcal{N} > 1$, even in the case of apparently disc-only systems. This population also displays $\mathcal{R}$ somewhat closer to unity, as a result of less pronounced differences in the colours and sizes of their bulge and disc components.

The luminosity dependence of $\mathcal{N}$ versus $\mathcal{R}$ in Chapter 3 can be understood as primarily due to lower-luminosity galaxies (at a given B/T or n) having closer bulge and disc colours, and hence $\mathcal{N}$ and $\mathcal{R}$ closer to unity. The variation in $\mathcal{N}$ and $\mathcal{R}$ with overall colour in V14 mainly appears to result from the correlation between colour and luminosity; the more luminous galaxies tend to have a greater difference between their bulge and disc colours, which results in a greater change in structural properties with wavelength.

5.4.2 Comparison of observed trends of component colours with other studies

I remind the reader that in this study I have applied a bulge-disc decomposition to all galaxies in my sample, regardless of whether there is a physical need for two components. I have done this primarily to avoid building a dichotomy into my results, but this has also resulted in some interesting observations, in particular the sample of visually classified ellipticals seen in Fig. 5.11 which have *strong* discs associated with them. I do, however, apply a cleaning algorithm to distinguish between potentially unnecessary components and eliminate bulges which are significantly fainter than their corresponding disc (and vice versa). See section 5.2.1 for more details. The purpose of this cleaning is to avoid considering the properties of components that make an insignificant contribution to the galaxy light.

My analysis has shown that the redder and more luminous a galaxy, the greater the difference between the colour of its bulge and disc. Hudson et al. (2010) have performed bulge-disc decompositions simultaneously in B and R bands for ~ 900 galaxies in nearby clusters, and find that the reddest (and brightest) galaxies have a larger gap between bulge and disc colours. Although I find a small dependence of disc colour on magnitude in my low-n population, this effect is minimal compared to the strong dependence of bulge colour on magnitude, which is also consistent with the findings of Hudson et al. (2010). In agreement with this, Head et al. (2014) also observe a greater difference between bulge and disc colours for brighter objects in their sample of $S0$ galaxies.

Regardless of visual morphology I see that bulges are consistently redder than their associated discs; Lackner & Gunn (2012) (and references therein) find that discs around classical bulges are redder than lone discs or discs around pseudo-bulges, which supports our observation that bulge and disc colour are correlated.

The work of Peletier & Balcells (1996), however, suggests that the colour variations from galaxy to galaxy are much larger than the colour differences observed between the bulges and discs of individual galaxies, for a small sample of inclined, bright, early-type spirals. This is somewhat at odds with my work, which suggests that the overall colour of a galaxy is driven by the relative

colours of the bulge and disc. Nonetheless, Peletier & Balcells (1996) find a $B-D$ colour, $\Delta(U-R)$, of 0.126 ± 0.165, which (within error) is consistent with both my study and Cameron et al. (2009).

By looking at the colours of bulges and discs, we can infer their star formation histories and eventual quenching. The negative colour gradients seen in the majority of galaxies (as studied in Chapter 4; also see Prochaska Chamberlain et al. 2011; Roediger et al. 2011 and references therein) tells us that older, redder stars tend to lie in the central, collapsed regions of galaxies, whilst the (rotationally supported) outskirts of a galaxy are generally dominated by younger, bluer stellar populations. On average over my six subsamples, bulges are 0.285 mag redder than their corresponding discs, and are indeed smaller and more concentrated. With my detailed analysis, however, I am able to see that this mean magnitude difference is a combination of the larger and smaller B-D colour differences seen in *red* and *blue* populations respectively, and has a significant dependence on luminosity.

5.5 Summary

I remind the reader that in this work we fit a bulge and disc (n = free and $n = 1$ respectively) to all galaxies in my sample. I make no attempt to remove objects for which a 2-component fit is inappropriate, nor do I substitute single-Sérsic measurements in these cases. I do, however, remove bulges which are more than 3 magnitudes fainter than their corresponding discs, and vice versa (see section 5.2.1 for more details). I also note that I use the terms 'bulge' to refer generally refer to the central component of a galaxy (thus, bars, lenses, pseudo bulges, classical bulges, and their superpositions, are all swept up in this term), whilst I use 'disc' to refer to a more extended component with an exponential light profile.

- The difference between bulge and disc colours of both high- and low-n galaxies remains constant regardless of redshift (see Fig. 5.3). The overall distribution of B/T flux ratios is similar at different redshifts, with perhaps a slightly higher proportion of low-z galaxies appearing to be disc-dominated in the lowest redshift bin.

- $\mathcal{N}$ & $\mathcal{R}$ (single-Sérsic wavelength dependence) give us information about a galaxy's bulge and disc properties (see Figs. 5.7 and 5.8):
  - The wavelength dependence of Sérsic index, $\mathcal{N}$, indicates whether an object is likely to contain a disc; $\mathcal{N}$ >1 ⇒ likely to have a disc present, $\mathcal{N}$ <1 ⇒ bulge-dominated galaxy
  - The wavelength dependence of $R_{\rm e}$ is a less effective classifier of structure than $\mathcal{N}$. Little change in $R_{\rm e}$ with wavelength suggests that a disc is present, whereas more change in $R_{\rm e}$ with wavelength suggests that the galaxy could be bulge-dominated.
  - A strong wavelength dependence of n is correlated with a redder B-D colour, i.e. a larger difference between the colour of the bulge and the colour of the disc.
  - Irrespective of the B/T flux ratio of the system, galaxies with similarly coloured components exhibit a weaker dependence of $R_{\rm e}$ on wavelength than galaxies with a bulge redder than its disc.
  - For the entire V14 sample I see little dependence of $\mathcal{N}$ on B/D size ratio. However, once I split the sample into bulge-dominated and disc-dominated galaxies (B/T flux ratio >0.5 and B/T flux ratio <0.5, respectively), I see that the disc-dominated galaxies show an increase in $\mathcal{N}$ with B/D size ratio, whilst the bulge-dominated population decreases in $\mathcal{N}$ with increasing B/D size ratio.
  - The relative size of the bulge and disc have little effect on $\mathcal{N}$, but there is a correlation with $\mathcal{R}$; as one would expect, galaxies with a smaller $R_e(B)/R_e(D)$ display a stronger wavelength dependence of single-Sérsic effective radius.
- Bulges are generally redder than their associated discs (see Fig. 5.9), regardless of the overall galaxy colour or Sérsic index. The bulge and disc are closer in colour for galaxies that are bluer in overall colour. Rather than all bulges being red and all discs being blue, there appears to be a colour difference within a given galaxy. For example, the median colour of *green* high-n bulges is actually bluer than the median colour of *red* high-n discs, which is what one might expect if bulges in bluer galaxies are likely to be younger, perhaps including a pseudo-bulge element.

- Regardless of morphology, the majority of galaxies exhibit a bulge that is redder than its corresponding disc (see Fig. 5.11). This is particularly interesting in the case of galaxies that have been visually classified as ellipticals, yet still appear to have a *strong*, comparatively blue, disc component.

- For the low-n population, brighter galaxies exhibit a lower B/T flux ratio, whereas the high-n population shows no significant change in B/T with luminosity (see Fig. 5.12). Bulges and discs get closer in colour for fainter galaxies (regardless of n). For both high- and low-n populations, the fainter the galaxy, the bluer its overall colour.

Chapter 6

Stellar Populations

6.1 Overview

In this chapter I consolidate the results of previous chapters by comparing colour information to the predictions of a stellar population model.

The colour of a galaxy is closely linked to the intrinsic properties of its stellar populations. As described in section 1.5, there are three main variables which can influence the observed color of a galaxy: dust, age and metallicity. In this thesis I have frequently divided galaxies into six subsamples, defined by colour and Sérsic index cuts. I will therefore begin by exploring the nature of these subsamples in terms of the age and metallicity of their stellar populations. In Chapter 3 I demonstrated that, although dust goes some way to explaining the trends seen in the wavelength dependence of Sérsic index and effective radius, the intrinsic properties of the underlying stellar populations must be the driving factor. In Chapter 4 I showed that the behaviour of structure with wavelength could be considered in terms of colour gradients, and in Chapter 5 I showed that the results in previous chapters could be better understood by considering the colours of bulges and discs. From this we can gain a more physical understanding of the contrasting properties of bulges and discs, as well as how they vary with overall galaxy type. In this chapter I therefore begin by looking at the properties of galaxies in each of my colour/Sérsic index subsamples to ascertain whether previous inferences are reasonable, before studying the stellar populations of the bulge and disc components within these

galaxies.

6.2 Data

As in previous chapters, I use the V14 volume-limited sample of galaxies for which we have both single-Sérsic fits and bulge-disc decompositions. The age and metallicity data used in this chapter has been derived through stellar population synthesis modelling of broadband optical (*ugriz*) photometry from our GALFITM fits. The photometry for the single-Sérsic, bulge, and disc components are each modelled independently. The modelling was kindly performed by Ned Taylor using the methods described in Taylor et al. (2011), which uses the Bruzual & Charlot (2003) stellar evolution models, assuming a Chabrier (2003) stellar initial mass function (IMF) and the Calzetti et al. (2000) dust curve, with exponentially declining star formation histories. The SPS models used in the fitting are defined via four output parameters, including the two parameters considered in this chapter: *i*-band luminosity-weighted mean stellar age, and stellar metallicity. As a starting point, in this study I naïvely assume that the results of the fitting procedure are a reasonable match to the star formation history of each bulge, disc or galaxy. Future work will be able to delve deeper into the variation in stellar populations within each component.

6.3 Results

In previous chapters I speculated as to the likely nature of the stellar populations within each of my six subsamples. Here I study this in more detail, using age and metallicity. Due to the relationship between age and metallicity described in Section 1.5, I will discuss them together in this chapter.

6.3.1 Do age and metallicity measurements support the distinction between the colour/Sérsic index subsamples?

In Chapters 3-5 I discussed how my six subsamples, divided by colour and Sérsic index, could be considered to represent different types of galaxies with different stellar populations. Galaxies with a low-n profile were found to have a stronger dependence of Sérsic index on wavelength than high-n galaxies, whilst the reverse was observed for the wavelength dependence of effective radius. I concluded that the low-n population appeared to be dominated by discs, whist the high-n population was dominated by bulges. This holds true when looking at bulge:total flux ratio within these galaxies, and when studying the wavelength dependence of n and $R_{\rm e}$.

To discover whether these inferences agree with stellar population models averaged over the galaxy as a whole, I show in Figures 6.1 and 6.2 the distribution of ages and metallicities (respectively) from the single-Sérsic photometry for each for each subsample. We can see that the *red* galaxies (represented in orange for the low-n, and red for the high-n populations) are both older and more metal-rich than the bluer subsamples, thereby in agreement with the inferences described above. To re-iterate: the populations previously thought of as bulge-dominated are indeed older (by approx. 3.5 Gyr on average) and more metal-rich than the bluest galaxies, which points to their formation having occurred in a deep potential well. The *green* high- and low-n subsamples have low metallicities consistent with the *blue* low-n population, which was selected in order to separate out the bluest star-forming galaxies. This implies that the *green* populations formed in discs, in much the same way as the *blue* low-n population, but they are older. The *blue* high-n population is both young ($\sim$ 1.2 Gyr) *and* metal-rich, which is consistent with recent star bursts having occurred in the centre of these galaxies, or in mergers in which material is already metal-rich.

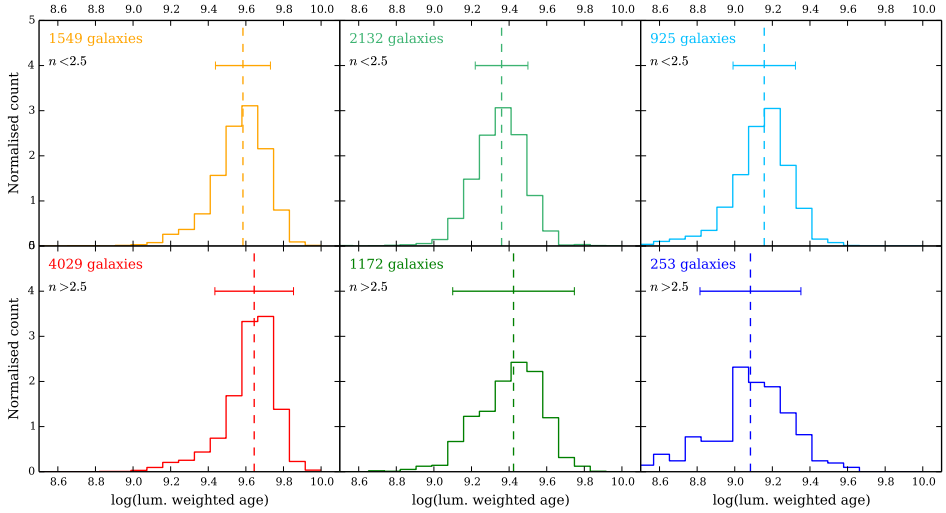

Figure 6.1. Age histograms for the six subsamples. Colours are as in previous plots, representing the colour/Sérsic index subsamples described previously. The median value of each subsample is plotted as a dashed line, with the standard deviation shown as a horizontal error bar.

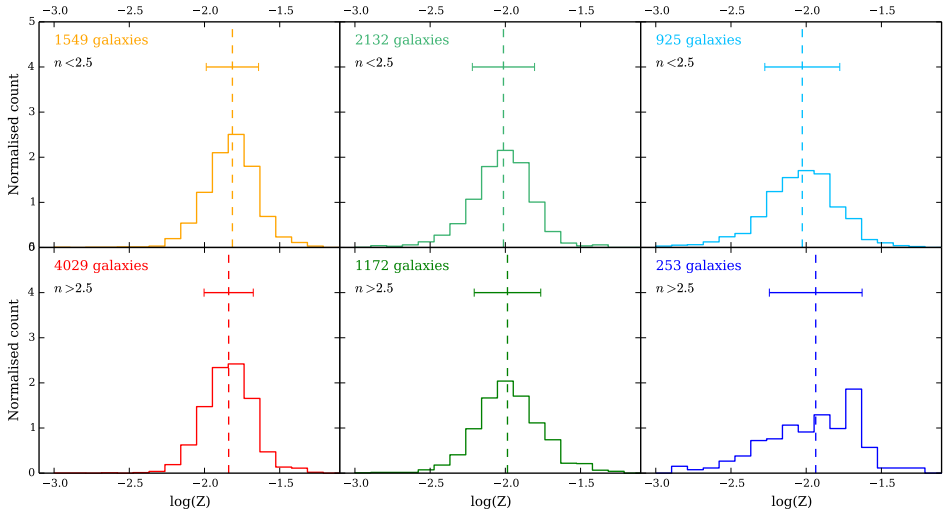

Figure 6.2. Metallicity histograms for the six subsamples. Colours are as in previous plots, representing the colour/Sérsic index subsamples described previously. The median value of each subsample is plotted as a dashed line, with the standard deviation shown as a horizontal error bar.

6.3.2 Bulge & disc age

In Figure 6.3 I study the ages of bulges and discs in each colour/Sérsic index subsample. It can be seen here that the oldest bulges ($\sim$ 4 Gyr) reside in the *red* high-n galaxies, which is consistent with them being bulge-dominated systems. The youngest discs reside in the *blue* low-n population, which is consistent with them being young starburst galaxies.

Figure 6.3 also allows us to compare the ages of bulges and discs in each subsample. *Green* galaxies have bulges and discs with very similar age distributions, which implies that both the bulge and disc in these two-component systems formed at similar times. Conversely, *red* galaxies show a greater difference in their bulge and disc age distributions; the bulges are consistently older than their associated discs in high-n galaxies, whilst the inverse is true for low-n galaxies. We have previously inferred that a large number of these high-n objects are likely to be a large spheroid component with a faint disc, which formed later through accretion of either gas or lower-mass galaxies in wet or dry minor mergers. In principle we could distinguish between these two origins using the ages and metallicities of the discs (see Section 1.3.2). The bulges of *red*, low-n galaxies are similar in age to the bulges of *green* low-n galaxies, but their associated discs are older. This implies that the bulges of *red* low-n galaxies continued to grow via continued star formation for a period after their discs have quenched. This seems at odds with the usual inside-out picture of galaxy formation (see section 1.3.2). It is, however, consistent with the growth of pseudo-bulges from residual gas reservoirs in the centres of galaxies, perhaps fed by bar instabilities and/or wet minor mergers. This result also agrees with spectroscopic studies which find that the bulges of some S0 galaxies are in fact younger than their discs (e.g. Johnston, Aragón-Salamanca & Merrifield 2014; Tabor et al. 2017).

Blue galaxies show contain the youngest components in the sample. The colour cut which defines the *blue* subsample was chosen in an attempt to isolate starburst galaxies, which are undergoing an intense phase of star formation. Here we can see that these galaxies are young throughout, with low-n galaxies displaying discs which are slightly younger than their bulges.

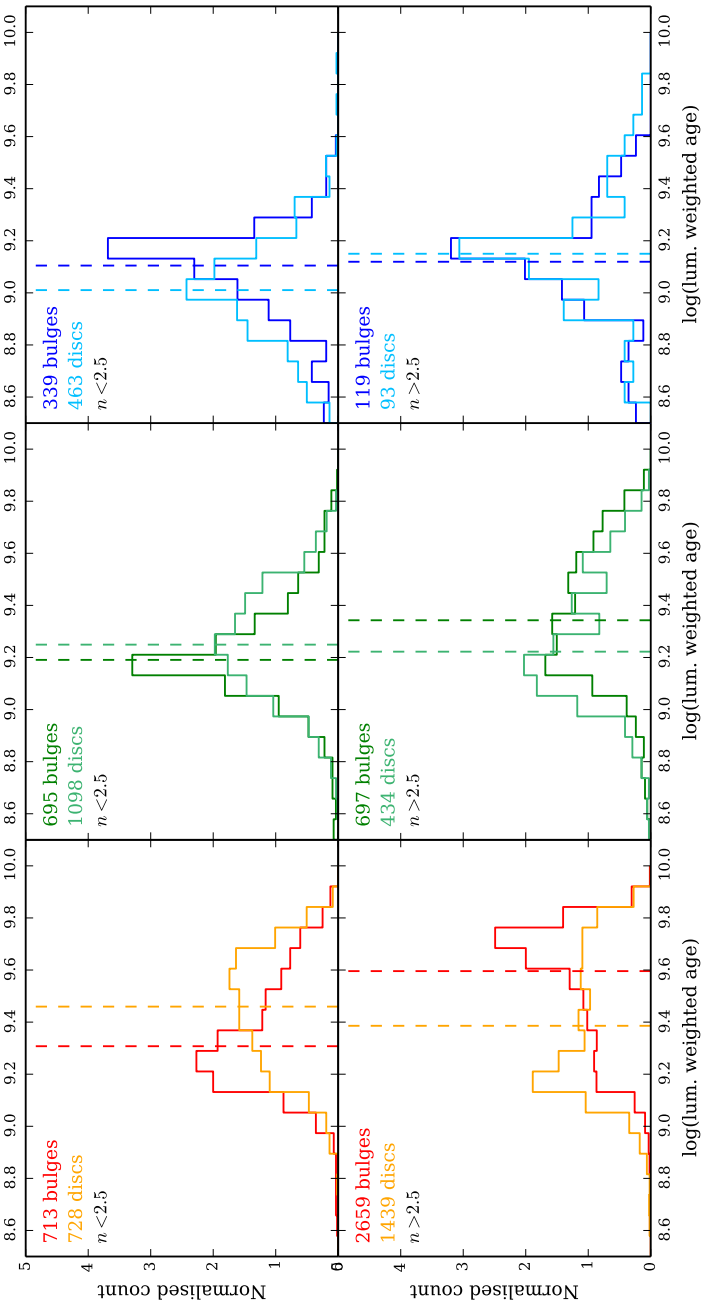

Figure 6.3. Age histograms for bulges and discs in each of the six subsamples. Colours are as in previous plots, representing the colour/Sérsic index subsamples described previously. The median value of each subsample is plotted as a dashed line, and the distribution of the entire V14 volume-limited subsample is shown in black, with the median value plotted as a solid vertical black line.

6.3.3 Bulge & disc metallicity

Figure 6.4 shows the distribution of bulge and disc metallicities for galaxies in each subsample. Bulges are more metal-rich on average than discs in every subsample, but this difference between bulges and discs is more pronounced in low-n galaxies, with significantly different bulge and disc distributions. The consistent, high metallicities of bulges point to their stellar populations forming from self-enriched gas in deep potential wells. The distribution of disc metallicities is much wider than the distribution of bulge metallicities in all subsamples, which is consistent with multiple disc formation mechanisms, as previously discussed in section 1.3.

Although in section 6.3.2 they were found to be relatively old, the discs of *red* galaxies are more metal-poor than the bulges of these galaxies, with a wide distribution. This is to be expected if these discs are in fact the accreted remnants of lower-mass (and less metal-rich) galaxies.

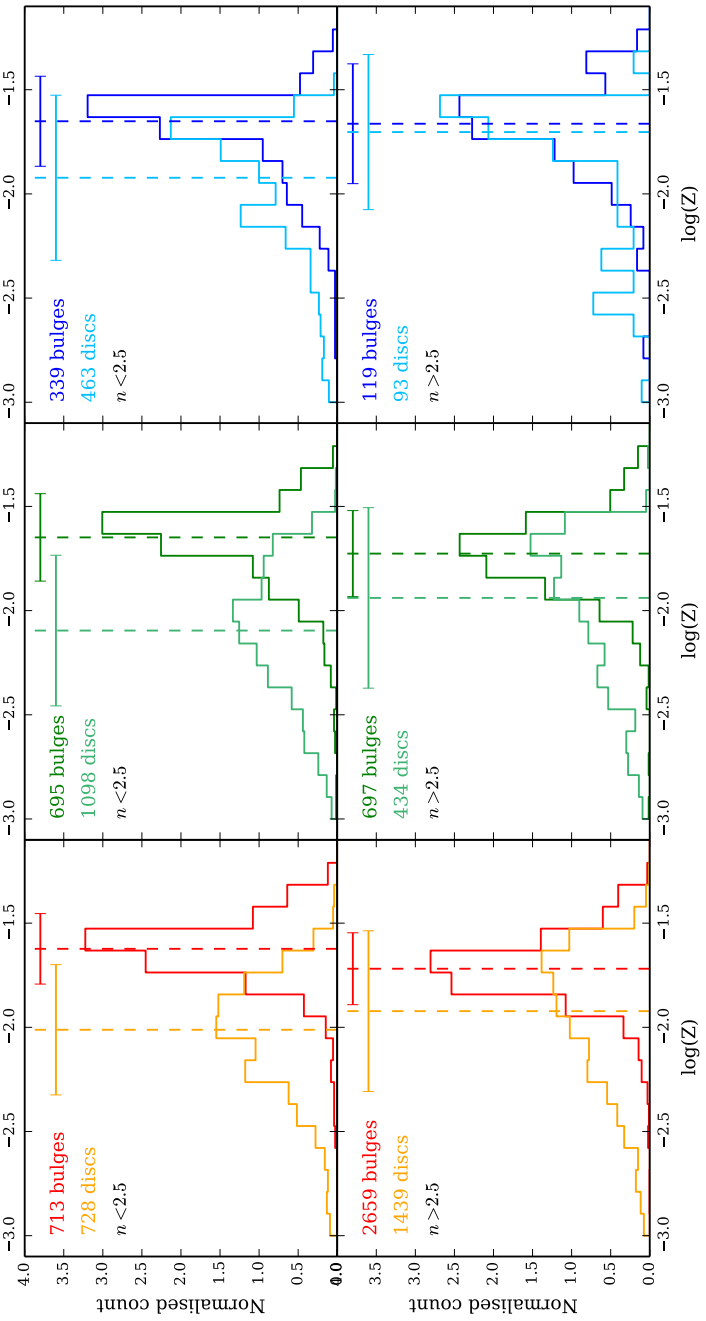

Figure 6.4. Metallicity histograms for bulges and discs in each of the six subsamples. Colours are as in previous plots, representing the colour/Sérsic index subsamples described previously. The median value of each subsample is plotted as a dashed line, and the distribution of the entire V14 volume-limited subsample is shown in black, with the median value plotted as a solid vertical black line.

Age vs. metallicity

The joint distribution of age vs. metallicity for bulges and discs in each subsample is shown in Figure 6.5. The difference in the properties of bulges and discs is clear: old discs are found to be metal-poor, whilst old bulges are metal rich. This difference in metallicity with age reflects the different environments in which these two populations formed.

At all times, stars formed in spheroids have their metallicity enhanced by self enrichment in a "closed-box" environment (see Pagel & Patchett 1975 and references therein). Discs, on the other hand, reflect the metallicity of their gas supply, since the metals produced by star-formation are more easily ejected. At earlier times, discs contain a high fraction of newly accreted gas, containing only the lightest elements. Stars formed in early discs are therefore also relatively metal poor. At later times gas accretion slows and discs become more dominated by gas which has been enriched by previous generations of star-formation (see e.g. Tonini et al. 2017 and references therein). Another possible contributing mechanism responsible for this is the migration of older stars towards the centre of the disc over time, and continued metal-poor gas accretion into the outskirts of the disc.

In previous chapters I have discussed the presence of discs in *red* high-n galaxies, which were previously thought to be elliptical galaxies. Using MegaMorph has allowed us to see that, when naïvely fitting a bulge *and* a disc to every galaxy, even the *red* high-n population is found to have 'meaningful' discs associated with their bulges. Figure 6.5 shows us that these discs follow the same age–metallicity trends as the discs in other subsamples, thus supporting the idea that these are 'real' structures that have either accreted from minor mergers, or are the faded remnants of a galaxy's original disc.

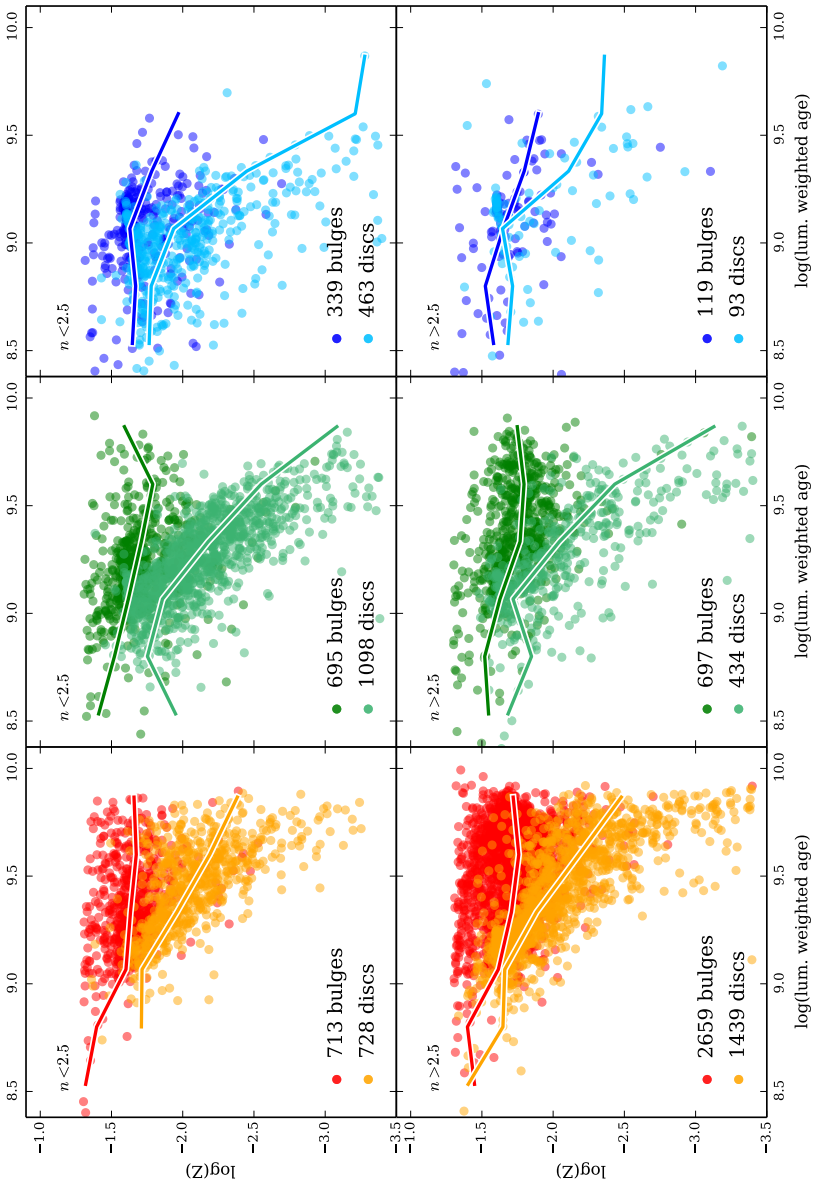

Figure 6.5. Age vs metallicity for bulges and discs in each of the six subsamples. Colours are as in previous plots, representing the colour/Sérsic index subsamples described previously. The median is overplotted.

6.4 Discussion

In Section 5.3.2 I showed that regardless of the overall Sérsic index and colour of the galaxy in which a bulge and a disc reside, there is a colour difference between those two components: in a given galaxy, the bulge is likely to be redder than its associated disc. With the application of stellar population models used in this chapter, we can begin to untangle the source of this colour difference. We can see in Figures 6.3 and 6.4 that this colour difference, particularly in low-n galaxies, is mostly driven by a metallicity difference between the bulge and the disc, which can be seen more clearly in Figure 6.5.

Two particularly interesting populations are the *blue* high- and low-n samples; these galaxies show very close bulge and disc colours, but different ages and metallicities for each component. Looking at the absolute ages of the bulges and discs in these populations, we see that while the bulges are of a similar (but slightly younger) age to those in other subsamples, the discs are *significantly* younger, and also more metal-poor. We previously chose the *blue* colour cut in an attempt to isolate the bluest star-forming galaxies in the sample, which may contain star bursts, and this analysis shows that a) this subsample does indeed contain the youngest stellar populations within the sample, and b) the recent star formation in these galaxies occurs in their discs. We can infer from this information that the bulges in these galaxies formed slightly later than the rest of the galaxy population, and the stellar populations in the discs formed later still. It should be noted, however, that a recent burst of star formation is able to 'mask' older stellar populations, resulting in a skew towards a younger and less metal-rich observation.

I surmised in section 6.3.3 that the diverging metallicity with age for bulges and discs (i.e. old bulges are metal rich, old discs are metal-poor) demonstrates their differing formation histories. Discs in all six subsamples also show a much wider distribution of metallicities than bulges, which is consistent with simulations (e.g. Snaith et al. 2016). The presence of 'strong' discs even in the *red*, high-n subsample indicates that, rather than these just being the outer part of a single spheroid structure, we are detecting real disc components which formed from the accreted remnants of smaller galaxies, or originated from low-metallicity accreted gas. These results highlight the discriminatory

power of the MegaMorph multi-band decompositions, and demonstrate the value of performing these decompositions equally for all galaxies.

This foray into the ages and metallicities of galaxies in this study answers a number of questions, and raises many more to be investigated in future work.

Chapter 7

Summary and further work

In this thesis I have studied measurements of the wavelength dependence of galaxy structure in order to understand the mechanisms by which today's galaxies formed and evolved. In this chapter I will discuss the significance of my results in the context of contemporary studies, and what implications this has for the field of galaxy evolution.

The results of my analysis are summarised as follows:

- The structural properties of galaxies and their components can be reliably measured out to a redshift of 0.3 (lookback time of ~ 3.5 Gyr) using MegaMorph techniques on SDSS+UKIDSS imaging.
- Dust opacity and varying inclination can account for features in the joint distribution of $\mathcal{R}$ and $\mathcal{N}$ for late-type galaxies. However, these factors alone cannot explain the highest values of $\mathcal{R}$ and $\mathcal{N}$; the bulge-disc nature of galaxies must also contribute to the wavelength dependence of their structure.
- There is a bimodality in the luminosity dependence of colour gradients. This is due to the superposition of many different galaxy populations dominating the distribution at different luminosities.
- The ubiquity of strong negative colour gradients supports the picture of inside-out growth through gas accretion for blue, low-n galaxies, and through dry minor mergers for red, high-n galaxies. An exception is the

blue high-n population, which has properties indicative of dissipative major mergers.

- The presence of a disc drives the wavelength dependence of a galaxy's structure.
- The colours of bulges and discs within a given galaxy are linked; the redder the bulge, the redder the disc, and vice versa. This interdependency implies a shared formation history, the potential study of which is described in Section 7.2.
- The relative ages and metallicities of galaxy components shows that bulges and discs formed through different mechanisms and over different time scales.
- A large number of *red* high-n galaxies host significant discs, which are likely to be faded 'traditional' discs, or accreted material.

7.1 Discussion

By observing the wavelength dependence of galaxy structure we can uncover how galaxies may have formed and evolved.

Previous studies have attempted to use colour gradients to glean information about the stellar population gradients of both early- and late-type galaxies. Whilst the technique of measuring colour gradients by laying down ellipses at different radii (see e.g. La Barbera et al. 2010a) has its merits as a non-parametric method, it cannot reveal the internal structure of galaxies in the same way as studying the wavelength dependence of n and $R_{\rm e}$.

A strong correlation has been found between the wavelength-dependent properties of galaxies and their internal structure; in particular, Vulcani et al. (2014) find that low-n galaxies have a much stronger wavelength dependence of Sérsic index than high-n galaxies. They find that the joint wavelength dependence of Sérsic index and effective radius ($\mathcal{N}$ vs $\mathcal{R}$) could potentially be an effective classifier of bulge-disc systems.

However, before an inference is made about the relationship between galaxy structure and the wavelength dependence of its parameters, it is important

to consider other possible causes. In Chapter 3 I observe some change in $\mathcal{N}$ and $\mathcal{R}$ with luminosity; the sizes of bright high-n galaxies have a stronger wavelength dependence, whilst low-n galaxies statistically show no trend in $\mathcal{R}$. For all populations (although it is more pronounced for low-n galaxies) the brightest galaxies show the highest values of $\mathcal{N}$. Although I do see a luminosity dependence for $\mathcal{N}$ and $\mathcal{R}$, the overall effect is that the differences between low- and high-n galaxies becomes more pronounced with increasing luminosity, whilst distinctions between subsamples are maintained. Therefore, the process by which late-types grow must promote the variation of profile shape with wavelength, by perhaps accreting a disc of ample cool gas to fuel star formation (e.g. Stewart et al. 2011), whilst the growth of early-types must promote the wavelength variation of size. Oogi, Habe & Ishiyama (2016) find that simulations of dry major mergers can be responsible for the size growth of early-types, particularly in high density environments. As few as one or two dry major mergers can increase the size of a galaxy fourfold between z = 2 and z = 0, and support my observations of multiple stellar populations which are oldest and reddest in the centre of a galaxy, and younger and bluer at the outskirts.

I find that dust also goes some way to explaining the high- and low-n populations in $\mathcal{N}$ vs $\mathcal{R}$ space; increasing dust opacity decreases $\mathcal{R}$, whilst increasing inclination increases $\mathcal{N}$. These effects cannot, however, account for the full $\mathcal{N}$-$\mathcal{R}$ distribution. Having assessed the possible effects of luminosity and dust, I can now consider the meaning of the wavelength dependence of galaxy properties solely in terms of internal structure.

To some degree, all galaxies show radial variations with colour. Even in galaxies with a one-component morphology, multiple stellar populations can be present which contribute to these colour gradients. A galaxy's colour gradient reflects internal trends in age and metallicity, however these two properties are degenerate (Worthey, Trager & Faber 1995); a positive age gradient will be balanced by a negative metallicity gradient and vice versa. Different formation mechanisms predict different colour, age and metallicity gradients; models of monolithic collapse predict metal-rich central regions in elliptical galaxies, whilst models of mergers 'wash out' any trends in colour, age and metallicity (White 1980). In recent years, advances have been made in constraining age

and metallicity gradients in early-type galaxies using colour information (see e.g. La Barbera et al. 2010a; Carter et al. 2011). Similarly, studies of late-types have attempted to disentangle age and metallicity; these studies find that inside-out formation is supported by observations of metal-rich centres of spiral galaxies (particularly Bell & de Jong 2000), although it has been found that in low-inclination spiral galaxies age gradients do not necessarily correlate with metallicity gradients (see e.g. Tortora et al. 2010; Sánchez-Blázquez et al. 2014).

Previous studies have made contrasting conclusions regarding the luminosity dependence of colour gradients, with some studies reporting little or no luminosity dependence (e.g. Peletier, Valentijn & Jameson 1990; De Propris et al. 2005; La Barbera et al. 2005), and others reporting a strong correlation (e.g. Tamura & Ohta 2003; Balcells & Peletier 1994; Roche, Bernardi & Hyde 2010). La Barbera et al. (2010a) found that, for a sample of ETGs, the luminosity dependence of colour gradients depended on the wavebands in which colour gradient was measured; when measuring colour gradients in optical wavebands they find that the brightest galaxies have the shallowest colour gradients, whilst the opposite trend is observed when measuring colour gradients between optical-NIR wavebands. One particularly interesting case is the double-valued behavior observed in the ∇_{g-r} gradient, which becomes flatter for the faintest and brightest galaxies.

In this study I have used a much larger sample of high-resolution galaxies than ever before in a study of this nature, representing all morphological types (rather than just 'early-' or 'late-type'). In Chapter 4 I have studied the luminosity dependence of colour gradients for six subsamples, and find that the bimodality seen in colour gradients vs luminosity must arise from the different populations which are being observed simultaneously. For example, I find that *red* high-n galaxies are the only population observed at the bright end, so their shallower colour gradients dominate the distribution seen by La Barbera et al. (2010a). Observing the colour gradient vs luminosity relationship for different subsamples allows me to distinguish between likely formation mechanisms. I have discussed these possible mechanisms in detail in Section 4.4, so here I provide a summary. The strong negative colour gradients we see in disc-dominated systems are consistent with the gradual accretion of gas to

their outer regions (Lemonias et al. 2011; Wang et al. 2011). Whilst it has been widely postulated that elliptical galaxies are the product of major mergers, I observe weak colour gradients even in the bright, red, high-n population. Any colour gradients would have been flattened by a major merger (Kim & Im 2013 and references therein), so another mechanism must be responsible. Possibilities include dry minor mergers introducing metal-poor stellar populations into the outskirts of these galaxies (e.g. Eliche-Moral et al. 2013) or the fading of low-n galaxies (e.g. Bell et al. 2006).

Having studied in detail the signatures of evolutionary scenarios provided by single-Sérsic fits, in Chapter 5 I then looked at what we can learn from bulge-disc decompositions. Looking in more detail at the two main structures within a galaxy has allowed me to isolate these populations in order to discover their individual contributions to the wavelength dependence of galaxy properties.

The work of Vulcani et al. (2014) found that the joint wavelength dependence of Sérsic index and effective radius ($\mathcal{N}$ vs $\mathcal{R}$) could potentially be an effective classifier of bulge-disc systems. They consider *blue* low-n galaxies and *red* high-n galaxies, which are the main contrasting populations. The blue, low-n population (which is expected to contain bulge-disc galaxies) exhibits a strong wavelength dependence for n, implying that the Sérsic index of the disc is observed in bluer wavebands, and the Sérsic index of the bulge is observed in redder wavebands. Conversely, the population of *red* high-n galaxies (which we expect to be spheroids) shows little change in Sérsic index with wavelength, implying that there is just one stellar population present. Following this trend, we would expect that galaxies containing only a disc (i.e. one component) should also exhibit little wavelength dependence of $\mathcal{N}$.

In this thesis I have revealed that, whilst the joint distribution of $\mathcal{N}$ and $\mathcal{R}$ *can* be an effective classifier for the internal structure of a galaxy, the implications of Vulcani et al. 2014 are not as straightforward as previously thought. Rather than the number of components determining the wavelength dependence of Sérsic index, I find that the presence of a disc drives the wavelength dependence of a galaxy's structure. When looking at the wavelength dependence of effective radius I find that red, single-component systems have much smaller radii at longer wavelengths. This can be attributed to an extended, bluer component, which may have formed due to dry minor mergers adding

younger stellar populations to the outskirts of these high-n systems.

Low-n galaxies in particular have bulges and discs which are relatively close in size (i.e. $\mathcal{R} \sim 1$). This, combined with the luminosity dependence seen in Chapter 3, explains the variation in $\mathcal{N}$ and $\mathcal{R}$ with overall colour seen in Vulcani et al. (2014); the brighter a galaxy, the greater the colour difference between its bulge and disc. This in turn results in a greater change in structural properties with wavelength.

7.2 Further work

Whilst more data, and higher resolution data, will allow us to probe deeper into our understanding of galaxies, this comes at a price. Current analysis methods will struggle to handle the huge datasets that facilities like LSST will bring, so I believe that the future of our field lies in machine learning. The ability of neural networks to efficiently learn and process data will transform data pipelines, allowing us to extract every ounce of science from the data collected (e.g. Charnock & Moss 2016 who have demonstrated the ability of neural networks to classify supernovae). However, I have identified some specific topics for future study which will make use of data and facilities currently available; these will be discussed in the following sections.

7.2.1 Are we able to observe separate colour gradients in bulges and discs?

The results presented here provide evidence in support of inside-out growth through gas accretion for disc-dominated galaxies, and growth through stellar mergers for bulge-dominated galaxies (see Fig. 4.4, Chapter 4). Observing colour gradients of each component individually is the next step required to infer the separate formation histories of bulges and discs, thus dissecting the formation history of the galaxy and its components.

It is known that star-forming galaxies do not show significant colour gradients in their discs, whilst passive galaxies do. Meanwhile, ellipticals are thought to form with steep stellar population gradients (see e.g. Brough et al. 2007; Kuntschner et al. 2010 for more discussion). With the multiwavelength tech-

niques developed as part of the MegaMorph project it is possible to fit bulges and discs with wavelength-dependent profiles, allowing us to observe colour gradients within individual components.

To investigate the relative contribution of bulges and discs to the overall colour gradients of galaxies requires bulge-disc decompositions of a sample of bright galaxies.

The technique described above also allows for several other complementary projects. In addition to the kinematic data already available through (for example) CALIFA and MaNGA, MUSE will be able to provide spatially resolved spectroscopy for a sample of nearby galaxies spanning all traditional Hubble types. Instead of looking solely at colour gradients as a proxy for galaxy structure, spectral information will be available throughout each galaxy which can be used to look *directly* at the age and metallicity gradients themselves. This information can be used to calibrate colour gradient findings and then apply them to galaxies without IFU data, to improve statistics and/or observe galaxy properties at higher redshifts. In measuring the wavelength dependence of a galaxy's structure, it will be possible to greatly improve the accuracy of age and metallicity measurements, and thus further understand its formation history.

Addressing these open questions will transform our understanding of galaxy formation and evolution by revealing the mechanisms by which bulges and discs form and evolve.

7.2.2 How does environment impact galaxy formation and evolution?

It is well-documented that a galaxy's environment plays an important role in its formation and evolution; but what impact does environment have on the individual stellar components within a galaxy?

Previous studies (e.g. Carollo et al. 2013; Cibinel et al. 2013; Head et al. 2014; Head, Lucey & Hudson 2015) have already begun investigating this for galaxies in nearby groups and clusters ($z < 0.05$). However they either don't have the multi-component information in the optical and NIR afforded by using MegaMorph with GAMA data, or perform their analysis on a much

smaller sample spanning a smaller range of environments. I found in Chapter 5 that, regardless of morphology, the majority of galaxies exhibit a bulge which is redder than its corresponding disc. This colour difference is maintained regardless of the overall colour of Sérsic index of a galaxy, and shows that rather than all bulges being 'red' and all discs being 'blue', there appears to be a colour difference within a given galaxy. This results in the discs of some galaxies being redder than the bulges in other galaxies. This relationship between bulge and disc properties implies that the two components have a shared formation history. Could environment be responsible for quenching in the reddest bulge-disc systems we have observed? If not, what processes could be responsible?

Studying the environmental dependence of bulge and disc properties will provide unique insights into the shared formation history of these components.

Bibliography

Aguerri J. A. L., Elias-Rosa N., Corsini E. M., Muñoz-Tuñón C., 2005, AAP, 434, 109

Allen P. D., Driver S. P., Graham A. W., Cameron E., Liske J., De Propris R., 2006, MNRAS, 371, 2

Andredakis Y. C., Peletier R. F., Balcells M., 1995, MNRAS, 275, 874

Andredakis Y. C., Sanders R. H., 1994, MNRAS, 267, 283

Bahé Y. M., McCarthy I. G., 2015, MNRAS, 447, 969

Balcells M., Graham A. W., Domínguez-Palmero L., Peletier R. F., 2003, The Astrophysical Journal, 582, L79

Balcells M., Peletier R. F., 1994, AJ, 107, 135

Baldry I. K., Balogh M. L., Bower R., Glazebrook K., Nichol R. C., 2004, in American Institute of Physics Conference Series, Vol. 743, The New Cosmology: Conference on Strings and Cosmology, Allen R. E., Nanopoulos D. V., Pope C. N., eds., pp. 106–119

Baldry I. K., Balogh M. L., Bower R. G., Glazebrook K., Nichol R. C., Bamford S. P., Budavari T., 2006, MNRAS, 373, 469

Bamford S. P., Häußler B., Rojas A., Vika M., Cresswell J., 2012, Proceedings of the International Astronomical Union, 7, 301

Bamford S. P. et al., 2009, MNRAS, 393, 1324

Barazza F. D., Jogee S., Marinova I., 2008, ApJ, 675, 1194

Barden M., Häuß ler B., Peng C. Y., McIntosh D. H., Guo Y., 2012, MNRAS, 422, 449

Barden M. et al., 2005, ApJ, 635, 959

Bekki K., 1998, ApJ, 502, L133

Bekki K., Shioya Y., 1998, ApJ, 497, 108

Bell E. F., de Jong R. S., 2000, MNRAS, 312, 497

Bell E. F. et al., 2006, ApJ, 640, 241

Bendo G. J. et al., 2006, ApJ, 645, 134

Bertin E., Arnouts S., 1996, A&AS, 117, 393

Binggeli B., Jerjen H., 1998, A&A

Blanton M. R., Roweis S., 2007, AJ, 133, 734

Block D., Puerari I., Frogel J., Eskridge P., Stockton A., Fuchs B., 1999, Ap&SS, 5

Brinchmann J., Charlot S., White S. D. M., Tremonti C., Kauffmann G., Heckman T., Brinkmann J., 2004, MNRAS, 351, 1151

Brough S., Proctor R., Forbes D. A., Couch W. J., Collins C. A., Burke D. J., Mann R. G., 2007, MNRAS, 378, 1507

Bruzual A. G., 2000, ArXiv Astrophysics e-prints

Bruzual G., Charlot S., 2003, Monthly Notices of the Royal Astronomical Society, 344, 1000

Calzetti D., Armus L., Bohlin R. C., Kinney A. L., Koornneef J., StorchiBergmann T., 2000, The Astrophysical Journal, 533, 682

Cameron E., Driver S. P., Graham A. W., Liske J., 2009, ApJ, 699, 105

Caon N., Capaccioli M., D'Onofrio M., 1993, MNRAS, 265

Capaccioli M., Piotto G., Rampazzo R., 1988, AJ, 96, 487

Cappellari M. et al., 2011, MNRAS, 416, 1680

Carollo C. M., 1999, ApJ, 523, 566

Carollo C. M. et al., 2013, ApJ, 776, 71

Carollo C. M., Stiavelli M., de Zeeuw P. T., Mack J., 1997, AJ, 114, 2366

Carter D., Pass S., Kennedy J., Karick A. M., Smith R. J., 2011, MNRAS, 414, 3410

Cassata P. et al., 2010, ApJL, 714, L79

Chabrier G., 2003, PASP, 115, 763

Charnock T., Moss A., 2016, ArXiv e-prints

Cibinel A. et al., 2013, ApJ, 776, 72

Cimatti A. et al., 2008, A&A, 482, 21

Ciotti L., 1991, A&A, 249, 99

Combes F., Debbasch F., Friedli D., Pfenniger D., 1990, A&A, 233, 82

Conselice C. J., 2006, MNRAS, 373, 1389

Daddi E. et al., 2005, ApJ, 626, 680

Darg D. W. et al., 2010, MNRAS, 401, 1043

Darvish B., Mobasher B., Sobral D., Rettura A., Scoville N., Faisst A., Capak P., 2016, ApJ, 825, 113

Davari R. H., Ho L. C., Mobasher B., Canalizo G., 2017, ApJ, 836, 75

De Geyter G., Baes M., Camps P., Fritz J., De Looze I., Hughes T. M., Viaene S., Gentile G., 2014, MNRAS, 441, 869

de Jong R., van der Kruit P., 1994, Astronomy and Astrophysics Suppl. 106

de Jong R. S., Simard L., Davies R. L., Saglia R. P., Burstein D., Colless M., McMahan R., Wegner G., 2004, MNRAS, 355, 1155

de Lapparent V., Baillard A., Bertin E., 2011, A&A, 532, A75

De Propris R., Colless M., Driver S. P., Pracy M. B., Couch W. J., 2005, MNRAS, 357, 590

de Souza R. E., Gadotti D. A., dos Anjos S., 2004, ApJS, 153, 411

de Vaucouleurs G., 1948, AnAp, 11, 247

deJong R., 1996, A&A, 118, 557

den Brok M. et al., 2011, MNRAS, 414, 3052

Dressler A., 1980, ApJ, 236, 351

Dressler A. et al., 1997, ApJ, 490, 577

Driver S. P., Allen P. D., Liske J., Graham A. W., 2007a, ApJ, 657, L85

Driver S. P. et al., 2011, MNRAS, 413, 971

Driver S. P., Norberg P., Baldry I. K., Bamford S. P., Hopkins A. M., Liske J., Loveday J., Peacock J. A., 2009, Astronomy & Geophysics, 50, 5.12

Driver S. P., Popescu C. C., Tuffs R. J., Liske J., Graham A. W., Allen P. D., De Propris R., 2007b, MNRAS, 379, 1022

Drory N., Fisher D. B., 2007, The Astrophysical Journal, 664, 640

D'Souza R., Kauffman G., Wang J., Vegetti S., 2014, MNRAS, 443, 1433

Dullo B. T., Graham A. W., 2013, ApJ, 768, 36

Duncan K. et al., 2014, MNRAS, 444, 2960

Edge A., Sutherland W., Kuijken K., Driver S., McMahon R., Eales S., Emerson J., 2013, The Messenger, 154, 32

Efstathiou G., 2000, MNRAS, 317, 697

Eliche-Moral M. C., González-García A. C., Aguerri J. A. L., Gallego J., Zamorano J., Balcells M., Prieto M., 2013, A&A, 552, A67

Emsellem E. et al., 2011, MNRAS, 414, 888

Emsellem E. et al., 2007, MNRAS, 379, 401

Evans R., 1994, MNRAS, 266

Fabian A. C., 2012, ARAA, 50, 455

Fall S. M., Efstathiou G., 1980, MNRAS, 193, 189

Ferreras I., Lisker T., Carollo C. M., Lilly S. J., Mobasher B., 2005, ApJ, 635, 243

Gabor J. M., Davé R., Oppenheimer B. D., Finlator K., 2011, MNRAS, 417, 2676

Gadotti D. A., 2009, Monthly Notices of the Royal Astronomical Society, 393, 1531

Gadotti D. A., 2011, MNRAS, 415, 3308

Gargiulo A., Saracco P., Longhetti M., La Barbera F., Tamburri S., 2012, MNRAS, 425, 2698

Gonzalez-Perez V., Castander F. J., Kauffmann G., 2011, MNRAS, 411, 1151

Goudfrooij P., Hansen L., Jorgensen H., Norgaard-Nielsen H., deJong T., vandenHoek L., 1994, A&A Suppl. 104

Graham A. W., 2013, Elliptical and Disk Galaxy Structure and Modern Scaling Laws, Oswalt T. D., Keel W. C., eds., p. 91

Graham A. W., 2014, in Astronomical Society of the Pacific Conference Series, Vol. 480, Structure and Dynamics of Disk Galaxies, Seigar M. S., Treuthardt P., eds., p. 185

Graham A. W., Driver S. P., 2005, PASA, 22, 118

Graham A. W., Dullo B. T., Savorgnan G. A. D., 2015, ApJ, 804, 32

Graham A. W., Guzman R., 2003, AJ, 125, 2936

Graham A. W., Prieto M., 2001, Ap&SSS, 277, 465

Gunn J. E., Gott, III J. R., 1972, ApJ, 176, 1

Häußler B. et al., 2013, MNRAS, 430, 330

Head J. T. C. G., Lucey J. R., Hudson M. J., 2015, MNRAS, 453, 3729

Head J. T. C. G., Lucey J. R., Hudson M. J., Smith R. J., 2014, MNRAS, 440, 1690

Hill D. T. et al., 2011, MNRAS, 412, 765

Hinz J. L., Rieke M. J., Rieke G. H., Willmer C. N. A., Misselt K., Engelbracht C. W., Blaylock M., Pickering T. E., 2007, ApJ, 663, 895

Hodge P. W., 1971, ARA&A, 9, 35

Holwerda B. W. et al., 2012, A&A, 541, L5

Holwerda B. W., Gonzalez R. A., Allen R. J., van der Kruit P. C., 2005, AJ, 129, 1396

Holwerda B. W., Keel W. C., Williams B., Dalcanton J. J., de Jong R. S., 2009, AJ, 137, 3000

Hopkins P. F. et al., 2010, ApJ, 715, 202

Hopkins P. F., Bundy K., Murray N., Quataert E., Lauer T. R., Ma C.-P., 2009, MNRAS, 398, 898

Huang S., Ho L. C., Peng C. Y., Li Z. Y., Barth A. J., 2012, in American Astronomical Society Meeting Abstracts, Vol. 219, American Astronomical Society Meeting Abstracts, p. 102.07

Huang S., Ho L. C., Peng C. Y., Li Z.-Y., Barth A. J., 2013, The Astrophysical Journal, 768, L28

Hubble E., 1936, The Realm of the Nebulae. Yale University Press, p. 207

Hudson M. J., Stevenson J. B., Smith R. J., Wegner G. A., Lucey J. R., Simard L., 2010, MNRAS, 409, 405

Johnston E. J., Aragón-Salamanca A., Merrifield M. R., 2014, MNRAS, 441, 333

Kauffmann G. et al., 2003, MNRAS, 346, 1055

Keel W. C., White III R. E., 2001, AJ, 122, 1369

Keenan R. C. et al., 2014, ApJ, 795, 157

Kelvin L. S. et al., 2014, MNRAS, 439, 1245

Kelvin L. S. et al., 2012, MNRAS, 421, 1007

Kennedy R. et al., 2015, MNRAS, 454, 806

Kennedy R. et al., 2016a, MNRAS

Kennedy R., Bamford S. P., Häußler B., Brough S., Holwerda B., Hopkins A. M., Vika M., Vulcani B., 2016b, A&A, 593, A84

Khochfar S., Burkert A., 2001, ApJ, 561, 517

Khochfar S., Burkert A., 2003, ApJ, 597, L117

Kim D., Im M., 2013, ApJ, 766, 109

Ko J., Im M., 2005, JKAS, 38, 149

Kormendy J., 1977, ApJ, 217, 406

Kormendy J., 1993, in IAU Symposium, Vol. 153, Galactic Bulges, Dejonghe H., Habing H. J., eds., p. 209

Kormendy J., Bender R., 1996, ApJ, 464, L119

Kormendy J., Cornell M. E., Block D. L., Knapen J. H., Allard E. L., 2006, The Astrophysical Journal, 642, 765

Kormendy J., Kennicutt, Jr. R. C., 2004, ARA&A, 42, 603

Krajnovic D. et al., 2013, MNRAS, 432, 1768

Krajnović D. et al., 2011, MNRAS, 414, 2923

Kuntschner H. et al., 2010, MNRAS, 408, 97

La Barbera F., de Carvalho R. R., 2009, ApJ, 699, L76

La Barbera F., De Carvalho R. R., De La Rosa I. G., Gal R. R., Swindle R., Lopes P. A. A., 2010a, AJ, 140, 1528

La Barbera F., De Carvalho R. R., De La Rosa I. G., Lopes P. A. A., Kohl-Moreira J. L., Capelato H. V., 2010b, MNRAS, 408, 1313

La Barbera F., de Carvalho R. R., Gal R. R., Busarello G., Merluzzi P., Capaccioli M., Djorgovski S. G., 2005, ApJ, 626, L19

La Barbera F., Ferreras I., de Carvalho R. R., Bruzual G., Charlot S., Pasquali A., Merlin E., 2012, MNRAS, 426, 2300

Lacey C., Cole S., 1993, MNRAS, 262, 627

Lackner C. N., Gunn J. E., 2012, MNRAS, 421, 2277

Lange R. et al., 2015, MNRAS, 447, 2603

Laurikainen E., Salo H., Buta R., Knapen J. H., 2007, MNRAS, 381, 401

Lawrence A. et al., 2007, MNRAS, 379, 1599

Lemonias J. J. et al., 2011, ApJ, 733, 74

Li Z., Han Z., 2007, A&A, 471, 795

Liller M. H., 1966, ApJ, 146, 28

Liske J. et al., 2015, MNRAS, 452, 2087

Longhetti M. et al., 2007, MNRAS, 374, 614

Masters K. L. et al., 2010, MNRAS, 404, 792

McDonald M., Courteau S., Tully R. B., Roediger J., 2011, Monthly Notices of the Royal Astronomical Society, 414, 2055

Mendez A. J., Coil A. L., Lotz J., Salim S., Moustakas J., Simard L., 2011, ApJ, 736, 110

Mo H. J., Mao S., White S. D. M., 1998, MNRAS, 295, 319

Moffett A. J. et al., 2016, MNRAS, 457, 1308

Möllenhoff C., 2004, A&A, 415, 63

Möllenhoff C., Popescu C. C., Tuffs R. J., 2006, A&A, 456, 941

Moore B., Katz N., Lake G., Dressler A., Oemler A., 1996, Nature, 379, 613

Morselli L., Renzini A., Popesso P., Erfanianfar G., 2016, MNRAS, 462, 2355

Naab T., Burkert A., 2001, The Astrophysical Journal, 555, L91

Naab T., Johansson P. H., Ostriker J. P., 2009, ApJL, 699, L178

Nieto J.-L., Capaccioli M., Held E. V., 1988, A&A, 195, L1

Oogi T., Habe A., Ishiyama T., 2016, MNRAS, 456, 300

Oser L., Ostriker J. P., Naab T., Johansson P. H., Burkert A., 2010, ApJ, 725, 2312

Pagel B. E. J., Patchett B. E., 1975, MNRAS, 172, 13

Park C., Choi Y.-Y., 2005, ApJ, 635, L29

Pastrav B. A., Popescu C. C., Tuffs R. J., Sansom A. E., 2013a, A&A, 553, A80

Pastrav B. A., Popescu C. C., Tuffs R. J., Sansom A. E., 2013b, A&A, 557, A137

Peletier R., Valentijn E., Jameson R., 1990, A&A, 233, 62

Peletier R. F., Balcells M., 1996, The Astronomical Journal, 111, 2238

Peng C. Y., Ho L. C., Impey C. D., Rix H.-W., 2002, AJ, 124, 266

Peng C. Y., Ho L. C., Impey C. D., Rix H.-W., 2010, AJ, 139, 2097

Peng Y., Maiolino R., Cochrane R., 2015, Nature, 521, 192

Pierini D., Gordon K. D., Witt A. N., Madsen G. J., 2004, ApJ, 617, 1022

Pipino A., D'Ercole A., Chiappini C., Matteucci F., 2010, MNRAS, 407, 1347

Poggianti B. M., Barbaro G., 1997, A&A, 325, 1025

Popescu C. C., Misiriotis A., Kylafis N. D., Tuffs R. J., Fischera J., 2000, A&A, 362, 138

Popescu C. C., Tuffs R. J., Völk H. J., Pierini D., Madore B. F., 2002, ApJ, 567, 221

Prochaska Chamberlain L. C., Courteau S., McDonald M., Rose J. A., 2011, MNRAS, 412, 423

Rees M. J., Ostriker J. P., 1977, MNRAS, 179, 541

Robotham A. S. G. et al., 2011, MNRAS, 416, 2640

Roche N., Bernardi M., Hyde J., 2010, MNRAS, 407, 1231

Roediger J. C., Courteau S., McDonald M., MacArthur L. A., 2011, MNRAS, 416, 1983

Rowlands K. et al., 2012, MNRAS, 419, 2545

Saglia R., Maraston C., Greggio L., Bender R., Ziegler B., 2000, A&A, 360

Sánchez-Blázquez P., Ocvirk P., Gibson B. K., Pérez I., Peletier R. F., 2011, MNRAS, 415, 709

Sánchez-Blázquez P. et al., 2014, A&A, 570, A6

Schawinski K. et al., 2014, MNRAS, 440, 889

Sérsic J. L., 1963, Boletin de la Asociacion Argentina de Astronomia, 6

Simard L., TrevorMendel J., Patton D., Ellison S., McConnachie A., 2011, VizieR On-line Data Catalog: J/ApJS/196/11. Originally published in: 2011ApJS..196...11S

Simien F., Michard R., 1990, A&A, 227, 11

Slater C. T., Bell E. F., 2014, ApJ, 792, 141

Smethurst R. J. et al., 2015, MNRAS, 450, 435

Snaith O. N., Bailin J., Gibson B. K., Bell E. F., Stinson G., Valluri M., Wadsley J., Couchman H., 2016, MNRAS, 456, 3119

Steinmetz M., Navarro J. F., 2002, NA, 7, 155

Stewart K. R., Kaufmann T., Bullock J. S., Barton E. J., Maller A. H., Diemand J., Wadsley J., 2011, ApJL, 735, L1

Stinson G., Seth A., Katz N., Wadsley J., Governato F., Quinn T., 2006, MNRAS, 373, 1074

Strateva I. et al., 2001, AJ, 122, 1861

Suh H., Jeong H., Oh K., Yi S. K., Ferreras I., Schawinski K., 2010, ApJS, 187, 374

Szomoru D., Franx M., van Dokkum P. G., 2012, ApJ, 749, 121

Tabor M., Merrifield M., Aragón-Salamanca A., Cappellari M., Bamford S. P., Johnston E., 2017, MNRAS, 466, 2024

Tamura N., Ohta K., 2003, AJ, 126, 596

Taylor E. N. et al., 2009, ApJS, 183, 295

Taylor E. N. et al., 2011, MNRAS, 418, 1587

Taylor V. A., Jansen R. A., Windhorst R. A., Odewahn S. C., Hibbard J. E., 2005, ApJ, 630, 784

Taylor-Mager V. A., Conselice C. J., Windhorst R. A., Jansen R. A., 2007, ApJ, 659, 162

Tolstoy E., Hill V., Tosi M., 2009, ARAA, 47, 371

Tonini C., Mutch S. J., Wyithe J. S. B., Croton D. J., 2017, MNRAS, 465, 4133

Tortora C., Napolitano N. R., Cardone V. F., Capaccioli M., Jetzer P., Molinaro R., 2010, MNRAS, 407, 144

Tuffs R. J., Popescu C. C., Vlk H. J., Kylafis N. D., Dopita M. A., 2004, A&A, 419, 821

van den Bergh S., 1976, ApJ, 206, 883

van der Wel A. et al., 2014, ApJ, 788, 28

van Dokkum P. G. et al., 2010, ApJ, 709, 1018

Vika M., Bamford S. P., Haussler B., Rojas A. L., 2014, MNRAS, 444, 3603

Vika M., Bamford S. P., Häussler B., Rojas A. L., Borch A., Nichol R. C., 2013, MNRAS, 435, 623

Vika M., Vulcani B., Bamford S., Häuß ler B., Rojas A., 2015, eprint arXiv:1502.05627

Vulcani B. et al., 2014, MNRAS, 441, 1340

Wang J. et al., 2011, MNRAS, 412, 1081

Weinzirl T., Jogee S., Khochfar S., Burkert A., Kormendy J., 2009, ApJ, 696, 411

White S. D. M., 1980, MNRAS, 191, 1P

Wild V., Kauffmann G., Heckman T., Charlot S., Lemson G., Brinchmann J., Reichard T., Pasquali A., 2007, MNRAS, 381, 543

Willman B., Governato F., Wadsley J., Quinn T., 2004, MNRAS, 355, 159

Worthey G., 1994, ApJS, 95, 107

Worthey G., 1999, in Astronomical Society of the Pacific Conference Series, Vol. 192, Spectrophotometric Dating of Stars and Galaxies, Hubeny I., Heap S., Cornett R., eds., p. 283

Worthey G., Trager S. C., Faber S. M., 1995, in Astronomical Society of the Pacific Conference Series, Vol. 86, Fresh Views of Elliptical Galaxies, Buzzoni A., Renzini A., Serrano A., eds., p. 203

Xu C. K., Zhao Y., Scoville N., Capak P., Drory N., Gao Y., 2012, ApJ, 747, 85

York D. G. et al., 2000, AJ, 120, 1579

Zwicky F., 1933, Helvetica Physica Acta, 6, 110